Lucrări științifice relevante

1. **Stan F,** Gudea A, Damian A, Gal AF, Papuc I, Pop AR, Martonos C., 2020, **Ultrasonographic Algorithm for the Assessment of Sentinel Lymph Nodes That Drain the Mammary Carcinomas in Female Dogs.** Animals (Basel). 2020 Dec 10;10(12):2366. doi: 10.3390/ani10122366. PMID: 33321917; PMCID: PMC7763578. https://pubmed.ncbi.nlm.nih.gov/33321917/

2. **Stan Florin Gheorghe**, (2018), **Comparative Study of the Liver Anatomy in the Rat, Rabbit, Guinea Pig and Chinchilla** Bulletin UASVM Veterinary Medicine 75(1)/2018, pg 33-40, Cluj Napoca, Romania, Print ISSN 1843-5270; Electronic ISSN 1843-5378, 2018. http://veterinarymedicinejournal.usamv.ro/pdf/2018/issue_1/Art2.pdf

3. **Florin Gheorghe STAN**, (2018), **Macroscopic anatomy of the gallbladder and extrahepatic biliary tract in the guinea pig (*Cavia porcellus*),** Scientific Works. Series C. Veterinary Medicine. Vol. LXIII (2), pg. 25-29, Bucuresti, Romania, ISSN 2065-1295; ISSN 2343-9394 (CD-ROM); ISSN 2067-3663 (Online); ISSN-L 2065-1295. http://veterinarymedicinejournal.usamv.ro/index.php/scientific-papers/past-issues?id=1580

4. **Stan Florin Gheorghe**, (2018), **Macroscopic anatomy of pancreas in rats, guinea pigs, chinchillas and rabbits**, Scientific Works Series C. Veterinary medicine volume LXIV (1), 2018, pag. 15-20. http://veterinarymedicinejournal.usamv.ro/pdf/2018/issue_1/Art2.pdf

5. **Stan Florin**, (2016), **Morphological Particularities of Anatomical Crown of the Teeth in Golden Jackal (Canis Aureus Moreoticus),** Scientific Works. Series C. Veterinary Medicine. Vol. LXII (2), pg. 44-51, ISSN 2065-1295; ISSN 2343-9394 (CD-ROM); ISSN 2067-3663 (Online); ISSN-L 2065-1295, Bucuresti, Romania. http://veterinarymedicinejournal.usamv.ro/pdf/2016/issue_2/Art7.pdf

6. **Stan Florin,** (2016), **Non-Invasive Assessment of Sentinel Lymph Nodes That Drain the Tumoral Mammary Glands in Female Dog**, Bulletin UASVM Veterinary Medicine 73(2) /pg. 382-388, 2016, Print ISSN 1843-5270; Electronic ISSN 1843-5378 DOI:10.15835/buasvmcn-vm: 12251. http://journals.usamvcluj.ro/index.php/veterinary/article/view/12251

7. **Stan, F.** (2015). **Anatomical Particularities of Male Reproductive System of Guinea Pigs (Cavia porcellus)** *Bulletin of University of Agricultural Sciences and Veterinary Medicine Cluj-Napoca. Veterinary Medicine*, *72*(2), 288-295. http://journals.usamvcluj.ro/index.php/veterinary/article/view/11410

8. **Stan F.** (2015). **Qualitative morphological assessement of tumor associated lymphatic vasculature in mammary gland neoplasia of female dog in relation with sentinel lymph nodes metastatic infiltration**. Scientific *Works. Series C. Veterinary Medicine*, Vol. LXI, p. 16-23. http://veterinarymedicinejournal.usamv.ro/pdf/2015/issue_2/Art2.pdf

9. **Stan, F.,** Crișan M., Damian A., Dezdrobitu C., Martonoș C., Gudea A. (2015), **Heart topography and pericardic ligaments of guinea pigs**. *Scientific Works. Series C. Veterinary Medicine, Vol. LXI,* 57-64. http://veterinarymedicinejournal.usamv.ro/pdf/2015/issue_1/Art9.pdf

10. **Stan, F.,** Gudea, A., Baba, A.I., Feier, D., Badea, R. (2012). **Correlation Between Ultrasonographic Features and Morphological Pattern after Blue Dye Injection of Normal Superficial Lymph Nodes in Carnivores** *Bulletin of University Agricultural Sciences and Veterinary Medicine Cluj-Napoca, Veterinary Medicine, 69* (1-2) p. 211 – 219 https://journals.usamvcluj.ro/index.php/veterinary/article/view/8430

animals

MDPI

Article

Ultrasonographic Algorithm for the Assessment of Sentinel Lymph Nodes That Drain the Mammary Carcinomas in Female Dogs

Florin Stan [1,*], Alexandru Gudea [1], Aurel Damian [1], Adrian Florin Gal [2], Ionel Papuc [3], Alexandru Raul Pop [4] and Cristian Martonos [1]

1 Department of Comparative Anatomy, Faculty of Veterinary Medicine, University of Agricultural Sciences and Veterinary Medicine, 3-5 Manastur Street, 400372 Cluj Napoca, Romania; alexandru.gudea@usamvcluj.ro (A.G.); aurel.damian@usamvcluj.ro (A.D.); cristian.martonos@usamvcluj.ro (C.M.)

2 Department of Cell Biology, Histology and Embryology, Faculty of Veterinary Medicine, University of Agricultural Sciences and Veterinary Medicine, 3-5 Manastur Street, 400372 Cluj Napoca, Romania; adrian.gal@usamvcluj.ro

3 Department of Semiology and Medical Imaging, Faculty of Veterinary Medicine, University of Agricultural Sciences and Veterinary Medicine, 3-5 Manastur Street, 400372 Cluj Napoca, Romania; ionel.papuc@usamvcluj.ro

4 Department of Reproduction, Obstetrics and Reproductive Pathology, Biotechnologies in Reproduction, Faculty of Veterinary Medicine, University of Agricultural Sciences and Veterinary Medicine, 3-5 Manastur Street, 400372 Cluj Napoca, Romania; alexandru.pop@usamvcluj.ro

* Correspondence: florin.stan@usamvcluj.ro; Tel.: +40-264-596384 (ext. 258)

Received: 12 October 2020; Accepted: 4 December 2020; Published: 10 December 2020

Simple Summary: Mammary neoplasms are one of the most common oncological diseases diagnosed in female dogs. Their staging also involves the evaluation of the sentinel lymph nodes that drain these tumors. Since non-invasive diagnosis is an important requirement in both human and veterinary medicine, by using simple and available ultrasound techniques, our study proposes a non-invasive assessment of the status of sentinel lymph nodes of the tumoral mammary glands. The algorithm consists of B-mode ultrasound, Doppler technique, contrast-enhanced ultrasound (CEUS), and real-time elastography. Diagnostic performance was established for each technique. The highest accuracy in identifying metastases in sentinel lymph nodes was given by the elasticity score followed by the short/long-axis ratio and resistivity index. CEUS had the same accuracy as the Doppler examination. By assigning a score to each parameter of the mentioned techniques and summing up these scores, we obtained a high accuracy of metastasis detection in sentinel lymph nodes (92.2%). This algorithm for examining the status of sentinel lymph nodes that uses simple and widely available techniques in the current practice can be extremely useful to practitioners for staging mammary malignant tumors in female dogs, leading to the right treatment decision.

Abstract: The status of sentinel lymph nodes (SLNs) is decisive in staging, prognosis, and therapeutic approach. Using an ultrasonographic examination algorithm composed of B-mode, Doppler technique, contrast-enhanced ultrasound (CEUS) and elastography, this study aimed to determine the diagnostic performance of the four techniques compared to histopathological examination. 96 SLNs belonging to 71 female dogs with mammary gland carcinomas were examined. After examinations, mastectomy and lymphadenectomy were performed. Histopathological examination confirmed the presence of metastases in 54 SLNs. The elasticity score had the highest accuracy—89.71%, identifying metastases in SLNs with 88.9.9% sensitivity (SE) and 90.5% specificity (SP), ROC analysis providing excellent results. The S/L (short axis/long axis) ratio showed 83.3% SE and 78.6% SP as a predictor of the presence of metastases in SLN having a good accuracy of 81.2%. On Doppler examination, the resistivity index(RI) showed good accuracy of 80% in characterizing lymph nodes with metastases versus unaffected

ones; the same results being obtained by CEUS examination. By assigning to each ultrasonographic parameter a score (0 or 1) and summing up the scores of the four techniques, we obtained the best diagnostic performance in identifying lymph node metastases with 92.2% accuracy. In conclusion, the use of the presented algorithm provides the best identification of metastases in SLNs, helping in mammary carcinoma staging and appropriate therapeutic management.

Keywords: sentinel lymph node; canine mammary tumor; staging; ultrasonography; non-invasive

1. Introduction

It is well known that the status of sentinel lymph nodes in mammary carcinomas in both women and female dogs is a prognostic factor of the disease and decisively influences the therapeutic approach. The correlations between the two species are justified because the spontaneous mammary tumors in dogs have biological and histopathological common appearances with those of the woman, being valuable experimental models in the study of breast cancers [1,2]. Another worth considering aspect is the similar mechanism of metastasis, through the lymphatic pathways, initially in the regional lymph nodes, for most of the carcinomas. Furthermore, tumor staging is dependent on the presence or absence of tumor invasion in these lymph nodes [3,4]. As a first instance, the lymph node that drains the tumor must be identified and then investigated to determine its status-unaffected or affected/metastatic. In breast cancer in women, there are standard protocols for the identification of SLNs (sentinel lymph nodes) by lymphoscintigraphy after peritumoral or subareolar injection of 99mTc followed by dye injection. [5–7]. The deficiency of this protocol is given by the side effects of Tc radioactivity, relatively high costs, and dye-related side effects (possible allergic reactions, local necrosis, and the inability to perform the biopsy technique in real-time). The newly developed technique of localization of sentinel lymph nodes (SLN), near-infrared fluorescence imaging, which used indocyanine green (ICG) as a mapping agent is successfully used in women [8,9] and is being investigated as a possible technique of mapping the SLNs of mammary tumors in bitches [10]. However, the best results in the identification and evaluation of SLNs are obtained by CT lymphography [11–13], Positron Emission Tomography–Computed Tomography (PET/CT), [14,15], or MRI [16], both in woman and bitch. Currently, ultrasonography is the first method of evaluation, being noninvasive, widely available, and easy to perform in clinical practice.

Using gray-scale ultrasonography, the criteria for differentiating benign from malignant lymph nodes refer to size, shape, nodal border, echogenicity, hilum appearance, calcification, or necrosis, alongside the appearance of vascularization at Doppler examination. It was stated that the malignant lymph nodes have a rounded shape, the S/L ratio is over 0.5, (short axis/long axis ratio), a hypoechoic pattern, absence of echogenic hilum, sharp borders, and chaotic, peripheral or mixed vascularization [17–20]. However, these findings are not significant for accurate differentiation of metastatic lymph nodes. Contrast-enhanced ultrasound (CEUS), a recent, novel technique for evaluating tissue perfusion in real time, became widely used in the evaluation of SLN in breast cancer in women [21–24]. This technique received attention in the evaluation of SLNs draining mammary tumors in bitches [25,26] or healthy draining mammary lymph nodes [10,27]. The accuracy of CEUS in identifying SLNs is limited if the contrast agent is injected intravenously, as there is a risk of evaluating a regional lymph node that does not drain the tumor. Another limitation of the lymph node assessment by CEUS lies in the fact that this method evaluates only the lymph node that has been identified presumed to be sentinel (because it is part of the lymph nodes that are anatomically present in the region of interest and usually drain the basin in which the tumor is located). With this method, the lymphatic drainage that can be followed at a given time is generally only one, meaning that different drainage basins are unlikely to be monitored at the same time. By intradermal or peritumoral injection, this deficiency is removed as much as possible.

Another recent technique that relevantly assesses SLNs is elastography. Considering that tumor infiltration increases the SLNs stiffness, this technique is increasingly applicable in animals lymph node evaluation. [28–30]. There are two main types of elastography—real-time elastography (or strain elastography) and share wave elastography (SWE) [31,32]. Real-time elastography qualitatively assess the degree of stiffness of the lymph node in the form of elasticity scores and quantitatively evaluates the strain ratio. SWE provides a quantitative value of tissue stiffness expressed in shear wave speed in meters/second or converted by the software and expressed in kPa requiring special modules incorporated in the ultrasound device.

The presence of metastases in the SLNs can be confirmed only after the true sentinel lymph node is identified and assessed. It may be possible that SLN is not the closest lymph node from the tumor drainage basin. This is due either to obstruction of the lymphatic pathways with tumor thrombi, or cause of an increased peritumoral lymphangiogenesis that changes the lymphatic pathway to another lymph node [33–35]. It is well-known that healthy mammary glands drain into two main lymph centers—axillary, through proper and accessory LNs, respectively the inguinofemoral lymph center through superficial inguinal LNs [36,37]. In the case of mammary neoplasia, the lymphatic drainage is altered, as other lymph centers might be involved—for example, the ventral thoracic lymph center through the cranial sternal lymph nodes or even the superficial cervical lymph center through the ventral superficial cervical lymph nodes [33,34].

Thus, it is imperative to identify and evaluate with the highest accuracy the real and corresponding SLN of the tumor drainage basin. Considering the above-mentioned facts and having as investigation methods the simple and available ultrasound methods (namely grayscale US, Doppler technique, CEUS, and elastography), this study aims to provide a non-invasive algorithm for SLNs evaluation. The accuracy of each method in differentiating between benign and metastatic SLN will be established having as reference the histopathological examination.

2. Materials and Methods

The study protocol and design complied with the guidelines of the Romanian national legislations, according to European Union standards regarding animals involved in clinical studies. The Bioethics Committee of the University of Agricultural Sciences and Veterinary Medicine approved the study (approval no. 79/17.11.2017). Informed consent was signed by the owners of animals included in the study.

A prospective cohort study was conducted including 71 female dogs of various pure and mixed breeds, diagnosed with malignant mammary tumors of the cranial thoracic (T1), cranial abdominal (A1), caudal abdominal (A2), and inguinal (I) mammary glands, histopathologically confirmed by biopsy. The subjects were chosen from patients presented for examination at the university hospital due to the presence of one or more mammary tumors. To be eligible for the study, the subjects were supposed to meet the following criteria: no previous therapy for the mammary tumor, no evidence of distant metastasis revealed by three-view thoracic radiographs and abdominal ultrasound, absence of another serious illness (severe heart and respiratory conditions, cachexia or other types of neoplasms, including lymphomas) and absence of pregnancy.

Clinical examination, complete blood count, serum biochemistry, and urine analysis were performed before the examinations. All animals were examined using an algorithm composed of greyscale ultrasound, Doppler technique, contrast-enhanced ultrasound, and real-time elastography. The dogs were examined in dorsal recumbency being closely monitored throughout the examinations. Sedation during examinations was achieved by the IV administration of acepromazine (Sedam, Pasteur Romania) at 0.2–0.3 mg/kg BW.

The procedure started with low doses of acepromazine being augmented during the examination protocol in cases that have required a much longer examination time. This approach was also a consequence of some cited effects of anesthetics on CEUS parameters that have been influencing the perfusion of different organs in dogs and cats [38,39].

2.1. Gray Scale Examination

The included subjects were examined with a Logiq E9 GE (MEDIST Imaging, GE Healthcare, Romania) ultrasound device or a Phillips IU-22 XMatrix Diamond Select (Danson Medicine, Bucuresti, Romania) device. For B–Mode examination a high-frequency linear probe, 6–15 MHz was used. A single experienced sonographer performed the examinations.

The study was conducted according to ARRIVE guidelines [40]. The examiner was unaware of the histopathological result of the SLNs throughout the ultrasonographic evaluation. On greyscale ultrasound, the following parameters were recorded: value (in cm) of the short and long axis (for the short/long ratio calculation), the internal structure (echostructure) classified as homogeneous or inhomogeneous, the echogenicity of the lymph node classified as hypoechoic, isoechoic or hyperechoic, hilum tissue definition recorded as present or absent/invisible and the capsule pattern recorded as well-defined or ill-defined. The measurements were made, having as reference a series of known reports and procedures in humans and animals [41–43].

2.2. Doppler US Examination

Doppler US examination used pulse repetition frequency 350 Hz and wall filter 45 Hz. Color Doppler technique (with pulse repetition frequency kept low—to maximize vessel detection—and the angle between the Doppler beam and long axis of the vessel being kept under 60°) studied the presence and distribution of the vascular signal. The region of interest was carefully examined without exerting pressure on the lymph node as compression may obliterate the vascular signal.

Four patterns of vascular signal localization were recorded: hilar pattern, peripheral pattern, mixed vascularisation (with both hilar and peripheral pattern), or absence of vascular signal. We used the same classification as in reports on vascularization found in mammary gland tumors in female dogs [43,44] and lymph nodes draining various tumors [42]. Regarding the type and distribution of vessels, two patterns were defined: ordered or chaotic vascularisation [41]. Pulse wave Doppler analysis was used for vascular indices assessment. After the best color signals were obtained, the spectral gate was placed on the main artery of the node which showed the fastest arterial signal.

Resistive index (RI), pulsatility index (PI), peak systolic velocity (PSV) and end-diastolic velocity (EDV) were measured using integrated software. The RI was calculated as follows: peak systolic velocity–end-diastolic velocity/peak systolic velocity. PI was calculated as follows: peak systolic velocity–end-diastolic velocity/time-averaged maximum velocity [28,45].

Two consecutive measurements were made and the average value for RI and PI was calculated for each lymph node.

2.3. CEUS Examination

CEUS examination used a 3–9 MHz linear transducer (range of gain: 86–90%, compression 38, low mechanical index of 0.07, and dedicated contrast software). In each subject, using a 2 mL syringe with a 26G needle, peritumoral administration of 0.5 mL SonoVue (Bracco Imaging SpA, Milan Italy), was performed in each point, at four symmetrical points around the tumor, in the subcutaneous cellular tissue, followed by gentle massage of the region. The microbubble contrast agent was reconstituted in 2 mL of saline water, containing 1 × 109 microbubbles/mL as previously reported [46].

The lymphatic channels were traced on contrast pulse sequencing until they reached the corresponding lymph node, which has been assumed to be the sentinel lymph node [26]. Three patterns of enhancement were defined: intense homogeneous pattern, inhomogeneous pattern with perfusion defects, and no enhancement [47].

The contrast transit times were recorded as perfusion phases, (wash-in time and wash-out time, in seconds). We defined wash-in time as the period from time zero (after the SonoVue injection) to first cortical enhancement, ending by complete medullary enhancement of lymph node parenchyma. Wash-out time was defined as the time from the visually-assessed first decrease in

medullary enhancement followed by a slower cortical enhancement (in the whole or in a part of the lymph node) resulting in hypoenhancement of the lymph node [44,48].

2.4. Real-Time Elastography (RTE)

Real time elastography was performed with a high-resolution 7–18 MHz real-time linear-array transducer and devices elastographic software. Before the RTE, conventional US was performed to obtain the most appropriate information of each SLN. The area where the lymph node was identified by CEUS was also considered. Then, the elastogram image was displayed along the B-mode image in a two-panel appearance. The region of interest (ROI) was established to encompass the entire lymph node and approximately the same part of adjacent tissue (excluding tissues like bone and blood vessels that may affect stiffness assessment). Light pressure along the radiation axis, followed by decompression was made until the same size and color images in sequential frames were obtained [31,49]. The direction of compression was upwards and downwards.

According to the color-graphic representation (in which blue indicated stiff, green and yellow indicated intermediate stiffness and red indicated soft), the lymph nodes were categorized using a five-point elasticity score proposed by Alam and collaborators (Table 1) [49]. Three to five measurements were made for each lymph node. The image that met at least twice the same classification was chosen for assigning the final score.

Table 1. Five-point elasticity scoring system.

Elasticity Score	Description	Interpretation
1	Total green or yellow, absent blue areas or very small blue area/s	Soft
2	Small scattered blue areas or total blue area <45%	Moderately soft
3	Large blue area/s, total blue area ≥45%	Moderately stiff
4	Peripheral large hard area and central small green areas suggesting central necrosis	Predominantly stiff
5	Hard area occupying the entire lymph node, with or without green rim	Stiff

The female dogs were carefully monitored for 24 h after the ultrasonographic examination.

All examinations were supervised by two experienced practitioners—one with experience in human imaging and the second in veterinary imaging.

Mastectomy and ipsilateral lymphadenectomy were performed in all subjects. Before surgery, lymphatic mapping was performed. In this respect, 0.25 mL Evans blue dye 1% (Sigma-Aldrich, Merck Company) was injected into the same locations as the contrast agent. The gentle massage was done on the injected site for 1–2 min. The dissection was performed on the operating table. Colored lymphatic vessels were identified and tracked to the sentinel lymph node.

The excised lymph nodes and mammary tissues were preserved in 10% formalin and submitted for histopathological analysis. The lymph nodes were examined at multiple levels of the paraffin block to optimize metastasis detection. Hematoxylin and eosin staining was used. Histopathological analysis was performed by a histopathologist with expertise in mammary gland pathology.

The sentinel lymph nodes were classified unaffected (absence of metastatic infiltration) and metastatic/affected (presence of metastasis or micrometastasis). When only inflammatory changes were noted, they were interpreted as benign and lymph nodes were classified as unaffected.

2.5. Statistical Analysis

Statistical analysis was performed using IBM SPSS Statistics, software version 20.0, and Microsoft Office Excel 2016. Standard descriptive statistics were used for analysis, means and standard deviations

were defined for numeric results. The normal distribution of continuous variables was assessed using the Kolmogorov-Smirnov test. Qualitative variables were compared with histopathological examination using the Chi-Square test. ROC analysis was performed for the evaluation of sensitivity, specificity, positive predictive value, negative predictive value, and overall accuracy of the four techniques defined parameters to differentiate benign from malignant lymph nodes by calculating the area under the curve (AUC). Cut-off values were determined considering the highest value of the Youden index. Significance was defined at a *p*-value lower than 0.05.

3. Results

A total of 96 sentinel lymph nodes were evaluated (79 superficial inguinal and 17 axillary lymph nodes belonging to the 71 female dogs enrolled in the study, aged 8–16 years (mean 10.6 ± 1.8).

The encountered histological type of mammary carcinomas (according to Goldschmidt et al., 2011) [50] is presented in Table 2. The affected mammary gland of each subject and their sentinel lymph nodes, alongside the demographic characteristics, are presented in Supplementary file 1.

Table 2. Histological classification of encountered mammary tumors.

Type of Neoplasms	Number of Neoplasms
Carcinoma in a mixed tumor	25
Carcinoma—simple tubular	19
Carcinoma—simple tubulopapillary	17
Carcinoma—solid	5
Carcinoma—complex type	3
Carcinoma—anaplastic	2
Total subjects	71

Of the total of 96 SLNs evaluated at the histopathological examination, 42 (43.75%) SLNs were classified as benign/unaffected and 54 (56.25%) SLNs were classified as metastatic/affected. The rate of metastasis was 56.33% (40 subjects out of 71).

The sonographic quantitative and qualitative characteristics of the SLNs are detailed in Table 3.

Table 3. Qualitative and quantitative variables evaluated by different ultrasonography methods: B-mode, Doppler technique, contrast-enhanced ultrasonography and real-time elastography.

Ultrasound Parameter *n* (%)	Unaffected Nodes (N = 42)	Metastatic/Affected Nodes (N = 54)	*p* Value
B-MODE ULTRASONOGRAPHY OF SENTINEL LYMPH NODES			
SA/LA ratio < 0.55	33 (78.57)	9(16.66)	<0.001
Short axis (mean ± SD) cm	0.67 ± 0.26	1.17 ± 0.53	
Long axis (mean ± SD) cm	1.33 ± 0.46	1.83 ± 0.79	
Internal structure (Echostructure)			
Homogeneous	36(85.71)	10(18.51)	<0.001
Inhomogeneous	6(14.28)	44(81.48)	
Echogenicity			
Hypoechoic	28(66.66)	37(68.51)	=0.81
Isoechoic	10(23.80)	14(25.92)	
Hyperechoic	4(9.52)	3(5.55)	
Hillum tissue definition			

Table 3. *Cont.*

Ultrasound Parameter *n* (%)	Unaffected Nodes (N = 42)	Metastatic/Affected Nodes (N = 54)	*p* Value
Present	30(71.48)	29(53.70)	=0.07
Absent/invisible	12(28.57)	25(46.29)	
Capsule (Borders)			
Well-defined	37(88.09)	39(72.22)	0.057
Ill-defined	5 (11.90)	15(27.77)	
COLOR DOPPLER ULTRASONOGRAPHY—VASCULAR PATTERN			
Localization			
Absence of vascular signal	2(4.76)	1(1.85)	<0.001
Hilar pattern	36(85.71)	12(22.22)	
Peripheral pattern	1(2.38)	30(55.55)	
Mixed	3(7.14)	11(20.37)	
Type and distribution			
Ordered	36(85.71)	5(9.25)	<0.001
Chaotic	4(9.52)	48(88.88)	
NA	2(4.76)	1(1.85)	
Intranodal vascular resistance (expressed by mean ± SD)			
RI	0.5060 ± 0.147	0.7011 ± 0.138	<0.001
PI	0.9828 ± 0.223	1.2426 ± 0.259	
CONTRAST-ENHANCED ULTRASONOGRAPHY (CEUS)			
Enhancement patterns			
Intense homogeneouss	32(76.19)	6(11.11)	<0.001
Inhomogeneous	8(19.04)	44(81.48)	
No enhancement	2(4.76)	4(7.40)	
Perfusion times (expressed by mean ± SD)			
Wash in time/s	18.12 ± 7.15	15.34 ± 7.23	=0.07
Wash out time/s	151.48 ± 34.62	104.26 ± 39.67	<0.001
REAL-TIME ELASTOGRAPHY—LYMPH NODE STIFFNESS ASSESSED BY ELASTICITY STIFFNESS SCORES			
Soft (scores 1 and 2)	38(90.47)	6(11.11)	<0.001
Hard (scores 3, 4 and 5)	6(14.28)	48(88.88)	

Legend: SA—short axis; LA—long axis; NA—not applicable; RI—resistivity index; PI—pulsatility index; s—seconds.

3.1. B-Mode Ultrasonography

At greyscale US, the S/L axis ratio value >0.55 was the most significant predictive sign for the presence of metastases in the SLNs (Figure 1), having a sensitivity of 83.3% and a specificity of 78.6%.

The mean S/L ratio was lower in the unaffected SLNs (0.50 ± 0.09), compared to the metastatic ones (0.65 ± 0.13) with $p < 0.001$. The same characteristic was maintained in terms of the mean value of the short axis—0.67 ± 0.26 in unaffected SLNs, versus 1.17 ± 0.53 in metastatic SLNs, respectively 1.33 ± 0.46 mean value of the long axis in unaffected SLNs versus 1.83 ± 0.79 in metastatic SLNs.

The homogeneity in the unaffected SLNs was obvious (Figure 1a,b), compared to the inhomogeneous metastatic lymph nodes, ($p < 0.001$) (Figure 1c,d). There was no statistically significant

difference between the echogenicity of the two categories of SLNs. The majority of the unaffected SLNs were hypoechoic (66.6%) or isoechoic (23.8%), features which were found in the metastatic SLNs too, rated as hypoechoic (68.51%) or isoechoic (25.92%), $p = 0.81$. The hyperechoic pattern was found in 9.52% of the unaffected SLNs and 5.55% of the metastatic SLNs.

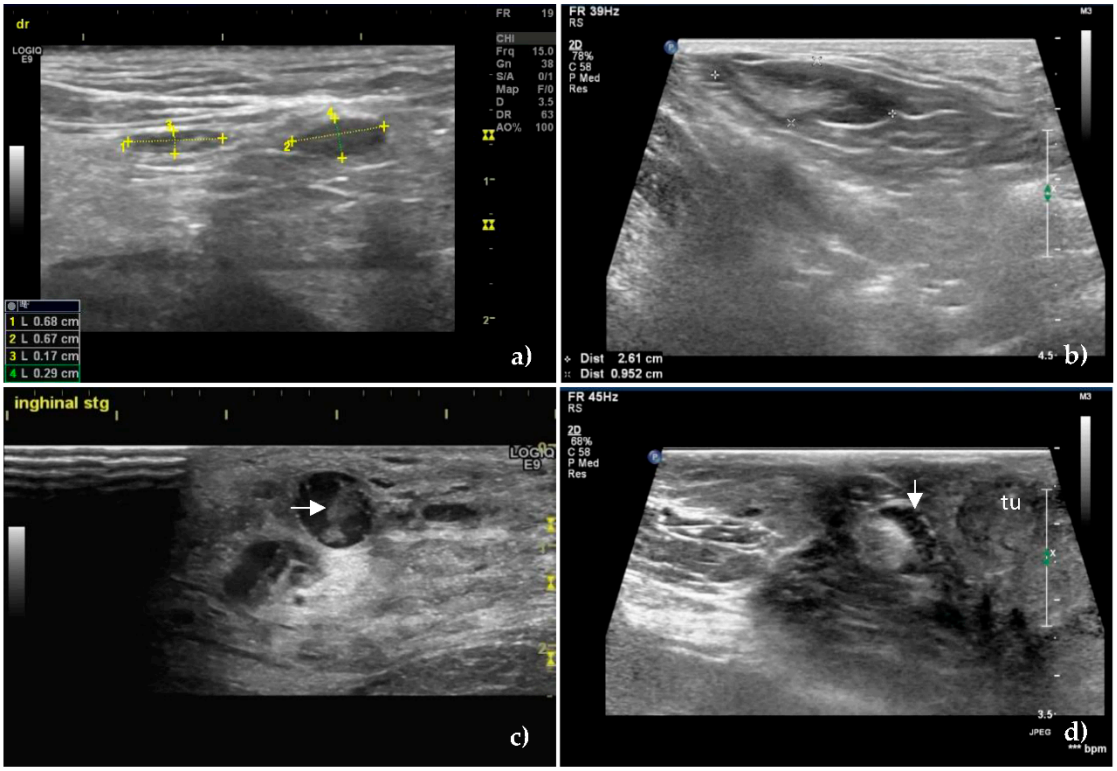

Figure 1. B-mode ultrasound images of unaffected (**a**,**b**) and metastatic, (**c**,**d**) sentinel lymph nodes. Oval shape, S/L ratio less than 0.5, homogeneous echostructure and hyperechoic hilum of unaffected superficial inguinal sentinel lymph nodes in (**a**) and axillary sentinel lymph node in (**b**). The numbers in the image and the lower left corner of Figure 1a represent the long axis (1 and 2) and short axis (3 and 4) measurements of the examined SLNs. The distance between the two "+"signs in Figure 1b represents the measurement of the long axis, and the distance between the two "×" signs represents the measurement of the short axis of SLN. The values are found in the lower left corner of Figure 1b. (**c**) Metastatic superficial inguinal sentinel lymph node showing rounded shape, hypoechoic pattern, and inhomogeneous echostructure with coagulation necrosis inside of lymph node (horizontal arrow) as an echogenic structure which leaves no shadows. (**d**) Cortical thickening of a metastatic superficial inguinal sentinel lymph node (down arrow) located near a tumor—tu.

Hilum was visualized in 71.48% of unaffected SLNs and most of the metastatic SLNs—53.70%. There was no significant difference between the two categories, $p = 0.07$, related to the visualization of the hilum.

Regarding the delimitation given by the lymph nodes capsule, no statistical difference was noted between the two categories of SLNs, $p = 0.057$, both unaffected (88.09%) and metastatic lymph nodes (72.22%) having a well-defined capsule.

However, a difference was noted regarding the appearance of the margins in the sense that the metastatic infiltrated SLNs had irregular and blurred margins compared to the smooth, sharp appearance in unaffected SLNs.

3.2. Color Doppler Ultrasonography

The Doppler technique certified the presence of a vascular signal in 40 unaffected SLNs and 53 metastatic SLNs, with different pattern between the groups, $p < 0.001$.

In 85.71% of non-metastatic SLNs, blood vessels started from the hilum and were orderly distributed toward the capsule (Figure 2a,b), whereas in 88.88% of the metastatic SLNs, the vascularization had a disordered, chaotic appearance, with predominantly peripherally location (55.55%) or mixed (20.37%) (Figure 2c,d). 12 metastatic SLNs had a perfused hilar region.

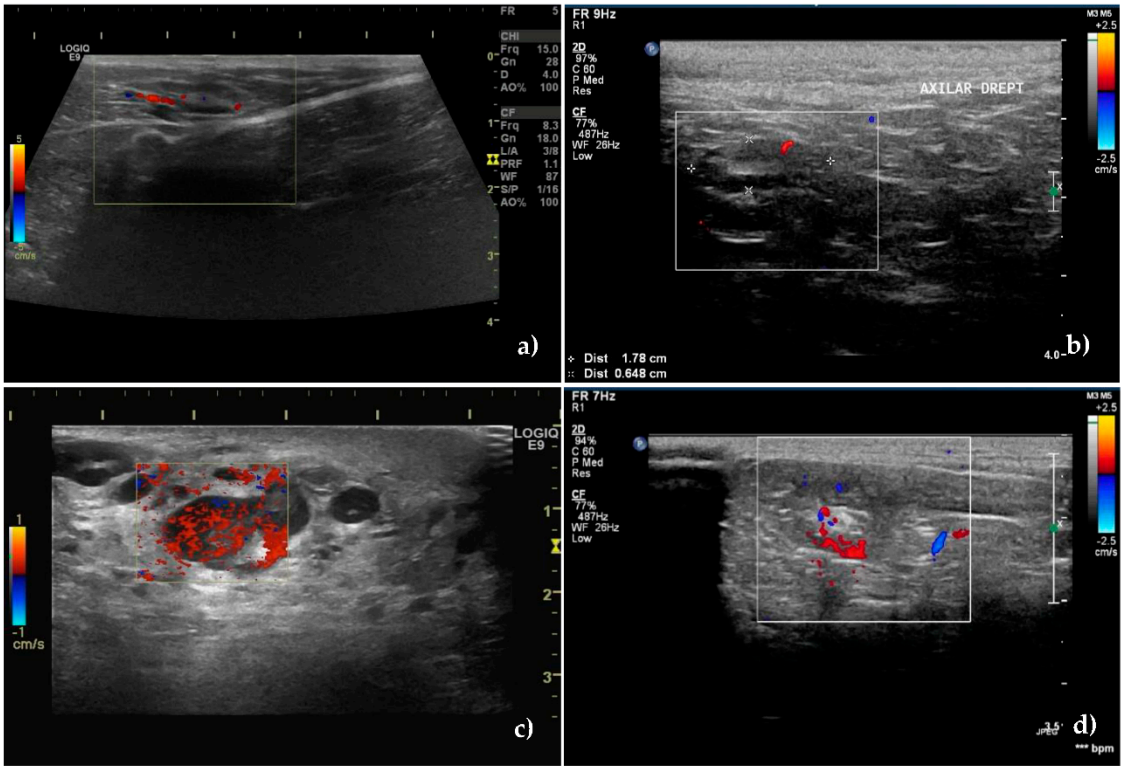

Figure 2. Vessels location and distribution assessed by Color Doppler ultrasound. (**a**) Central, hilar vessels of unaffected superficial inguinal sentinel lymph node and (**b**) unaffected axillary sentinel lymph node. (**c**) Presence of neovascularisation with an abnormal, hilar, and peripheral distribution of vessels in a metastatic superficial inguinal sentinel lymph node. (**d**) Mixed hilar and peripheral pattern with the parenchymal subcapsular location of vessels in a metastatic axillary sentinel lymph node.

Regarding the intranodal vascular resistance, the mean values of the resistivity index (RI), were lower in the unaffected nodes: 0.50 ± 0.14 vs. 0.70 ± 0.13 in the metastatic SLNs ($p < 0.001$).

The same trend was also recorded for the pulsatility index (PI). Its mean value was lower in the unaffected nodes 0.98 ± 0.22 compared to 1.24 ± 0.25 in the metastatic ones.

According to the ROC analysis, the cutoff value obtained for lymph node differentiation, for RI was 0.56 and for PI was 1.02 with 83% SE and 75% SP for RI and 83% SE respectively a 65% SP for PI (Figure 3b).

The accuracy of the two methods was 80% for RI and 75.14% for PI.

Considering above mentioned analyses, S/L ratio and RI were the best discriminators of the two categories of lymph nodes (Figure 3a,b).

3.3. Contrast-Enhanced Ultrasonography

After peritumoral injection of SonoVue, the lymphatic vessels were identified as hyperechoic and well-defined linear structures Initially, the route of the lymphatic vessels was superficial, then became deeper close to the SLNs (Figure 4).

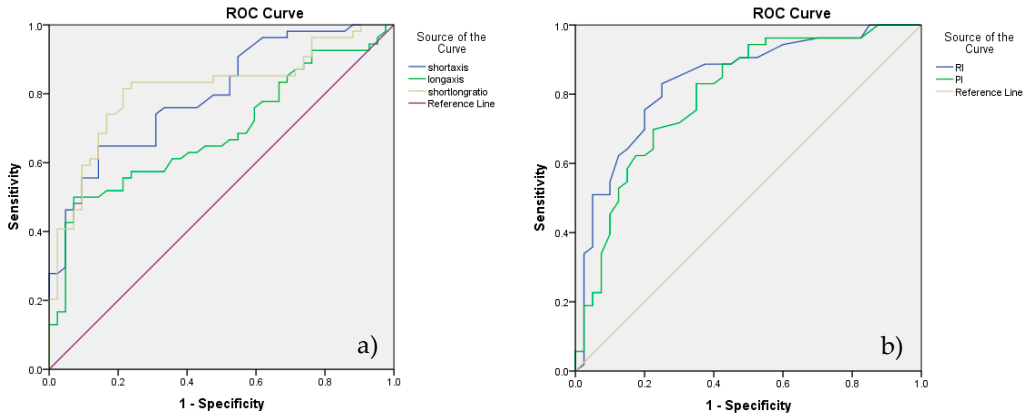

Figure 3. ROC analysis assessing the diagnostic accuracy of B-mode parameters—short axis, long axis, and short/long ratio in (**a**) and Doppler parameters—resistivity index (RI) and pulsatility index (PI) in (**b**).

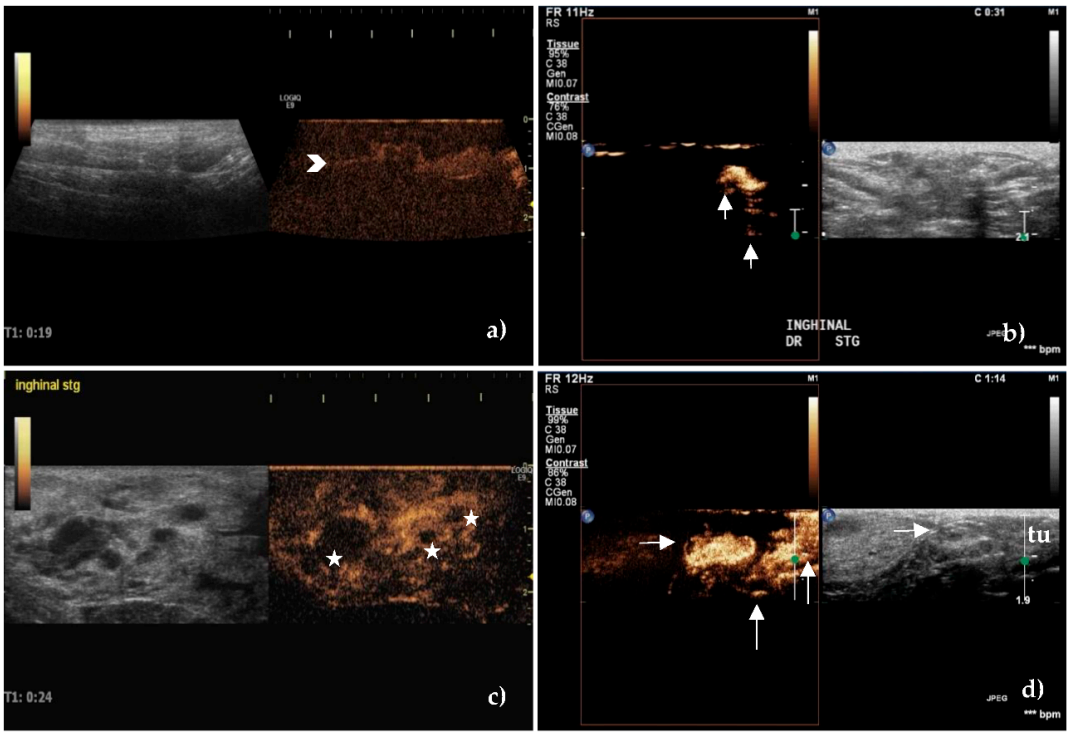

Figure 4. Contrast-enhanced ultrasound of sentinel lymph nodes after peritumoral administration of contrast agent. (**a**) Complete, homogeneous enhancement of an unaffected axillary sentinel lymph node with an evident hyperechoic lymphatic vessel—chevron arrow. (**b**) Intense enhancement of an unaffected superficial inguinal sentinel lymph node. Note the lymphatic vessels that bypass the lymph node leading to the next lymph node station—vertical arrows. (**c**) Inhomogeneous enhancement of a metastatic superficial inguinal sentinel lymph node. Areas with enhancement defects are present—stars. (**d**) The focal cortical area with no enhancement—horizontal arrow, of a metastatic superficial inguinal sentinel lymph node located in the vicinity of a tumor (tu) of the inguinal mammary gland. Note the multiple afferent lymphatic channels as hyperechoic linear structures that approach the lymph node and the contrast agent that was injected peritumorally—vertical arrows.

Three types of lymph node enhancement have been established: 1. intense or moderate but homogeneous enhancement without areas with no contrast; 2. inhomogeneous or partially inhomogeneous with the presence of areas without contrast, either peripherally or centrally, and 3. no enhancement.

The enhancement patterns were quantified as intense, centripetal, homogeneous, without enhancement defects in most unaffected SLNs (76.19%), belonging to type 1, (Figure 4a,b) compared to the inhomogeneous pattern (81.48%), with the presence of areas with no contrast in the metastatic ones ($p < 0.001$), belonging to type 2 (Figure 4c,d).

There was no enhancement in 4 female dogs (4 lymph nodes belonging to the axillary lymph center and 2 lymph nodes belonging to the superficial inguinal lymph center) belonging to type 3.

Considering that type 1 is found in unaffected and type 2 and 3 in metastatic SLNs, we obtained a sensitivity of 88.89%, a specificity of 76.19% with PPV 82.76%, NPV 84.21%, and good accuracy of 83.33%.

Regarding the contrast transit times, the mean values of the wash-in time of 18.12 ± 7.15 (s) in unaffected SLNs was not statistically different from the metastatic ones, 15.34 ± 7.23 ($p = 0.07$), having 64% SE and low SP of 59%, with PPV 68.15%, NPV 57.07%, and 62.92% accuracy. The established cutoff value was 17.5 s.

The shorter and more marked wash-out time of 104.26 ± 39.67 (s) in the metastatic SLNs, compared to 151.48 ± 34.62, in unaffected SLNs, ($p < 0.001$), was a better predictor of metastatic infiltration. If a cutoff value of 133 s for wash-out time determined by ROC analysis was considered, the SE and SP were 84% and 74.36%, respectively, with PPV 80.81% and NPV of 78.33% and 79.78% accuracy.

Enhancement patterns and contrast transit times are presented in Table 3.

3.4. Real-Time Elastography

Using the score proposed by Alam et al. [49], which quantified the relative proportion of the areas with low deformability (or high rigidity), a cutoff value between scores 2 and 3 was established.

Among metastatic SLNs, 88.9% were classified in scores 3, 4, or 5 (hard). These scores were recorded in only 9.5% of the unaffected SLNs. Scores 1 and 2 were recorded in 90.5% of unaffected SLNs (Figure 5a,b) and in 11.1% of metastatic SLNs, ($p < 0.001$) (Figure 5c,d).

The classification of SLNs in a certain score is presented in Table 4. Stiffness was significantly higher in metastatic SLNs compared to the unaffected ones (Figure 5) having a very good SE, SP, PPV, NPV, and accuracy to identify the metastatic lymph nodes, of 88.9%, 90.5%, 89.69%, 86.36%, and 89.71%.

Table 4. Lymph node characterization according to the elasticity score.

Lymph Nodes	1	2	3	4	5
Unaffected (N = 42)	25 (59.5)	13 (31.0)	3 (7.1)	-	1 (2.4)
Metastatic (N = 54)	2 (3.7)	4 (7.4)	14 (25.9)	19 (35.2)	15 (27.8)
p value			<0.001		

Note—number in parenthesis are percentages.

Considering the above mentioned analysis of CEUS, wash-out time was a better discriminator of the two categories of SLNs—Figure 6a. ROC analysis assessing the diagnostic accuracy of significant parameters of B-mode, Doppler technique, CEUS and real-time elastography is presented in Figure 6b.

The diagnostic performance of grayscale US, color Doppler, CEUS, and elastography is summarized in Table 5.

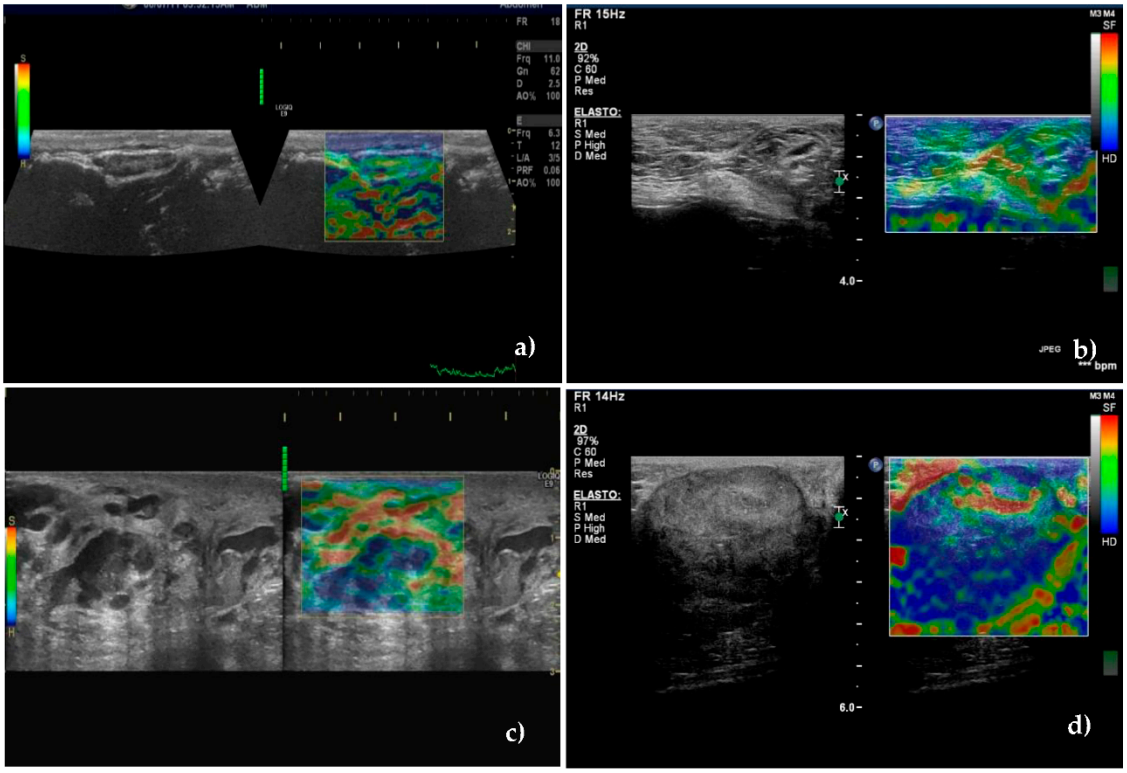

Figure 5. Sonoelastographic images of unaffected—(**a**,**b**)—and metastatic—(**c**,**d**)—sentinel lymph nodes. (**a**) Unaffected axillary sentinel lymph node showing soft appearance—total green with small blue areas corresponding to score of 1. (**b**) Moderately soft superficial inguinal sentinel lymph node with small scattered blue areas corresponding to score of 2. (**c**) Most of the superficial inguinal lymph node is blue with small green areas inside suggesting necrosis, corresponding to score of 4. (**d**) Hard-blue area occupying entire lymph node, with green rim corresponding to score of 5.

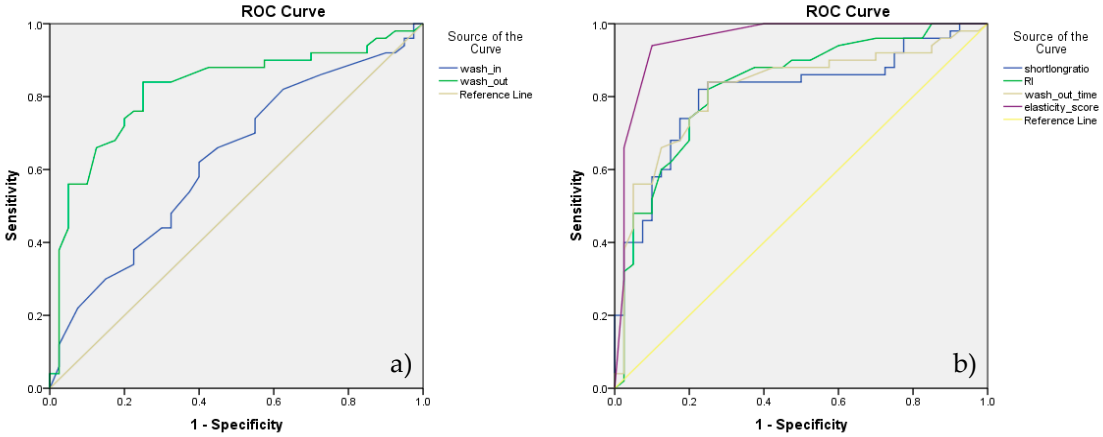

Figure 6. (**a**) ROC analysis assessing the diagnostic accuracy of contrast-enhanced ultrasound (CEUS) parameters, wash-in time and wash-out time; (**b**) ROC analysis assessing the diagnostic accuracy of significant parameters of the four techniques—B-mode, Doppler, CEUS, and elastography.

According to our results, the highest diagnostic accuracy for prediction SLNs metastases was given by the elasticity score (89.71%) followed by the S/L ratio (81.25%) and RI (80.0). The statistical significance of the AUC was preestablished according to the following qualification: 0.500–0.600—improper, failure; 0.600–0.700—poor, weak; 0.700–0.800—fair; 0.800–0.900—good; 0.900–1—excellent.

Combining the most significant parameters, namely short/long ratio, resistivity index, wash-out time and elasticity score, we obtained the best diagnostic performance with 92.27% accuracy, 94% SE and 90% SP.

Considering previous reports [48,51] and based on our results obtained by ultrasonographic examination and their correlation with the histopathological examination, we developed a US examination algorithm using the significant parameters of the four techniques—grayscale US, color Doppler, CEUS, and elastography. Each parameter receives a 0 or 1 score depending on its significance. Thus, the classification of SLNs in one of the two categories, unaffected or metastatic, was appreciated. The data is presented in Table 6.

Table 5. ROC analysis. Diagnostic performance of significant parameters of gray-sale US, Doppler US, CEUS, and sonoelastography in the detection of metastatic lymph nodes.

Criterion	AUC	SE (%)	SP (%)	Statistical Sig.	Cutoff Value	CI 95%	PPV (%)	NPV (%)	Acc (%)
S/L Ratio	0.812	83.3	78.6	Good	0.550	0.724–0.899	83.33	78.57	81.25
L axis	0.689	50.0	92.9	Poor	1.860	0.583–0.794	90.00	59.09	68.75
S axis	0.798	64.8	85.7	Fair	0.854	0.711–0.885	85.37	65.45	73.96
RI	0.837	83.0	75.0	Good	0.565	0.753–0.921	81.02	77.45	80.00
PI	0.798	83.0	65.0	Fair	1.025	0.705–0.891	75.31	74.86	75.14
WOT (s)	0.818	84.0	74.4	Good	133.0	0.727–0.910	80.81	78.33	79.78
ES	0.928	88.9	90.5	Excellent	2.5	0.871–0.986	89.69	86.36	89.71

Legend: AUC—area under the curve; SE—sensitivity; SP—specificity; PPV—positive predictive value; NPV—negative predictive value; Acc—accuracy; RI—resistivity index; PI—pulsatility index; WOT—wash-out time; ES—elasticity score.

Table 6. Proposed algorithm for differentiating between unaffected and metastatic sentinel lymph nodes using available ultrasound techniques—grayscale US, Doppler, CEUS and elastography.

	US Parameter	Pattern	Score
		Gray scale ultrasound	
1.	S/L ratio	<0.55	0
		≥0.55	1
2.	Echostructure	Homogeneous	0
		Inhomogeneous	1
		Doppler ultrasound	
3.	Localization	Hilar	0
		Peripheral	1
4.	Type and distribution	Ordered	0
		Chaotic	1
5.	RI	<0.54	0
		≥0.54	1
6.	PI	<0.83	0
		≥0.83	1
Score < 3—unaffected lymph node; Score = 3 CEUS and elastography should be performed; Score ≥ 3 metastatic lymph node should be taken into account			
		CEUS	
1.	Enhancement pattern	Intense, homogeneous	0
		Inhomogeneous ± no enhanced areas	1
2.	Wash-out time (s) peritumoral ad.	>133	0
		≤133	1
		Strain elastography	
3.	Stiffness	Soft or moderately soft (scores 1 and 2)	0
		Predominantly/moderately stiff or stiff (scores 3,4,5)	1

Considering CEUS and elastography: Score ≤ 1—unaffected lymph node; Score ≥ 2—malignant lymph node. Considering all significant US parameters: score = 3—unaffected lymph node: score ≥ 4—malignant lymph node. Legend: S—short axis; L—long axis; RI—resistivity index; PI—pulsatility index.

3.5. Lymphatic Mapping

After peritumoral injection of Evans Blue Dye, the identification rate of SLNs was 98.5% (70/71 subjects) average of 1,3 SLN/subject.

Out of 70 subjects, in 46 (65.71%) a single SLN was identified and in 24 subjects (34.28%) mammary tumor drainage was performed by 2 SLNs. In 8 subjects (11.28%) presenting A1, A2, and I tumors, the drainage was made both cranially (by proper axillary lymph node—5 subjects- or accessory axillary lymph node—3 subjects) and caudally (by the superficial inguinal lymph nodes)—in all subjects. In 2 subjects with T1 mammary gland tumor, a lymphatic vessel was identified which branched off, giving off an obvious lymphatic vessel which drained into the proper axillary lymph node and another lymphatic vessel bypassing the proper axillary lymph node to drain into the cranial sternal lymph node. The cranial sternal lymph node was considered also SLN.

The drainage pattern of each subject is presented in Supplementary file 1.

4. Discussion

The clinical applicability of US is fully recognized in the primary assessment of superficial drainage within a well-defined territory. Based on the hypothesis that the sum of available US methods can differentiate between unaffected and metastatic SLNs, our research analyzes and describes the normal and pathological aspects of draining lymph nodes of mammary carcinomas in female dogs.

In current practice, the surgical therapeutic approach by local mastectomy or excision of the whole unilateral mammary chain is accompanied by ipsilateral lymphadenectomy, if SLNs are identified intraoperatively [52–54]. As in breast cancer in women, the appearance of metastases in the lymph nodes correctly stages cancer, guides treatment, prognosis, and evolution [2–4,53–55]. There is debate about the influence of the lymph nodes metastatic burden on the histologic malignancy grade, prognosis, and disease-free survival time of both women and bitches [3,54]. Micrometastases (MICs) and isolated tumor cells (ITCs) detected by immunohistochemistry (IHC) are the subject of recent studies [4,55], but their influence on cancer evolution has not yet been clearly established, but there is a chance that in the absence of IHC these MIC and ITCs will not be detected [55].

Although it has been stated that there are no differences between the evolution of cases with negative lymph nodes and those in which the presence of MIC or ITCs was determined by IHC [3], future studies are needed to evaluate lymph nodes from this point of view. At the same time, the existence of correlations between the presence of MIC and ITCs and the ultrasonographic patterns must be appreciated. Excision of sentinel lymph nodes draining the tumoral mammary glands, without a prior evaluation, is unjustified from two perspectives. The first reason is that an SLN must be certified as a certain drainer of the tumor. Secondly, the excision of a benign SLN deprives a relatively large territory of lymphatic drainage, which also drains other structures, leading to the well-known secondary effects. These effects are encountered in both humans and animals: limb lymphedema, pain, diminished peripheral nerve sensitivity and reducing the local defense capacity [13,55,56]. That is why, through this study, we tried to avoid inguinal or axillary clearance and we created an evaluation algorithm using the simplest and most available ultrasound methods.

4.1. B-Mode Ultrasonography

It has been shown that on the grayscale US the S/L ratio is an important criterion for differentiating the categories of SLNs in both humans and animals [18,28,41,57,58].

The higher observed ratio in the malignant SLNs is due to the tumoral infiltration that causes a change in shape (the lymph node tends to be rounded), effect quantified by calculating this ratio [57,59]. Likewise, the local and regional inflammatory processes cause a clear rounding of the lymph nodes that drains the affected territory [30]. Compared to the metastatic lymph nodes, (whose modification is most often unilateral), depending on the path of the related lymphatic pathway that carries the malignant cells, enlargement of inflammatory lymph nodes, is uniform.

A similar feature regarding the uniformly-rounded shape of malignant lymph nodes is found in lymphomas, frequently diagnosed in dogs [17,18,28,58,60,61]. Most animal studies report statistically significant S/L ratio values, without specifying SE and SP values in discriminating lymph node categories.

In our study, the cutoff value of the S/L ratio obtained on the ROC analysis was 0.55 having 83.3% SE and 78.6% SP, these values being found in other reports too. Cited sources reported a SE of 48.8–87.1, 86.7, 86.8, 93% [28,48,62,63] and 55.6–97.3, 67.2, 72.5, 53% SP. In our study, the S/L ratio presented a good accuracy of 81.25% for the identification of metastatic SLNs.

In a recent study, Silva et al., (2018), [30] showed that the S/L ratio has a moderate discriminative power of around 60% in differentiating the altered lymph nodes. Mean values of this ratio calculated in free, altered, and metastatic lymph nodes, were non-specific and lower in comparison with other studies, namely 0.38, 0.37, and 0.34 for axillary lymph nodes and 0.47, 0.49 and 0.53 for superficial inguinal lymph nodes. The mean values of the S/L ratio in our study, 0.50 for unaffected SLNs and 0.65 for metastatic SLNs, were higher compared with the above-mentioned study.

Considering the clinical anatomy, there are significant differences between the shape of the normal lymph nodes depending on the topography and the lymphatic drainage basin which they serve, e.g., mesenteric lymph nodes in dogs are more elongated than medial iliac lymph nodes; superficial cervical lymph nodes and medial retropharyngeal lymph nodes have a much more fusiform appearance compared to the proper axillary lymph nodes or submandibular lymph nodes; benign parotid lymph nodes are more rounded than superficial cervical lymph nodes; the shape of popliteal lymph nodes is generally rounded [17,41,42,58,59,64,65]. Under these conditions, the S/L ratio must be combined with other techniques for a certain SLN classification.

The size of the lymph nodes established by measuring the two axes is not a relevant criterion for the differentiation of the metastatic lymph nodes. In most studies, the measurements of the two axes are related to the ratio calculation. Standard assessments cannot be made, either on deep lymph nodes or superficial lymph nodes, as long as the size of the lymph nodes is bodyweight, breed, body mass index, age or sagittal and longitudinal thoracic diameters- dependent [59,64,65] and the presence or absence of associated pathology. Certain studies report the average values established for the submandibular, medial retropharyngeal, cervical superficial, proper axillary, and superficial inguinal, normal lymph nodes, ranging from 1.35, 1.9, 1.48, 1.57, 1.79 cm for the longitudinal axis, 1.00, 0.98, 0.85, 0.81, 0.68 cm for the transverse axis and 0.41, 0.55, 0.41, 0.65, 0.31 cm for the sagittal axis [59,64,65].

In pathological cases, these values increase significantly, reaching up to 2.61–5.5 cm for the longitudinal axis and 1.15–2.8 cm for the transverse axis [17,28] being comparable to the average values recorded in our study, respectively 1.33 cm for LA and 0.67 cm for SA in unaffected SLNs and 1.83 cm for LA and 1.17 cm for SA in metastatic SLNs.

The fact that SA had better accuracy (73.96%) compared to LA (68.75%) has an anatomical explanation. First of all, normal afferent or potential vessels that carry the malignant cells, approach the node on the capsular level, causing SA growth in the first phase. Secondly, the arrangement of the superficial lymph nodes is, either in the subcutaneous cellular tissue or in the intermuscular spaces with the long axis oriented towards the lymphatic drainage, which relatively limits the expansion of LA.

Another aspect related to the variability of lymph node size is age-dependent, with an inverse correlation between age and size [66–68]. This is due to the immunosenescence and atrophy of the lymph nodes based on the specific degenerative changes responsible for the altered immune response and an increased rate of cancers in old ages.

Under these conditions, the shape and size of the lymph nodes cannot be used as a unique criterion for differentiation. In contrast, their size may provide important data for monitoring treatment response, especially in lymphoma, by significantly decreasing the LA value [69].

In our study, the SLNs margins or capsule was not a significant criterion for differentiating the two categories, similar to other reports [17,30,42] in animals, but different from reports of sentinel

lymph nodes margins in humans [48,70]. The majority of both unaffected (88/09%) and metastatic (72.22%) SLNs in our study, were well delimited to surrounding tissue. The sharp appearance of most of the capsules in the metastatic SLNs, is due to capsule and nodal parenchyma infiltration with tumor cells (that causes an increase in acoustic impedance difference between the inside and the surrounding tissue [42,71,72]).

The reports regarding the appearance of the lymph node capsule are very heterogeneous. Some stated that both, benign lymph nodes and malignant ones have irregular contour but well-defined margins [28] but most of the malignant nodes were diagnosed with lymphoma and a small number were represented by metastasis of local tumors. On the other hand, studying cervical lymph nodes in healthy dogs, it has been shown that benign lymph nodes can have both irregular and smooth margins [65].

The internal structural features of the SLNs examined in our study are consistent with studies that evaluated superficial or profound normal or pathological lymph nodes in animals and humans. It has been proved that homogeneity is a specific feature of benign lymph nodes, compared to the inhomogeneous appearance of malignant lymph nodes [18,41,48,73,74]. Focal cortical nodules, intranodal necrosis, calcifications are responsible for the inhomogeneous appearance of the malignant lymph nodes [41]. These structural changes are obvious in superficial SLNs, compared to the deep ones, where these changes may be influenced by certain artifacts or by the difficulty of the examination.

In contrast, other studies have reported that these two characteristics (homogeneity and inhomogeneity) are not always associated with the presence of metastases in lymph nodes. Cited sources state that the categories of sentinel lymph nodes cannot be differentiated considering only this criterion [30] as long as the lymphomatous nodes are homogeneous similar to the benign ones [17,42]. These studies differ from the present one, both in the variety of lymph nodes evaluated (submandibular, superficial cervical, popliteal, medial iliac, mesenteric, hepatic, or even cranial sternal and cranial mediastinal) as well as the variety of disorders that have determined the lymph node structural changes.

The lack of significant difference in the echogenicity of the malignant lymph nodes compared to the unaffected sentinel lymph nodes from our study is similar to other reports regarding this criterion [17,28,65]. Although in humans, the hypoechoic pattern of the lymph nodes is commonly associated with malignancy [41,48,72], in animals, most of the lymph nodes have hypoechoic or isoechoic appearance, while the hyperechoic pattern is found in both malignant and benign lymph nodes.

In our study, the hypoechoic pattern was more prevalent compared to isoechoic or hyperechoic appearance. It should be specified that the echogenicity of a lymph node is not necessarily related to its homogeneity as long as the heterogeneous lymph nodes can be cataloged in some circumstances as hypoechoic [18,19]. Furthermore, the lymph node cortex that contains few sinuses in a connective tissue network is responsible for the hypoechoic pattern of the lymph nodes, because the interfaces are few and the reflection is poor. A hypoechoic cortex (>3 mm in size) is considered to have metastatic infiltration in both animals and humans [54,75]. However, attention must be paid to this criterion because for the measurement it is necessary the presence of a hilum and on the other hand in animals, the size of the lymph nodes is dependent on breed and condition. Therefore, malignant lymph nodes may appear hypoechoic and homogeneous or heterogeneous/inhomogeneous, as cited for some mammary tumors, the heterogeneity being produced by the clusters of malignant cells on conjunctive support [43,44,50,52]. Intranodal necrosis is generally heterogeneous, depending on the stage of necrosis, being seen as coagulation or liquefaction necrosis [41,71].

On the other hand, the echogenicity is debatable, as long as different locations of the lymph nodes induce different appreciations. For example, the medial retropharyngeal lymph node (located caudally to the digastric muscle, ventrally to the long muscle of the neck, covered by the sternocephalic muscle and the mastoid end of the brachiocephalic muscle) may appear hyperechoic in relation to the above-mentioned muscles or isoechoic to the deeper adjacent portion of the salivary gland [65]. The proper axillary lymph nodes examined after pulling the anterior limb extended forward may appear hyperechoic if we refer to the large round muscle insertion, or slightly hypoechoic if we refer to

the subscapular and axillary veins [20]. The accessories axillary lymph nodes are hyperechoic if we compare them to the dorsal edge of the ascending pectoral muscle. The most important conclusion from the comparisons of the echogenicity is that this cannot be considered a reliable parameter for differentiation of the metastatic from the benign or unaffected lymph nodes.

The hilum was visualized in the majority of SLNs, both unaffected (71.48%) and metastatic (53.70%), as previously has been reported in animals [17,19,28]. Not the same conclusions were recorded in certain studies related to the SLNs that drain the female breast cancer [70,75,76] or in different neoplasms in animals [18,42,51] that associated the presence of metastases with the lack of hilum echogenicity. The metastatic infiltration of the hilum occurs in the relatively late stages of metastatic dissemination, in which the echogenic structures represented by multiple medullary sinuses, are replaced by the tumor cells, reducing the reflectivity of the interfaces [41,71,77]. The presence of a thin, effaced hilum associated with cortical focal hypoechogenicity raises the suspicion of metastatic infiltration [51]. It is also considered that ischemic degeneration at the level of the hilum may be a consequence of its visualization as a thin, hyperechoic structure [19,78] an aspect also encountered in this study. In these conditions, on the grayscale US, the presence or absence of hilum is not reliable enough in differentiating between metastatic and benign lymph nodes.

4.2. Color Doppler Ultrasonography

The evaluation of lymph node vascularization by the Doppler technique offers a very good appreciation of their status, many authors suggesting the possibility of differentiation the metastatic from the benign or unaffected lymph nodes, both in humans and animals [41,42,51,58,71,79]. It has been stated that with respect to the histopathological examination, Doppler US is capable to detect and evaluate with great accuracy the blood flow in superficial lymph nodes [58].

In the present study, we defined the presence of the Doppler signal in three locations: hilar, peripheral, and mixed. The absence of the vascular signal was recorded in 3 SLNs. The absence of the Doppler signal can be recorded in the benign or unaffected lymph nodes of small size. In these nodes, the small vessels contain a small number of red blood cells at one time, which leads to the decrease of the Doppler signal intensity. A similar situation is noted in the metastatic lymph nodes in which the necrosis areas are lacking Doppler signal [71,80,81]. Most unaffected SLNs in the present study showed hilar vascularization (85%), the anatomical place of entry of the lymphatic vessels, but hilar and mixed vascularization was found in the metastatic lymph nodes too. A similar pattern was found in SLNs that drain the breast cancer in women [70,76,82].

The presence of hilar vascularization in metastatic lymph nodes is found in the early stages of metastasis, where the hilar vessels are not yet destroyed by the tumor invasion. The peripheral identification of the Doppler signal in most of the metastatic sentinel lymph nodes in our study is similar to other reports that concluded that this aspect is associated with the presence of metastases in lymph nodes having high specificity and variable sensitivity [19,58,77,83].

Contrary to these claims, evaluating the vascularization of malignant and benign tumors of the mammary glands in bitches, Soler and collaborators (2016) [43] showed that the peripheral distribution of vessels detected by the Doppler technique is significantly different in benign tumors compared to malignant ones. They concluded that this is because initially benign tumors have wider vessels at the periphery of the tumor while malignant tumors in need of increased vascular support show the mixed type of vascular distribution [43]. Tumor cells that first approach the lymph node in the cortical sinuses and then medullary sinuses, by secretion of angiogenic factors, determine angiogenesis and recruitment of peripheral vessels making peripheral identification possible through the Doppler technique [19,41,71,81].

In our study in 88% of the metastatic SLNs, the distribution of vessels had a disordered, chaotic distribution, this pattern being previously reported [48,84]. This feature is determined by the shape changes caused by the invasion of the tumor cells that displace the ordered pathway of the vessels from the hilum to the lymph node parenchyma and, on the other hand, it is the result of the development of

new blood vessels induced by the tumor angiogenic factors which determine anarchic and distorted growth of newly formed arterial vessels [81,83–86].

The analysis of vascular indices revealed their high values in the metastatic lymph nodes, the predictive cutoff values established on the ROC analysis being 0.56 for RI and 1.02 for PI. The increase of these values in the metastatic lymph nodes is a consequence of the compression given by the tumor cells to the parenchyma and the blood vessels causing an increased vascular resistance but also the induction of desmoplasia (fibrous tissue hyperplasia). These events multiply the structural changes leading to a greater increase in the vascular resistance [71,87]. The cutoff values, for RI and PI for which we obtained the best sensitivity and specificity, are lower compared to other values for dogs, namely 0.67 and 1.02 [87] 0.68 and 1.49 [42] 0.69 and 1.49 [28] or in humans 0.7 and 1.4 [71]. The differences are probably because these studies evaluated different lymph nodes, located both superficially and deeply, being considered SLNs in different neoplasms, compared to the uniform group of this study in which the axillary SLNs and superficial inguinal SLNs were evaluated.

To the best of our knowledge, there is no report regarding the vascular indices of SLNs that drained strictly the neoplastic mammary glands in female dogs. In another research regarding the status of draining lymph nodes of neoplastic mammary glands in bitches [30], in addition to grayscale and ARFI Elastography, Doppler examination evaluated only the presence of the vascular signal and its location without determining the RI and PI. Bellota et al. (2019) [28] besides the superficial cervical, submandibular, and popliteal lymph nodes that drained the locoregional tumors, investigated only 1 axillary lymph node and 12 superficial inguinal lymph nodes that drained mammary carcinomas. In our study, we found a good accuracy of 80% for RI in distinguishing between the two categories of lymph nodes.

4.3. Contrast-Enhanced Ultrasonography

Considering that the high density of peritumoral lymphatic vessels is a reliable criterion for predicting the presence of metastases in SLNs [5,85,88] and taking into account that SLN may be other than locoregional lymph nodes [33,34], we injected the contrast agent (SonoVue), peritumorally. In a preliminary study of our team, we administered the contrast agent both intravenously and peritumorally, focusing on the description of the aspects encountered [26]. The cases were few and no relevant statistics were performed.

The peritumoral administration of SonoVue in the present study was considered optimal for the identification of the true lymph node draining the carcinoma in question. In this way, we tried to avoid examining another regional lymph node that does not drain the carcinoma. In this respect, Goldberg and collaborators (2004; 2005) [89,90] showed that by modifying the injection site of AC with only 1 cm, different lymph nodes could be identified as SLNs than those of the tumor in question. On the other hand, the functional anatomy of the region must be considered. Intradermal or subareolar administration of a dye or radioactive tracer certainly identifies a large number of lymphatic vessels, but for the contrast agent to penetrate the lymphatic vessels, higher interstitial pressure than that of the dermis is required [91,92].

We considered that subcutaneous peritumoral administration of CA is justified due to the increased interstitial pressure given by the tumor itself and the tumor-induced lymphangiogenesis which causes an increase in peritumoral lymphatic density. From the injection site, the lymphatic vessels were identified in all subjects as hyperechoic linear structures that led to corresponding SLN. Similar reports were made after intradermal of SonoVue in pigs and women [93–95] or subdermal injection in the dog [10]. The dose of contrast agent that we have used for the peritumoral injection was determined based on previous research of our team [26] and other reports [46,47]. The doses used by reference studies are variable and there is still no protocol regarding this aspect. The learning period of the procedure is relatively short and does not require a large number of cases, and can be successfully performed in the clinic.

In the present study, in six subjects no SLN was enhanced. The explanation could be related to the obstruction of the associated lymphatic vessels by the tumor thrombi or the reduced size of the unaffected non-enhanced SLNs.

In our research we defined 3 types of enhancements: 1. homogeneous, complete, without enhancement defects; 2. inhomogeneous, incomplete, with areas without CA and 3. difficult to quantify/no enhancement as it was previously reported [47,96]. Type 1 was associated with benignity and type 2 and 3 were associated with metastatic infiltration. Other authors [48,95] have defined 4 types of enhancements: 1. uniform, complete; 2. uneven with the presence of areas with high or low enhancement; 3. peripheral complete or incomplete ring enhancement with low or no enhanced areas inside; 4. no enhancement associated with a related lymphatic vessel. Type 1 were considered negative nodes and types 2, 3, and 4 were considered metastatic. In our study, the majority of metastatic SLNs had type 2 enhancement (44 SLNs out of 54 metastatic SLNs), but the inhomogeneous aspect of enhancement was also found in 8 SLNs that were diagnosed as negative on histopathological examination. This may occur due to hyperplasia of the lymphoid follicles, adipose tissue deposits, chronic inflammation, or proliferation of fibrous tissue, leading to the uneven and inhomogeneous distribution of the contrast agent [95,96].

The sensitivity and specificity of 88.89% respectively 76.19%, with PPV of 82.76% and NPV of 84.21% obtained regarding enhancement type, are comparable with another reports [47], in which a SE of 81.8% and SP of 86.2% with PPV 75.0% and NPV of 90.3% was obtained. These results are different from those obtained by Liu and collaborators., (2019), [95] which obtained a high SE of 98.04% and a low SP of 49.23%. According to our results, after the peritumoral injection of the contrast agent and the enhancement type analysis, we obtained a good accuracy of 83.33% in differentiating the categories of SLNs.

Perfusion times analysis returned surprising results in the sense that wash-in time was not different in metastatic vs. unaffected SLNs, ($p = 0.07$). Studies performed in women after IV administration of CA and quantification of perfusion times are very heterogeneous, reporting different SE, SP, PPV and NPV of 59%, 87%, 63%, and 85%, [97] or 92.6%, 76.0%, 80.6%, and 90.5% [98]. Although it was specified that in metastatic SLNs, wash-in time is shorter (<15.90 s) [99] and clear, we did not observe this aspect. Indeed, overall, the wash-in time was faster and shorter in the metastatic SLNs, but there was no statistical difference between the mean values of the two categories (17.35 s in unaffected SLNs vs. 15.12 s in metastatic SLNs).

In contrast, wash-out time was significantly different between unaffected and metastatic SLNs (149.48 s in unaffected SLNs vs. 104.12 s in metastatic SLNs) but our values were higher than other reports, the cutoff value being <133 s compared to <60 s previously established [100] for metastasis. Regarding these results, it should be taken into account that CA was peritumorally injected, under these conditions the longer duration of the perfusion times is explained because migration through the lymphatic pathways lasts longer than the intravenous route. In metastatic SLNs washout time was shorter than in unaffected SLNs, $p < 0.001$, having 84% SE, 74.4% SP, PPV 80.81%, NPV 78.33%, and 79.78% accuracy. However, we consider that these results should be taken into consideration with caution, as large-scale studies are needed to validate this method.

The centripetal enhancement revealed in our study in both unaffected and metastatic lymph nodes is because CA has entered lymph nodes on the related afferent lymphatic pathways, approaching the lymph node at the capsule level, following anatomical pathways. Comparatively, after IV administration, a criterion of differentiation is the centrifugal enhancement in unaffected SLNs and centripetal one in the metastatic SLNs [98,101]. The appearance is of a disorganized type, with areas of unequal vascularization, achieved through several vascular pedicles whose presence is explained by subcapsular neoangiogenesis induced by subcapsular cortical metastases [102]. Regarding the enhancement direction, comparative studies are needed to establish if the administration of the contrast agent should be done both IV and peritumoral.

4.4. Real Time Elastography

Another current ultrasonographic technique applied in our research, real-time elastography, had the highest accuracy—89.71% in SLNs differentiation—obtaining 88.9% SE, 90.5% SP, PPV—89.69%—and NPV—86.36%. The high elasticity score of the metastatic SLNs between the values 2 and 3, of the five-point scoring system, was statistically significant to differentiate between the two categories corroborating other reports [29,103]. It is known that the stiffness of metastatic lymph nodes is much higher compared to adjacent tissue or benign lymph nodes in humans and animals [30,49,104,105] and following the compression exerted by the transducer, their displacement is absent. These findings are correlated with palpable clinical evaluation, in which the metastatic lymph nodes are much harder and well anchored in the adjacent tissue [25].

Elasticity scoring systems are based on color-coded elastograms that allow visual appreciation of the proportion of hard tissue in a lymph node, relative to adjacent structures [29,106,107]. On the other hand, due to its components, the cortical area of a lymph node is slightly harder than the medullary, even in benign lymph nodes [108]. However, metastatic lymph nodes are specifically characterized by increased cortical stiffness [109,110]. This is due to multiple factors, including focal cortical stiffness caused by metastatic cell islands, tumor infiltration associated with desmoplasia, and increased angiogenesis and lymphangiogenesis [107,111,112]. Metastatic lymph nodes with areas of necrosis are less hard than those without necrosis. All these structural changes are qualified in different elasticity scores from four, five, or even eight patterns [49,104,109], each of which establishes cutoff value between scores 2 and 3 or between scores 3 and 4 in an eight-point scoring system. Elasticity scores were initially applied in the evaluation of the superficial cervical lymph nodes, but the same score was adapted to SLNs of mammary glands. Although Seiler and Griffith (2017) [29], using both, a four- and five-point scoring system to discriminate cervical lymphadenopathies, stated that the value of the four-point and the five-point score is similar in differentiating the metastatic from the benign SLNs, we applied the five-point scoring system. We applied Alam's elasticity scoring system because this score also analyses the possibility of the presence of necrotic areas in metastatic SLNs. Compared to the score of Bhatia [104] and compared to other studies [29,106,109], Alam's scoring system [49] had the highest accuracy of 89% with 83% SE, 100% SP, PPV of 100% and NPV of 78%. Even if the accuracy of the method is high in the above-mentioned study, studies in the field in animals are quite heterogeneous, obtaining various SE values of 53–67% to 83%, 85% and values of 75% and 80–83%, 100% for SP [28,30,103]. Moreover, there is no standardized elasticity scoring system for SLNs that drains the mammary glands with tumors in bitches, the score applied by us being extrapolated from the human evaluation. However, in our study, the elasticity stiffness scoring system provided the best results in differentiating the lymph node categories. These results are consistent with a recent study in which using Acoustic Radiation Force Impulse (ARFI) elastography to identify metastases in axillary and inguinal lymph nodes in dogs with mammary tumors, it was shown that ARFI shear wave velocity (SWV) identified with excellent accuracy (around 90%), the presence of metastases in SLNs [30]. In a recent study, using qualitative assessment (4-point elasticity scores) and semi-quantitatively (mean hue histogram and stiffness area ratio) of mandibular lymph nodes in dogs, the authors found 100% SE and 92% SP for hue histogram and 86% SE and 100% SP for stiffness area ratio in malignancy prediction [103].

Share wave elastography is a novel technique that performs absolute measurement of stiffness in kilo-pascal (kPa) units. Recently two-dimensional Shear Wave Elastography (2D SWE) was used to evaluate liver, pancreas, kidney, thyroid, prostate, and submandibular, retropharyngeal, axillary and inguinal lymph nodes in nine Beagle dogs. All lymph nodes were visualized with a uniform color map and constant contour lines on 2D-SWE while SWS (share wave speed) was not significantly different between lymph nodes [113]. All these procedures are still in their experimental use in veterinary medicine, with few studies and special requirements in terms of used software. A limitation of the qualitative elastography used in the present study is that this method is examiner-dependant. We applied this method in our algorithm because the elastography module is incorporated in most

devices used in current practice. The evaluation and assignment of a score can be easily done by practitioners.

4.5. Lymphatic Mapping

SLNs identification after peritumoral injection of the dye provided similar results to other reports that used the dye injections at various locations to identify SLNs in female breast cancer [5,114–116]. The most commonly used identification technique is the association of 99mTc (labeled colloids) with a dye (patent blue, isosulfan blue, or indocyanine green) injected after colloid administration, and detection by scintigraphy, SPECT or using a gamma probe [8,72,117–120].

In recent years, multiple attempts have been made to improve lymphatic migration by developing new small radiocolloids to which is added either the dye or other molecules. These molecules, by binding to macrophage receptors and dendritic cells in lymph nodes, increase the possibility of retaining the identification agents inside of lymph nodes [116,118,121]. In female breast cancer, the use of the fluorescent spectrum emitted by indocyanine green (ICG) detected intraoperatively was most commonly used, with an increased identification rate of over 95% [118,122]. The newer identification technique using superparamagnetic iron oxide (SPIO) and its ability to be identified due to its magnetic properties using a detector, provided slightly higher results of the identification rate of 97.6% compared to the classical identification using radiocolloid and blue dye—96.8% [123,124]. Tracer injection is usually peritumoral or subareolar. Even today, there are debates about the injection site, and whether the same SLNs are identified after administration in different locations.

We administered both the contrast agent and the dye peritumorally because we started from the hypothesis of lymphatic drainage variability in bitch demonstrated by numerous studies [13,33,34]. These studies have shown that mammary glands with tumors drain variably, recognizing as sentinel lymph nodes other lymph nodes that are not known to be characteristic of mammary glands drainage, respectively, cranial sternal lymph nodes, or superficial cervical lymph nodes for cranial mammary glands, and popliteal lymph nodes or medial iliac lymph nodes for the caudal mammary glands. The fact that we encountered in a subject a bypass vessel of the proper axillary lymph node that drained into the cranial sternal lymph node, sustains this statement. On the other hand, different pathways of lymphatic vessels, namely superficial, deep and penetrating lymphatic channels, in both women and bitches are also recognized [33,34,93,114,115,125].

However, at present, it is not possible to specify the route of the lymphatic draining vessels of a mammary gland with a tumor. Basically, a tumor is drained by both the deep and the superficial network. What is known is that peritumoral lymphatic density is increased, either on account of pre-existing vessels or those newly formed by tumor-induced lymphangiogenesis itself [126,127]. Under these conditions, we cannot omit these newly formed vessels that may have a different route than those coming from the lymphatic network of the mammary gland. Lymphatic drainage regardless of a certain territory or organ is uneven and unpredictable [25,35]. We consider that the peritumoral administration of both the dye and the contrast agent is justified to identify the true SLN.

Although this is a relatively large study using four ultrasonographic methods, some limitations can be stated. The first would be related to the small number of evaluated cases; we evaluate the lymph nodes as study units, therefore studies with a higher number of cases are needed. Another limitation could be given by the fact that the images were acquired by the same researcher, but by using two devices in the evaluation we tried to solve this impediment. All procedures were supervised by two experienced practitioners, one in human imaging and one in veterinary imaging. The ultrasonographic methods used in our study were very simple and can be performed by any practitioner who deals with the evaluation and treatment of mammary gland tumors in dogs and does not require a long period of learning. Moreover, the costs associated with performing these techniques are low because current ultrasound devices have incorporated contrast and elastography software. That is why even for the more advanced techniques like CEUS and elastography we used their simplest approaches. Subjectivism can be controlled by combining all the techniques for obtaining a good diagnostic performance.

On the other hand, the methods are not fully standardized in terms of evaluation of lymph nodes that drain mammary gland tumors in the females' dog requiring extensive studies to validate the ultrasonographic algorithm. The differentiation between various pathologies in which sentinel lymph nodes are the first station of metastatic dissemination or independent pathology (lymphoma) should be made. The addition of the quantitative parameters of the CEUS and elastography techniques will lead to a substantial increase in the diagnostic performance of the ultrasonographic evaluation algorithm.

5. Conclusions

The accuracy of a single ultrasound method is not sufficient to diagnose the presence of metastases in the SLNs of mammary glands with tumors. B-mode ultrasonography through S/L ratio and ecostructure guides the diagnosis; the location of the blood vessels, their type, distribution and the resistivity index, examined by the Doppler technique, increase the confidence of the diagnosis; enhancement pattern and wash-out time evaluated by CEUS are high predictors for the presence of metastases and the lymph nodes stiffness evaluated by the elasticity scores, strengthens the diagnostic certainty. All these techniques, available for most of the veterinary practitioners, are easy to perform and the described algorithm helps in staging mammary gland tumors, guiding the appropriate therapeutic approach, thus avoiding the unjustified excision of SLNs.

Results obtained in our study support the use of the four techniques as non-invasive identification and primary assessment of sentinel lymph nodes in help selecting further interventions, determining therapeutic approach and prognosis.

Supplementary Materials: The following are available online at http://www.mdpi.com/2076-2615/10/12/2366/s1. File 1: Demographic characteristics, histological diagnosis of mammary tumor and lymphatic drainage of involved tumoral mammary gland.

Author Contributions: Conceptualization, F.S.; methodology, C.M., A.F.G. and A.R.P.; software and validation A.G.; formal analysis, A.D.; investigation and resources, C.M.; data curation, A.G.; writing—original draft preparation, F.S.; writing—review and editing, F.S.; A.G.; A.F.G.; visualization, I.P., A.R.P. and A.D.; supervision, F.S.; project administration, A.F.G. All authors have read and agreed to the published version of the manuscript.

Funding: This research received no external funding.

Acknowledgments: We would like to thank Robert Purdoiu and Diana Feier for their technical support.

Conflicts of Interest: The authors declare no conflict of interest.

References

1. Abadie, J.; Nguyen, F.; Loussouarn, D.; Peña, L.; Gama, A.; Rieder, N.; Belousov, A.; Bemelmans, I.; Jaillardon, L.; Ibisch, C.; et al. Canine invasive mammary carcinomas as models of human breast cancer. Part 2: Immunophenotypes and prognostic significance. *Breast Cancer Res. Treat.* **2018**, *167*, 459–468. [CrossRef] [PubMed]
2. Nguyen, F.; Peña, L.; Ibisch, C.; Loussouarn, D.; Gama, A.; Rieder, N.; Belousov, A.; Campone, M.; Abadie, J. Canine invasive mammary carcinomas as models of human breast cancer. Part 1: Natural history and prognostic factors. *Breast Cancer Res. Treat.* **2018**, *167*, 635–648. [CrossRef] [PubMed]
3. Coleto, A.F.; Wilson, T.M.; Soares, N.P.; Gundim, L.F.; Castro, I.P.; Guimarães, E.C.; Bandarra, M.B.; Medeiros-Ronchi, A.A. Prognostic value of occult isolated tumour cells within regional lymph nodes of dogs with malignant mammary tumours. *J. Comp. Pathol.* **2018**, *158*, 32–38. [CrossRef] [PubMed]
4. Chocteau, F.; Abadie, J.; Loussouarn, D.; Nguyen, F. Proposal for a histological staging system of mammary carcinomas in dogs and cats. part 1: Canine mammary carcinomas. *Front. Vet. Sci.* **2019**, *6*, 1–12. [CrossRef] [PubMed]
5. Bauer, T.W.; Spitz, F.R.; Callans, L.S.; Alavi, A.; Mick, R.; Weinstein, S.P.; Bedrosian, I.; Fraker, D.L.; Bauer, T.L.; Czerniecki, B.J. Subareolar and peritumoral injection identify similar sentinel nodes for breast cancer. *Ann. Surg. Oncol.* **2002**, *9*, 169–176. [CrossRef] [PubMed]

6. Edwina Doting, M.H.; Annemiek Stiekema, H.M.; de Vries, J.; Lemstra, C.; Hoekstra, H.J.; Vrieling, M.; Rietman, L.; Jager, P.L. Immediate dynamic lymphoscintigraphy delivers no additional value to lymphoscintigraphy 3 hr after tracer injection in sentinel lymph node biopsy in breast cancer patients. *J. Surg. Oncol.* **2007**, *95*, 469–475. [CrossRef] [PubMed]
7. Tuttle, T.M.; Colbert, M.; Christensen, R.; Ose, K.J.; Jones, T.; Wetherille, R.; Friedman, J.; Swenson, K.; McMasters, K.M. Subareolar injection of 99mTc facilitates sentinel iymph node identification. *Ann. Surg. Oncol.* **2002**, *9*, 77–81. [CrossRef]
8. McGregor, A.; Pavri, S.N.; Tsay, C.; Kim, S.; Narayan, D. Use of indocyanine green for sentinel lymph node biopsy: Case series and methods comparison. *Plast. Reconstr. Surg. Glob. Open* **2017**, *5*, 1–4. [CrossRef]
9. Vermersch, C.; Raia-Barjat, T.; Chapelle, C.; Lima, S.; Chauleur, C. Randomized comparison between indocyanine green fluorescence plus 99m technetium and 99m technetium alone methods for sentinel lymph node biopsy in breast cancer. *Sci. Rep.* **2019**, *9*, 1–6. [CrossRef]
10. Favril, S.; Stock, E.; Hernot, S.; Hesta, M.; Polis, I.; Vanderperren, K.; de Rooster, H. Sentinel lymph node mapping by near-infrared fluorescence imaging and contrast-enhanced ultrasound in healthy dogs. *Vet. Comp. Oncol.* **2019**, *17*, 89–98. [CrossRef]
11. Kawase, K.; Gayed, I.W.; Hunt, K.K.; Kuerer, H.M.; Akins, J.; Yi, M.; Grimes, L.; Babiera, G.V.; Ross, M.I.; Feig, B.W.; et al. Use of lymphoscintigraphy defines lymphatic drainage patterns before sentinel lymph node biopsy for breast cancer. *J. Am. Coll. Surg.* **2006**, *203*, 64–72. [CrossRef]
12. Rossi, F.; Körner, M.; Suárez, J.; Carozzi, G.; Meier, V.S.; Roos, M.; Rohrer Bley, C. Computed tomographic-lymphography as a complementary technique for lymph node staging in dogs with malignant tumors of various sites. *Vet. Radiol. Ultrasound* **2018**, *59*, 155–162. [CrossRef] [PubMed]
13. Soultani, C.; Patsikas, M.N.; Karayannopoulou, M.; Jakovljevic, S.; Chryssogonidis, I.; Papazoglou, L.; Papaioannou, N.; Papadopoulou, P.; Pavlidou, K.; Ilia, G.M.; et al. Assessment of sentinel lymph node metastasis in canine mammary gland tumors using computed tomographic indirect lymphography. *Vet. Radiol. Ultrasound* **2017**, *58*, 186–196. [CrossRef] [PubMed]
14. Seiler, S.M.F.; Baumgartner, C.; Hirschberger, J.; Beer, A.J.; Brühschwein, A.; Kreutzmann, N.; Laberke, S.; Wergin, M.C.; Meyer-Lindenberg, A.; Brandl, J.; et al. Comparative oncology: Evaluation of 2-deoxy-2-[18F]. Fluoro-d-glucose (FDG) Positron emission tomography/computed tomography (PET/CT) for the staging of dogs with malignant tumors. *PLoS ONE* **2015**, *10*, 1–15. [CrossRef] [PubMed]
15. Sánchez, D.; Romero, L.; López, S.; Campuzano, M.; Ortega, R.; Morales, A.; Guadarrama, M.; Cesarman-Maus, G.; García-Pérez, O.; Lizano, M. 18F-FDG—PET/CT in canine mammary gland tumors. *Front. Vet. Sci.* **2019**, *6*, 1–10. [CrossRef]
16. Suga, K.; Yuan, Y.; Ogasawara, N.; Okada, M.; Matsunaga, N. Localization of breast sentinel lymph nodes by MR lymphography with a conventional gadolinium contrast agent. *Acta Radiol.* **2003**, *44*, 35–42. [CrossRef]
17. De Swarte, M.; Alexander, K.; Rannou, B.; D'Anjou, M.A.; Blond, L.; Beauchamp, G. Comparison of sonographic features of benign and neoplastic deep lymph nodes in dogs. *Vet. Radiol. Ultrasound* **2011**, *52*, 451–456. [CrossRef]
18. Llabrés-Díaz, F.J. Ultrasonography of the medial iliac lymph nodes in the dog. *Vet. Radiol. Ultrasound* **2004**, *45*, 156–165. [CrossRef]
19. Nyman, H.T.; O'Brien, R.T. The sonographic evaluation of lymph nodes. *Clin. Tech. Small Anim. Pract.* **2007**, *22*, 128–137. [CrossRef]
20. Stan, F.; Gudea, A.; Baba, A.I.; Feier, D.; Badea, R. Correlation between ultrasonographic features and morphological pattern after blue dye injection of normal superficial lymph nodes in carnivores. *Bull. Univ. Agric. Sci. Vet. Med. Cluj Napoca Vet. Med.* **2012**, *69*, 211–219. [CrossRef]
21. Cox, K.; Taylor-Phillips, S.; Sharma, N.; Weeks, J.; Mills, H.; Sever, A.; Lim, A.; Haigh, I.; Hashem, M.; De Silva, T.; et al. Enhanced pre-operative axillary staging using intradermal microbubbles and contrast-enhanced ultrasound to detect and biopsy sentinel lymph nodes in breast cancer: A potential replacement for axillary surgery. *Br. J. Radiol.* **2018**, *91*, 1082. [CrossRef]
22. Mei, M.; Ye, L.; Quan, J.; Huang, P. Contrast-enhanced ultrasound for the differential diagnosis between benign and metastatic superficial lymph nodes: A meta-analysis. *Cancer Manag. Res.* **2018**, *10*, 4987–4997. [CrossRef]

23. Nielsen Moody, A.; Bull, J.; Culpan, A.M.; Munyombwe, T.; Sharma, N.; Whitaker, M.; Wolstenhulme, S. Preoperative sentinel lymph node identification, biopsy and localisation using contrast enhanced ultrasound (CEUS) in patients with breast cancer: A systematic review and meta-analysis. *Clin. Radiol.* **2017**, *72*, 959–971. [CrossRef]
24. Sharma, N.; Cox, K. Axillary nodal staging with contrast-enhanced ultrasound. *Curr. Breast Cancer Rep.* **2017**, *9*, 259–263. [CrossRef]
25. Liptak, J.M.; Boston, S.E. Nonselective lymph node dissection and sentinel lymph node mapping and biopsy. *Vet. Clin. North Am. Small Anim. Pract.* **2019**, *49*, 793–807. [CrossRef]
26. Stan, F.G. Non-invasive assessment of sentinel lymph nodes that drain the tumoral mammary glands in female dog. *Bull. UASVM Vet. Med.* **2016**, *73*, 382–388. [CrossRef]
27. Gelb, H.R.; Freeman, L.J.; Rohleder, J.J.; Snyder, P.W. Feasibility of contrast-enhanced ultrasound-guided biopsy of sentinel lymph nodes in dogs. *Vet. Radiol. Ultrasound* **2010**, *51*, 628–633. [CrossRef]
28. Belotta, A.F.; Gomes, M.C.; Rocha, N.S.; Melchert, A.; Giuffrida, R.; Silva, J.P.; Mamprim, M.J. Sonography and sonoelastography in the detection of malignancy in superficial lymph nodes of dogs. *J. Vet. Intern. Med.* **2019**, *33*, 1403–1413. [CrossRef]
29. Seiler, G.S.; Griffith, E. Comparisons between elastographic stiffness scores for benign versus malignant lymph nodes in dogs and cats. *Vet. Radiol. Ultrasound* **2018**, *59*, 79–88. [CrossRef]
30. Silva, P.; Uscategui, R.A.R.; Maronezi, M.C.; Gasser, B.; Pavan, L.; Gatto, I.R.H.; de Almeida, V.T.; Vicente, W.R.R.; Feliciano, M.A.R. Ultrasonography for lymph nodes metastasis identification in bitches with mammary neoplasms. *Sci. Rep.* **2018**, *8*, 1–8. [CrossRef]
31. Choi, Y.J.; Lee, J.H.; Baek, J.H. Ultrasound elastography for evaluation of cervical lymph nodes. *Ultrasonography* **2015**, *34*, 157–164. [CrossRef]
32. Kim, H.J.; Kim, S.M.; Kim, B.; La Yun, B.; Jang, M.; Ko, Y.; Lee, S.H.; Jeong, H.; Chang, J.M.; Cho, N. Comparison of strain and shear wave elastography for qualitative and quantitative assessment of breast masses in the same population. *Sci. Rep.* **2018**, *8*, 1–11. [CrossRef]
33. Pereira, C.T.; Rahal, S.C.; De Carvalho Balieiro, J.C.; Ribeiro, A.A.C.M. Lymphatic drainage on healthy and neoplasic mammary glands in female dogs: Can it really be altered? *J. Vet. Med. Ser. C Anat. Histol. Embryol.* **2003**, *32*, 282–290. [CrossRef]
34. Patsikas, M.N.; Karayannopoulou, M.; Kaldrymidoy, E.; Papazoglou, L.G.; Papadopoulou, P.L.; Tzegas, S.I.; Tziris, N.E.; Kaitzis, D.G.; Dimitriadis, A.S.; Dessiris, A.K. The lymph drainage of the neoplastic mammary glands in the bitch: A lymphographic study. *J. Vet. Med. Ser. C Anat. Histol. Embryol.* **2006**, *35*, 228–234. [CrossRef]
35. Stan, F. Correlation between subareolar and peritumoral blue dye injection to identify sentinel lymph nodes in canine mammary neoplazia. *Lucr. Ştiinţifice Ser. Med. Vet. Iasi* **2012**, *55*, 125–132.
36. Patsikas, M.N.; Dessiris, A. The lymph drainage of the mammary glands in the bitch: A lymphographic study. Part I: The 1st, 2nd, 4th and 5th mammary glands. *Anat. Histol. Embryol.* **1996**, *25*, 131–138. [CrossRef]
37. Patsikas, M.N.; Dessiris, A. The lymph drainage of the mammary glands in the bitch: a lymphographic study. Part II: The 3rd mammary gland. *Anat. Histol. Embryol.* **1996**, *25*, 139–143. [CrossRef]
38. Rossi, F.; Fina, C.; Stock, E.; Vanderperren, K.; Duchateau, L.; Saunders, J.H. Effect of sedation on contrast-enhanced ultrasonography of the spleen in healthy dogs. *Vet. Radiol. Ultrasound* **2016**, *57*, 276–281. [CrossRef]
39. Stock, E.; Vanderperren, K.; Van der Vekens, E.; Haers, H.; Duchateau, L.; Polis, I.; Hesta, M.; Saunders, J.H. The effect of anesthesia with propofol and sedation with butorphanol on quantitative contrast-enhanced ultrasonography of the healthy feline kidney. *Vet. J.* **2014**, *202*, 637–639. [CrossRef]
40. Du Sert, N.P.; Hurst, V.; Ahluwalia, A.; Alam, S.; Avey, M.T.; Baker, M.; Browne, W.J.; Clark, A.; Cuthill, I.C.; Dirnagl, U.; et al. The arrive guidelines 2.0: Updated guidelines for reporting animal research. *PLoS Biol.* **2020**, *18*, 1–12. [CrossRef]
41. Dudea, S.M.; Lenghel, M.; Botar-Jid, C.; Vasilescu, D.; Duma, M. Ultrasonography of superficial lymph nodes: benign vs. malignant. *Med. Ultrason.* **2012**, *14*, 294–306.
42. Nyman, H.T.; Kristensen, A.T.; Skovgaard, I.M.; McEvoy, F.J. Characterization of normal and abnormal canine superficial lymph nodes using gray-scale b-mode, color flow mapping, power, and spectral doppler ultrasonography: A multivariate study. *Vet. Radiol. Ultrasound* **2005**, *46*, 404–410. [CrossRef] [PubMed]

43. Soler, M.; Dominguez, E.; Lucas, X.; Novellas, R.; Gomes-Coelho, K.V.; Espada, Y.; Agut, A. Comparison between ultrasonographic findings of benign and malignant canine mammary gland tumours using b-mode, colour doppler, power doppler and spectral doppler. *Res. Vet. Sci.* **2016**, *107*, 141–146. [CrossRef]
44. Feliciano, M.A.R.; Uscategui, R.A.R.; Maronezi, M.C.; Simões, A.P.R.; Silva, P.; Gasser, B.; Pavan, L.; Carvalho, C.F.; Canola, J.C.; Vicente, W.R.R. Ultrasonography methods for predicting malignancy in canine mammary tumors. *PLoS ONE* **2017**, *12*, 1–14. [CrossRef]
45. Choi, M.Y.; Lee, J.W.; Jang, K.J. Distinction between benign and malignant causes of cervical, axillary, and inguinal lymphadenopathy: Value of doppler spectral waveform analysis. *Am. J. Roentgenol.* **1995**, *165*, 981–984. [CrossRef]
46. Sever, A.R.; Mills, P.; Jones, S.E.; Mali, W.; Jones, P.A. Sentinel node identification using microbubbles and contrast-enhanced ultrasonography. *Clin. Radiol.* **2012**, *67*, 687–694. [CrossRef]
47. Xie, F.; Zhang, D.; Cheng, L.; Yu, L.; Yang, L.; Tong, F.; Liu, H.; Wang, S.; Wang, S. Intradermal microbubbles and contrast-enhanced ultrasound (CEUS) is a feasible approach for sentinel lymph node identification in early-stage breast cancer. *World J. Surg. Oncol.* **2015**, *13*, 1–8. [CrossRef]
48. Poanta, L.; Serban, O.; Pascu, I.; Pop, S.; Cosgarea, M.; Fodor, D. The place of CEUS in distinguishing benign from malignant cervical lymph nodes: A prospective study. *Med. Ultrason.* **2014**, *16*, 7–14. [CrossRef]
49. Alam, F.; Naito, K.; Horiguchi, J.; Fukuda, H.; Tachikake, T.; Ito, K. Accuracy of sonographic elastography in the differential diagnosis of enlarged cervical lymph nodes: Comparison with conventional b-mode sonography. *Am. J. Roentgenol.* **2008**, *191*, 604–610. [CrossRef]
50. Goldschmidt, M.H.; Peña, L.; Rasotto, R.; Zappulli, V. Classification and grading of canine mammary tumors. *Vet. Pathol.* **2011**, *48*, 117–131. [CrossRef]
51. Vassallo, P.; Edel, G.; Roos, N.; Naguib, A.; Peters, P.E. In-vitro high-resolution ultrasonography of benign and malignant lymph nodes. *Invest. Radiol.* **1993**, 698–705. [CrossRef] [PubMed]
52. Cassali, G.D.; Lavalle, G.E.; de Nardi, A.B.; Ferreira, E.; Bertagnolli, A.C.; Estrela-Lima, A.; Alessi, A.C.; Daleck, C.R.; Salgado, B.S.; Fernandes, C.G.; et al. Consensus for the diagnosis, prognosis and treatment of canine mammary tumors. *Braz. J. Vet. Pathol.* **2011**, *4*, 153–180.
53. Karin, U.; Sorenmo, D.R.; Worley, M.H.G. Tumors of the mammary gland. In *Small Animal Clinical Oncology*; Stephen, J., Withrow, D.M., Vail, R.L.P., Eds.; Saunders Company: Philadelphia, PA, USA, 2013; pp. 538–556.
54. De Araújo, M.R.; Campos, L.C.; Ferreira, E.; Cassali, G.D. Quantitation of the regional lymph node metastatic burden and prognosis in malignant mammary tumors of dogs. *J. Vet. Intern. Med.* **2015**, *29*, 1360–1367. [CrossRef] [PubMed]
55. Beserra, H.E.O.; Grandi, F.; Dufloth, R.M.; Pinheiro, L.G.P.; Miot, H.A.; Vexenat, S.C.O.R.; Rocha, N.S. Metastasis of mammary carcinoma in bitches: Evaluation of the sentinel lymph node technique. *Adv. Breast Cancer Res.* **2016**, *5*, 58–65. [CrossRef]
56. Lorek, A.; Stojčev, Z.; Zarębski, W.; Kowalczyk, M.; Szyluk, K. Analysis of postoperative complications after 303 sentinel lymph node identification procedures using the sentimag®method in breast cancer patients. *Med. Sci. Monit.* **2019**, *25*, 3154–3160. [CrossRef]
57. Luigi Solbiati, V.; Cioffi, E.B. Ultrasonography of the neck. *Radiol. Clin. N. Am.* **1992**, *30*, 941–954.
58. Nyman, H.T.; Nielsen, O.L.; McEvoy, F.J.; Lee, M.H.; Martinussen, T.; Hellmén, E.; Kristensen, A.T. Comparison of b-mode and doppler ultrasonographic findings with histologic features of benign and malignant mammary tumors in dogs. *Am. J. Vet. Res.* **2006**, *67*, 985–991. [CrossRef]
59. Silver, T.I.; Lawson, J.A.; Mayer, M.N. Sonographic characteristics of presumptively normal main axillary and superficial cervical lymph nodes in dogs. *Am. J. Vet. Res.* **2012**, *73*, 1200–1206. [CrossRef]
60. Salwei, R.M.; O'Brien, R.T.; Matheson, J.S. Characterization of lymphomatous lymph nodes in dogs using contrast harmonic and power doppler ultrasound. *Vet. Radiol. Ultrasound* **2005**, *46*, 411–416. [CrossRef]
61. Zandvliet, M. Canine Lymphoma: A Review. *Vet. Q.* **2016**, *36*, 76–104. [CrossRef]
62. Alvarez, S.; Añorbe, E.; Alcorta, P.; López, F.; Alonso, I.; Cortés, J. Role of sonography in the diagnosis of axillary lymph node metastases in breast cancer: A systematic review. *Am. J. Roentgenol.* **2006**, *186*, 1342–1348. [CrossRef] [PubMed]
63. Chen, X.; Li, X.; Fan, Z.; Li, J.; Xie, Y.; Wang, T.; Ouyang, T. Ultrasound as a replacement for physical examination in clinical staging of axillary lymph nodes in breast cancer patients. *Thorac. Cancer* **2020**, *11*, 48–54. [CrossRef] [PubMed]

64. Mayer, M.N.; Lawson, J.A.; Silver, T.I. Sonographic characteristics of presumptively normal canine medial iliac and superficial inguinal lymph nodes. *Vet. Radiol. Ultrasound* **2010**, *51*, 638–641. [CrossRef] [PubMed]
65. Ruppel, M.J.; Pollard, R.E.; Willcox, J.L. Ultrasonographic characterization of cervical lymph nodes in healthy dogs. *Vet. Radiol. Ultrasound* **2019**, *60*, 560–566. [CrossRef]
66. Burns, G.O.; Scrivani, P.V.; Thompson, M.S.; Erb, H.N. Relation between age, body weight, and medial retropharyngeal lymph node size in apparently healthy dogs. *Vet. Radiol. Ultrasound* **2008**, *49*, 277–281. [CrossRef]
67. Krol, L.; O'Brien, R. Ultrasonographic assessment of abdominal lymph nodes in puppies. *Vet. Radiol. Ultrasound* **2012**, *53*, 455–458. [CrossRef]
68. Ahmadi, O.; Mccall, J.L.; Stringer, M.D. Does senescence affect lymph node number and morphology? A systematic review. *ANZ J. Surg.* **2013**, *83*, 612–618. [CrossRef]
69. Xin, L.; Yan, Z.; Zhang, X.; Zang, Y.; Ding, Z.; Xue, H.; Zhao, C. Parameters for contrast-enhanced ultrasound (CEUS) of enlarged superficial lymph nodes for the evaluation of therapeutic response in lymphoma: A preliminary study. *Med. Sci. Monit.* **2017**, *23*, 5430–5438. [CrossRef]
70. Dialani, V.; James, D.F.; Slanetz, P.J. A Practical approach to imaging the axilla. *Insights Imaging* **2015**, *6*, 217–229. [CrossRef]
71. Ahuja, A.T.; Ying, M.; Ho, S.Y.; Antonio, G.; Lee, Y.P.; King, A.D.; Wong, K.T. Ultrasound of malignant cervical lymph nodes. *Cancer Imaging* **2008**, *8*, 48–56. [CrossRef]
72. Nieciecki, M.; Dobruch-Sobczak, K.; Wareluk, P.; Gumińska, A.; Białek, E.; Cacko, M.; Królicki, L. Rola badania ultrasonograficznego oraz limfoscyntygrafii w diagnostyce węzłów chłonnych pachowych u pacjentek z rakiem piersi. *J. Ultrason.* **2016**, *16*, 5–15. [CrossRef] [PubMed]
73. Kinns, J.; Mai, W. Association between malignancy and sonographic heterogeneity in canine and feline abdominal lymph nodes. *Vet. Radiol. Ultrasound* **2007**, *48*, 565–569. [CrossRef] [PubMed]
74. Agthe, P.; Caine, A.R.; Posch, B.; Herrtage, M.E. Ultrasonographic appearance of jejunal lymph nodes in dogs without clinical signs of gastrointestinal disease. *Vet. Radiol. Ultrasound* **2009**, *50*, 195–200. [CrossRef] [PubMed]
75. Maxwell, F.; De Margerie Mellon, C.; Bricout, M.; Cauderlier, E.; Chapelier, M.; Albiter, M.; Bourrier, P.; Espié, M.; De Kerviler, E.; De Bazelaire, C. Diagnostic strategy for the assessment of axillary lymph node status in breast cancer. *Diagn. Interv. Imaging* **2015**, *96*, 1089–1101. [CrossRef]
76. Choi, H.Y.; Park, M.; Seo, M.; Song, E.; Shin, S.Y.; Sohn, Y.M. Preoperative Axillary Lymph Node Evaluation in Breast Cancer: Current Issues and Literature Review. *Ultrasound Q.* **2017**, *33*, 6–14. [CrossRef]
77. Prativadi, R.; Dahiya, N.; Kamaya, A.; Bhatt, S. Chapter 5 ultrasound characteristics of benign vs malignant cervical lymph nodes. *Semin. Ultrasound CT MRI* **2017**, *38*, 506–515. [CrossRef]
78. Ying, M.; Bhatia, K.S.S.; Lee, Y.P.; Yuen, H.Y.; Ahuja, A.T. Review of ultrasonography of malignant neck nodes: Greyscale, doppler, contrast enhancement and elastography. *Cancer Imaging* **2014**, *13*, 658–669. [CrossRef]
79. Almerey, T.; Villacreses, D.; Li, Z.; Patel, B.; McDonough, M.; Gibson, T.; Maimone, S.; Gray, R.; McLaughlin, S.A. Value of axillary ultrasound after negative axillary mri for evaluating nodal status in high-risk breast cancer. *J. Am. Coll. Surg.* **2019**, *228*, 792–797. [CrossRef]
80. Misra, D.; Panjwani, S.; Rai, S.; Misra, A.; Prabhat, M.; Gupta, P.; Talukder, S. Diagnostic efficacy of color doppler ultrasound in evaluation of cervical lymphadenopathy. *Dent. Res. J. (Isfahan)* **2016**, *13*, 217–224. [CrossRef]
81. Stan, F.G. Power Dopler Ultrasonography vs color dopler of the sentinel lymph mammary glands at female dog. *Bull. Univ. Agric. Sci. Vet. Med. Cluj Napoca Vet. Med.* **2010**, *67*, 298–304. [CrossRef]
82. Park, S.H.; Jeong, Y.M.; Cho, S.H.; Jung, H.K.; Kim, S.J.; Ryu, H.S. imaging findings of variable axillary mass and axillary lymphadenopathy. *Ultrasound Med. Biol.* **2014**, *40*, 1934–1948. [CrossRef]
83. Ahuja, A.T.; Ying, M.; Ho, S.S.Y.; Metreweli, C. Distribution of intranodal vessels in differentiating benign from metastatic neck nodes. *Clin. Radiol.* **2001**, *56*, 197–201. [CrossRef] [PubMed]
84. Rotim, T.; Kristek, B.; Turk, T.; Kretić, D.; Perić, M.; Pušeljić, I.; Pandurović, T.; Štefanić, M. Measurable and unmeasurable features of ultrasound lymph node images in detection of malignant infiltration. *Acta Clin. Croat.* **2017**, *56*, 415–424. [CrossRef] [PubMed]
85. Stan, F. Qualitative Morphological Assessement of Tumor Associated Lymphatic Vasculature in Mammary Gland Neoplasia of Female Dog in Relation With Sentinel Lymph Nodes Metastatic Infiltration. *Sci. Work. Ser. C. Vet. Med.* **2015**, *61*, 16–23.

86. Apple, S.K. Sentinel lymph node in breast cancer: review article from a pathologist's point of view. *J. Pathol. Transl. Med.* **2016**, *50*, 83–95. [CrossRef] [PubMed]
87. Prieto, S.; Gomez-Ochoa, P.; De Blas, I.; Gascón, M.; Aceña, C.; Corda, A.; Sosa, I.; Gregori, T.; Couto, G. Pathologic correlation of resistive and pulsatility indices in canine abdominal lymph nodes. *Vet. Radiol. Ultrasound* **2009**, *50*, 525–529. [CrossRef]
88. El-Gohary, Y.M.; Metwally, G.; Saad, R.S.; Robinson, M.J.; Mesko, T.; Poppiti, R.J. Prognostic significance of intratumoral and peritumoral lymphatic density and blood vessel density in invasive breast carcinomas. *Am. J. Clin. Pathol.* **2008**, *129*, 578–586. [CrossRef]
89. Goldberg, B.B.; Merton, D.A.; Liu, J. Contrast-enhanced sonographic imaging of lymphatic channels and sentinel lymph nodes. *J. Ultrasound Med.* **2005**, *24*, 953–965. [CrossRef]
90. Goldberg, B.B.; Merton, D.A.; Liu, J.; Thakur, M.; Murphy, G.F.; Needleman, L.; Tornes, A. Sentinel lymph nodes in a swine model with melanoma: contrast enhanced lymphatic US. *Radiology* **2004**, *230*, 727–734. [CrossRef]
91. Platt, A.M.; Randolph, G.J. *Dendritic Cell Migration Through the Lymphatic Vasculature to Lymph Nodes*, 1st ed.; Elsevier Inc.: Amsterdam, The Netherlands, 2013; Volume 120. [CrossRef]
92. Skobe, M.; Detmar, M. Structure, function, and molecular control of the skin lymphatic system. *J. Investig. Dermatol. Symp. Proc.* **2000**, *5*, 14–19. [CrossRef]
93. Sever, A.; Broillet, A.; Schneider, M.; Cox, K.; Jones, S.; Weeks, J.; Mills, P.; Fish, D.; Jones, P. Dynamic visualization of lymphatic channels and sentinel lymph nodes using intradermal microbubbles and contrast-enhanced ultrasound in a swine model and patients with breast cancer. *J. Ultrasound Med.* **2010**, *29*, 1699–1704. [CrossRef] [PubMed]
94. Shimazu, K.; Ito, T.; Uji, K.; Miyake, T.; Aono, T.; Motomura, K.; Naoi, Y.; Shimomura, A.; Shimoda, M.; Kagara, N.; et al. Identification of sentinel lymph nodes by contrast-enhanced ultrasonography with sonazoid in patients with breast cancer: a feasibility study in three hospitals. *Cancer Med.* **2017**, *6*, 1915–1922. [CrossRef] [PubMed]
95. Liu, J.; Liu, X.; He, J.; Gou, B.; Luo, Y.; Deng, S.; Wen, H.; Zhou, L. Percutaneous contrast-enhanced ultrasound for localization and diagnosis of sentinel lymph node in early breast cancer. *Sci. Rep.* **2019**, *9*, 1–6. [CrossRef] [PubMed]
96. Zhao, J.; Zhang, J.; Zhu, Q.L.; Jiang, Y.X.; Sun, Q.; Zhou, Y.D.; Wang, M.Q.; Meng, Z.L.; Mao, X.X. The value of contrast-enhanced ultrasound for sentinel lymph node identification and characterisation in pre-operative breast cancer patients: a prospective study. *Eur. Radiol.* **2018**, *28*, 1654–1661. [CrossRef]
97. Mori, N.; Mugikura, S.; Miyashita, M.; Kudo, Y.; Suzuki, M.; Li, L.; Mori, Y.; Takahashi, S.; Takase, K. Perfusion contrast-enhanced ultrasound to predict early lymph-node metastasis in breast cancer. *Jpn. J. Radiol.* **2019**, *37*, 145–153. [CrossRef]
98. Ouyang, Q.; Chen, L.; Zhao, H.; Xu, R.; Lin, Q. Detecting metastasis of lymph nodes and predicting aggressiveness in patients with breast carcinomas. *J. Ultrasound Med.* **2010**, *29*, 343–352. [CrossRef]
99. Zenk, J.; Bozzato, A.; Hornung, J.; Gottwald, F.; Rabe, C.; Gill, S.; Iro, H. Neck lymph nodes: prediction by computer-assisted contrast medium analysis? *Ultrasound Med. Biol.* **2007**, *33*, 246–253. [CrossRef]
100. Yang, H.K.; Burns, P.N.; Jang, H.J.; Kono, Y.; Khalili, K.; Wilson, S.R.; Kim, T.K. Contrast-enhanced ultrasound approach to the diagnosis of focal liver lesions: the importance of washout. *Ultrasonography* **2019**, *38*, 289–301. [CrossRef]
101. Piscaglia, F.; Nolsøe, C.; Dietrich, C.F.; Cosgrove, D.O.; Gilja, O.H.; Bachmann Nielsen, M.; Albrecht, T.; Barozzi, L.; Bertolotto, M.; Catalano, O.; et al. The EFSUMB guidelines and recommendations on the clinical practice of contrast enhanced ultrasound (CEUS): Update 2011 on non-hepatic applications. *Ultraschall der Medizin* **2012**, *33*, 33–59. [CrossRef]
102. Badea, R.; Ciobanu, L. Contrast enhanced and doppler ultrasonography in the characterization of the microcirculation. expectancies and performances. *Med. Ultrason.* **2012**, *14*, 307–317.
103. Choi, M.; Yoon, J.; Choi, M. Semi-quantitative strain elastography may facilitate pre-surgical prediction of mandibular lymph nodes malignancy in dogs. *J. Vet. Sci.* **2019**, *20*, 1–11. [CrossRef] [PubMed]
104. Bhatia, K.S.; Cho, C.C.; Yuen, Y.H.; Rasalkar, D.D.; King, A.D.; Ahuja, A.T. Real-time qualitative ultrasound elastography of cervical lymph nodes in routine clinical practice: Interobserver agreement and correlation with malignancy. *Ultrasound Med. Biol.* **2010**, *36*, 1990–1997. [CrossRef] [PubMed]

105. Sigrist, R.M.S.; Liau, J.; El Kaffas, A.; Chammas, M.C.; Willmann, J.K. Ultrasound elastography: Review of techniques and clinical applications. *Theranostics* **2017**, *7*, 1303–1329. [CrossRef] [PubMed]
106. Lo, W.C.; Liao, L.J. Comparison of two elasticity scoring systems in the assessment of the cervical lymph nodes. *J. Med. Ultrasound* **2014**, *22*, 140–144. [CrossRef]
107. Zhao, Q.L.; Xia, X.N.; Zhang, Y.; He, J.J.; Sheng, W.; Ruan, L.T.; Yin, Y.M.; Hou, H.L. Elastosonography and two-dimensional ultrasonography in diagnosis of axillary lymph node metastasis in breast cancer. *Clin. Radiol.* **2018**, *73*, 312–318. [CrossRef] [PubMed]
108. Wojcinski, S.; Dupont, J.; Schmidt, W.; Cassel, M.; Hillemanns, P. Real-time ultrasound elastography in 180 axillary lymph nodes: Elasticity distribution in healthy lymph nodes and prediction of breast cancer metastases. *BMC Med. Imaging* **2012**, *12*, 35. [CrossRef]
109. Lenghel, L.M.; Bolboacă, S.D.; Botar-Jid, C.; Băciut, G.; Dudea, S.M. The value of a new score for sonoelastographic differentiation between benign and malignant cervical lymph nodes. *Med. Ultrason.* **2012**, *14*, 271–277.
110. Bhatia, K.S.S.; Lee, Y.Y.P.; Yuen, E.H.Y.; Ahuja, A.T. Ultrasound elastography in the head and neck. part ii. accuracy for malignancy. *Cancer Imaging* **2013**, *13*, 260–276. [CrossRef]
111. Bhatia, K.S.S.; Lee, Y.Y.P.; Yuen, E.H.Y.; Ahuja, A.T. Ultrasound elastography in the head and neck. part, i. basic principles and practical aspects. *Cancer Imaging* **2013**, *13*, 253–259. [CrossRef]
112. Dietrich, C.F.; Barr, R.G.; Farrokh, A.; Dighe, M.; Hocke, M.; Jenssen, C.; Dong, Y.; Saftoiu, A.; Havre, R.F. 1 introduction to elastography. *Elastography* **2016**. [CrossRef]
113. Jung, J.W.; Je, H.; Lee, S.K.; Jang, Y.; Choi, J. Two-Dimensional shear wave elastography of normal soft tissue organs in adult beagle dogs; interobserver agreement and sources of variability. *Front. Bioeng. Biotechnol.* **2020**, *8*, 1–15. [CrossRef] [PubMed]
114. Wang, M.; Zhou, W.; Zhao, Y.; Xia, T.; Zha, X.; Ding, Q.; Liu, X.; Zhao, Y.; Ling, L.; Chen, L.; et al. A novel finding of sentinel lymphatic channels in early stage breast cancer patients: which may influence detection rate and false-negative rate of sentinel lymph node biopsy. *PLoS ONE* **2012**, *7*, e51226. [CrossRef] [PubMed]
115. Wang, Y.; Zhou, W.; Li, C.; Gong, H.; Li, C.; Yang, N.; Zha, X.; Chen, L.; Xia, T.; Liu, X.; et al. variation of sentinel lymphatic channels (SLCs) and sentinel lymph nodes (SLNs) assessed by contrast-enhanced ultrasound (CEUS) in breast cancer patients. *World J. Surg. Oncol.* **2017**, *15*, 1–7. [CrossRef] [PubMed]
116. Guo, J.; Yang, H.; Wang, S.; Cao, Y.; Liu, M.; Xie, F.; Liu, P.; Zhou, B.; Tong, F.; Cheng, L.; et al. Comparison of sentinel lymph node biopsy guided by indocyanine green, blue dye, and their combination in breast cancer patients: A prospective cohort study. *World J. Surg. Oncol.* **2017**, *15*, 1–7. [CrossRef]
117. Joseph, F.J.; Van Oepen, A.; Friebe, M. Breast sentinel lymph node biopsy with imaging towards minimally invasive surgery. *Biomed. Tech.* **2017**, *62*, 547–555. [CrossRef] [PubMed]
118. Takemoto, N.; Koyanagi, A.; Yamamoto, H.; Shimura, K.; Fujii, R. Comparison of the indocyanine green dye method versus the combined method of indigo carmine blue dye with indocyanine green fluorescence imaging for sentinel lymph node biopsy in patients with stage i or ii breast cancer. *Ann. Oncol.* **2014**, *25*, i3. [CrossRef]
119. Siddique, M.; Nawaz, M.K.; Bashir, H. The usefulness of SPECT/CT in sentinel node mapping of early stage breast cancer patients showing negative or equivocal findings on planar scintigraphy. *Asia Ocean. J. Nucl. Med. Biol.* **2018**, *6*, 80–89. [CrossRef]
120. Taumberger, N.; Pernthaler, B.; Schwarz, T.; Bjelic-Radisic, V.; Pristauz, G.; Aigner, R.M.; Tamussino, K. lymphoscintigraphy for sentinel lymph node biopsy in breast cancer: do we need a delayed image? *Breast Care* **2020**, *15*, 55–59. [CrossRef]
121. Niu, G.; Chen, X. Lymphatic imaging: Focus on imaging probes. *Theranostics* **2015**, *5*, 686–697. [CrossRef]
122. Ahmed, M.; Purushotham, A.D.; Horgan, K.; Klaase, J.M.; Douek, M. Meta-Analysis of superficial versus deep injection of radioactive tracer and blue dye for lymphatic mapping and detection of sentinel lymph nodes in breast cancer. *Br. J. Surg.* **2015**, *102*. [CrossRef]
123. Zada, A.; Peek, M.C.L.; Ahmed, M.; Anninga, B.; Baker, R.; Kusakabe, M.; Sekino, M.; Klaase, J.M.; Haken, B.; Douek, M. Meta-analysis of sentinel lymph node biopsy in breast cancer using the magnetic technique. *Br. J. Surg.* **2016**. [CrossRef] [PubMed]

124. Karakatsanis, A.; Michael, P.; Lone, C. The nordic sentimag trial: A comparison of super paramagnetic iron oxide (spio) nanoparticles versus tc 99 and patent blue in the detection of sentinel node (sn) in patients with breast cancer and a meta-analysis of earlier studies. *Breast cancer Res. Treat.* **2016**, 281–294. [CrossRef] [PubMed]
125. Martonos, C.; Gudea, A.; Dezdrobitu, C.; Damian, A.; Crisan, M.; Bud, I.; Pentea, M. Morphological description of sentinel lymphatic channels in canine mammary tumours. In Proceedings of the Multidisciplinary Conference on Sustainable Development, Timisoara, Romania, 23–24 May 2019; Filodiritto Editore: Bologna, Italy, 2019; pp. 637–643, ISBN 978-88-85813-60-1.
126. Zhao, Y.C.; Ni, X.J.; Li, Y.; Dai, M.; Yuan, Z.X.; Zhu, Y.Y.; Luo, C.Y. Peritumoral lymphangiogenesis induced by vascular endothelial growth factor c and d promotes lymph node metastasis in breast cancer patients. *World, J. Surg. Oncol.* **2012**, *10*, 1. [CrossRef] [PubMed]
127. Widodo, I.; Dwianingsih, E.K.; Utoro, T.; Anwar, S.L.; Aryandono, T. Prognostic value of lymphangiogenesis determinants in luminal and non-luminal breast carcinomas. *Asian Pacific J. Cancer Prev.* **2018**, *19*, 2461–2467. [CrossRef]

Scientific Works. Series C. Veterinary Medicine. Vol. LXI (2)
ISSN 2065-1295; ISSN 2343-9394 (CD-ROM); ISSN 2067-3663 (Online); ISSN-L 2065-1295

QUALITATIVE MORPHOLOGICAL ASSESSEMENT OF TUMOR ASSOCIATED LYMPHATIC VASCULATURE IN MAMMARY GLAND NEOPLASIA OF FEMALE DOG IN RELATION WITH SENTINEL LYMPH NODES METASTATIC INFILTRATION

Florin STAN

University of Agricultural Sciences and Veterinary Medicine of Cluj-Napoca, Faculty of Veterinary Medicine, Mănăştur Street, No. 3-5, Cluj-Napoca, Romania, Email: flodvm@yahoo.com

Corresponding author email: flodvm@yahoo.com

Abstract

Metastasis, the spread of tumor cells from the primary site to lymph nodes and the distant organs is the most aggressive and specific feature of malignant cancer. The mechanisms by which malignant cells leave the primary tumor, invade lymphatics and metastasize are complex and interconnected being directly related to biological behavior of tumor. However, the lymphatic vasculature is often neglected. The aim of this study is to establish if there is a correlation between the peritumoral and intratumoral lymphatic vascular density and the presence of metastatic infiltration in sentinel lymph nodes of mammary gland tumor. Injecting the coloring solution in mammary gland tumor of nine female dogs it was noted the pattern of lymphatic vessels at the injection site, their density, size distribution area, their trajectory to the first lymph node. Also the status of the tumor draining lymph node was histological assessed. The architecture and density of intratumoral and peritumoral lymphatic vessels was determined by their function in absorbing interstitial fluid together with the tumoral cells, due to their permeability. The coloring solution show the sinuous pattern of peritumoral lymphatic vessels, with a rich chaotic vascular network compared with reticular or plexiform pattern of lymphatic vasculature of healthy mammary gland. The size of peritumoral lymphatic colored area was dependant on the histological type of the tumor and on its size. Also, a malignant tumor size >1cm was associated with the presence of the metastatic infiltration in the first tumor draining lymph node. The density of intratumoral lymphatic vessels was low compared with the peritumoral lymphatics. In conclusion, qualitative morphological assessment of lymphatic vasculature of malignant mammary gland tumors of female dog revealed an increased density of lymphatic vessels in the peritumoral region and a lesser degree intratumoraly. The size of peritumoral lymphatic area was directly related with the presence of metastases in sentinel lymph nodes. Although great progression has been made in revealing the lymphangiogenic markers, additional studies are required to understand the paradoxical significance of intratumoral and peritumoral lymphatics density and lymph nodes metastases for prognosis and development of metastases in vital organs.

Key words: *lymphatic, metastasis, mammary gland tumor, dog.*

INTRODUCTION

Mammary gland is a common site of malignancies in female dogs (Sorenmo et al., 2011; Santos et al., 2014). Although the importance of the lymphatic system in tumor dissemination is fully recognized, lymphatic vessels were not considered as active factors involved in tumor progression. In canine mammary tumors characteristics of lymphangiogenesis is not fully known, and its role in tumor progression and metastasis is not completely understood.

Tumor lymphangiogenesis in most human cancers were associated with increased metastatic potential and lymphatic vessels density becomes another prognostic factor in overall survival of patients (Steven et al., 2014, Alitalo and Detmar 2012). More recently, lymph nodes lymphangiogenesis itself proved to be another circumstance that contributes to the dissemination of tumor cells.

Considering the above, there seems to be multiple causes for the apparition of metastasis (Tamela and Alitalo, 2010).

However, two concepts are conveyed in this direction: one directly related to the tumor type (Sorenmo et al., 2011) and the second connected to the anatomical and functional particularities of mammary drainage (Pereira et al., 2003; Stan 2009, 2012).

Therefore, our study analyzes the morphology and density of peritumoral lymphatic vessels, and their correlation with clinicopatological and staging parameters, namely the presence of metastases in mammary glands sentinel lymph nodes.

MATERIALS AND METHODS

The study was conducted on a group of nine subjects: two female dogs without pathology of mammary glands and seven female dogs who have visible tumors in cranial thoracic, cranial and caudal abdominal mammary gland and in inguinal mammary glands. One female presented mammary tumors on the entire left mammary chain, with impairment of contra lateral cranial abdominal (A1), cranial caudal (A2), and inguinal (I) mammary gland. Subjects with mammary gland tumors received a peritumoral 0.5% Blue Dye injection, in four points: cranial, caudal, medial and lateral of interest area. The same injection was performed subareolar in healthy subjects. The total amount of dye was 0.2ml on the injected point. To facilitate dye diffusion, a gentle massage of injected area was made. Previous to injection, the subjects were sedated, using 0.2mg/kg/bw of ketamine. Subjects were continuously monitored. Twenty four hours later euthanasia was made by IV administration of Euthasol (Virbach AH Inc.), 0.22ml/kg/bw. Regional stratigraphic dissection was performed. Histopatological examination of sentinel lymph nodes was made.

RESULTS

In case of malignancy, lymphatic vessels appear with an aberrant morphology, and a sinuous route, with relatively visible lumen and numerous branches (Fig. 1). Evaluation of lymphatic vessel density was achieved for

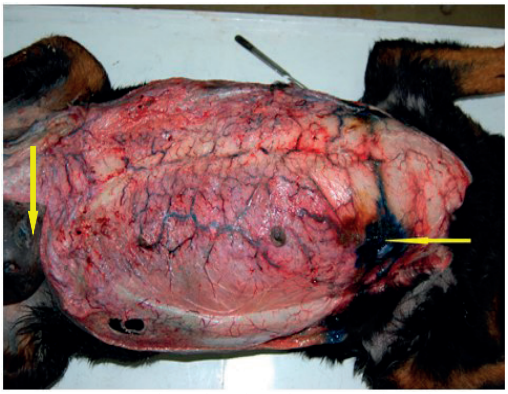

Fig. 1 Numerous branch of lymphatic vessels with contra lateral anastomosis in a subject with cranial thoracic mammary gland and inguinal mammary gland-arrows

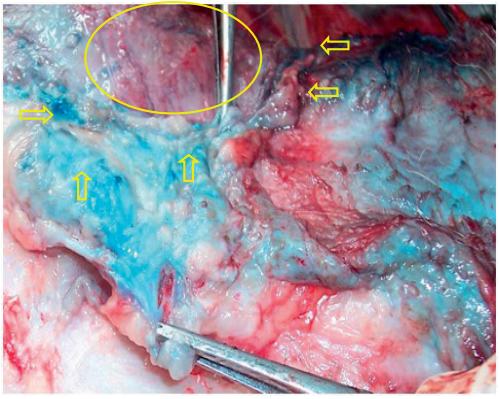

Fig. 2 Chaotic distribution of lymphatic vessels-arrows-around a cranial abdominal mammary gland tumor-oval shape

neoplastic mammary glands differentiated in two areas: a) we noted the presence of numerous well stained peritumoral lymphatic vessels, having a winding pattern, seemingly to supplement tumors lymphatic vessels in adjacent territory (Fig. 2).

These vessels were located especially at tumor-parenchyma interface, with chaotic distribution, without a typical morphology and uneven walls.

The corresponding area was also unclear delimitated (Fig.3); b) within the tumor, lymph vessels have a very low density relative to the peritumoral area or normal parenchyma, with small diameter, that appeared to be lacking in content. Around the tumor we noted a higher density of lymphatic vessels compared to less numerous lymphatic vessels inside the tumors.

Lymphatic's of healthy mammary glands

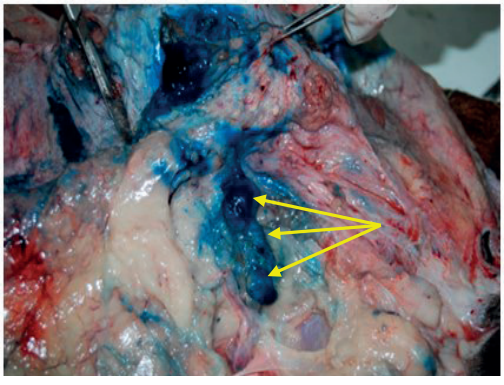

Fig. 3 The inguinal superficial lymph nodes draining a inguinal tumoral mammary gland-small arrows. Well defined lymphatic vessels are seen toward to the sentinel lymph nodes-joined arrow

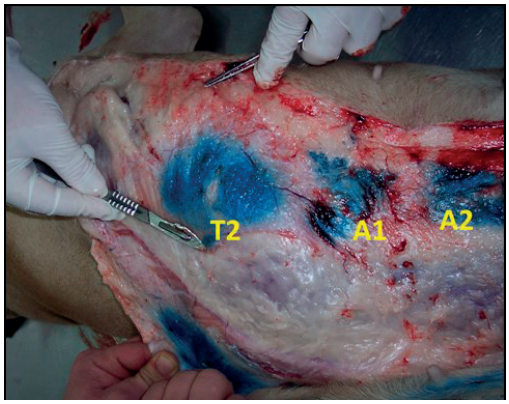

Fig. 4 Well defined lymphatic vascular area in healthy mammary gland. Note the ordered distribution of lymphatics of superficial dermis toward to the areola

were well stained highlighting the two drainage areas: deep and superficial (Fig.4).
Deep injection in mammary gland parenchyma revealed the lymphatic vessels that arise around glandular lobes, with an upward centripetal trajectory, accompanying milk ducts, toward the areola.
Periareolar injection of dye, colored the numerous subareolar lymphatic vessels, which made multiple anastomoses with parenchyma and dermis lymphatic vessels. These lymphatics had a relatively superficial centrifugal path, towards the mammary gland periphery. In absence of pathology, the parenchyma mammary lymphatic vessels were orderly distributed, showing a reticular model in deep parenchyma and a plexiform model toward the surface (Fig.4). In healthy subjects the superficial lymphatic vessels that were stained after dye injection realized well circumscribed areas around the mammary areola. The lymphatic vessels in their path to the corresponding lymph nodes were followed. Lymphatic vessels that drained the neoplastic cranial abdominal mammary gland (A1) and inguinal mammary gland (I) leave the peritumoral area, confluencing and creating well defined afferent lymphatic

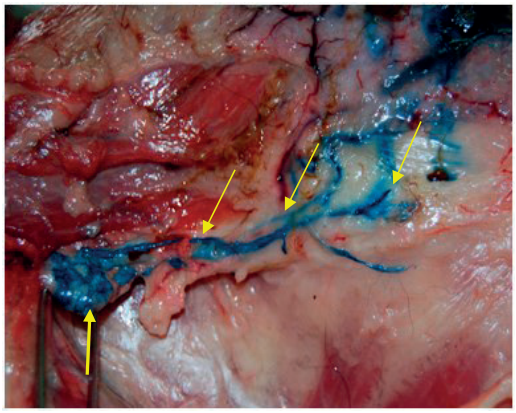

Fig. 5 Axillary lymph center draining cranial thoracic tumoral mammary gland. Vizible lymphatic paths to the proper axillary lymph node

vessels draining into inguinal lymph nodes. This aspect was seen in five subjects. In two subjects, when neoplastic T1 mammary gland was injected, we note that lymphatic vessels has not achieved so much confluence, rather had a separate route to the axillary lymph node (Fig. 5). Regarding lymphatic drainage of healthy mammary glands, axillary lymph center was well stained. In one case it consists in two lymph nodes, proper and accessories respectively, and in the other subject it was colored one axillary lymph node. In caudal direction it was obvious colored inguinal lymph nodes as sentinel lymph nodes for healthy A1 and inguinal mammary glands. In the present research the same lymph nodes were sentinel lymph nodes to neoplastic mammary glands. In a case of neoplastic A1 mammary gland, lymphatic vessels had only a cranial route toward axillary lymph center, without caudal direction to inguinal lymph nodes. Moreover, lymphatic vessels of apparently healthy neighborhood A2 mammary gland were stained.
Table 1 present the study protocol and the results concerning each subject of the study.

Table 1. The study protocol and the results related to the lymphatic drainage of injected mammary gland and the presence of metastatic infiltration into draining lymph nodes

Dog	Characteristics and tumor location	Site of dye injection	Draining lymph nodes	Lymph node metastatic infiltration
1	No tumor present	Left subareolarT1,A1 and right I	Left axillary ln and right superficial inguinal ln	Absent
2	No tumor present	Subareolar Left and right A1	Axillary ln	Absent
3	Right T1,T2	Peritumoral T1	Right axilary and cranial sternal ln	Present
4	Right A1,A2,I	Peritumoral A1	Right axillary ln	Present
5	Left A2,I	Peritumoral A2	Left superficial inguinal ln	Present
6	Left I	Peritumoral I	Left superficial inguinal ln	Absent
7	Left I	Peritumoral I	Left superficial inguinal ln	Present
8	Right and left I	Peritumoral I	Left and right superficial inguinal ln and left popliteal ln	Present
9	Left mammary chain and contralateral A1,A2,I	Left peritumoral T1, I and right peritumoral A1	Left and right superficial inguinal ln, popliteal ln and a lymphatic plexus on the medial aspect of the left tigh	Present in all mentioned draining sites

T1-cranial thoracic; T2-caudal thoracic; A1-cranial abdominal; A2-caudal abdominal; I-inguinal mammary gland; ln-lymph node

Histopathological examinations of lymph nodes which drained the neoplastic mammary glands confirm the presence of metastatic infiltration in suspicious lymph nodes (Fig. 6).

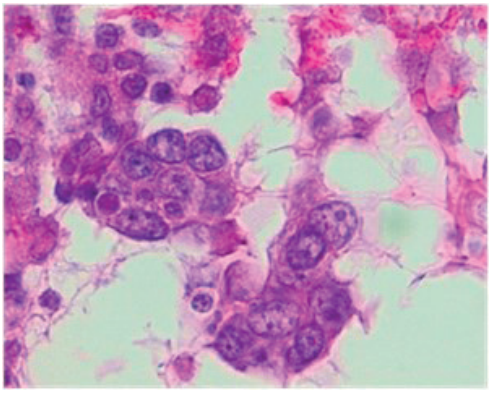

Fig.6 Metastatic infiltration of lymph nodes. The large poliglonal tumor cells possess finely granular cytoplasm. H&E40x

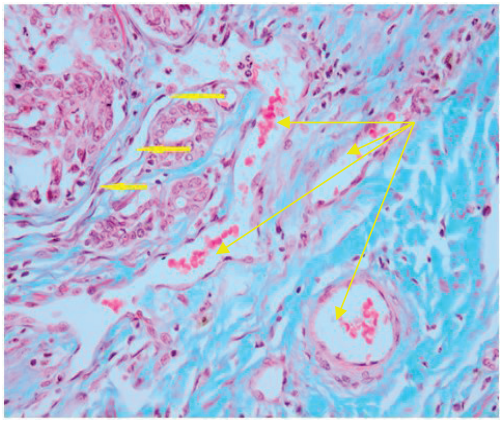

Fig. 7 Lymphatic channel into a mammary carcinoma (arrows) and numerous intratumoral blood vessels-(joined arrows). Goldner Trichrome 40x

Inside the tumor the lymphatic vessels appears like tiny channels with no content (Fig. 7). Contrary, the blood vessels were numerous proving high angiogenesis.

DISCUSSIONS

It is well known that mammary tumor metastasis into regional lymph nodes, their status being considered a major criterion to prognosis and lead to a different approach in therapy (Patsikas et al., 2006; Stan 2012). This feature is due to certain tumors type. Most of mammary tumors are carcinomas, a small percentage sarcomas, fibrosarcomas and osteosarcomas. Epithelial malignant mammary tumors as carcinomas metastasize through lymphatic vessels, while mesenchymal tumors metastasize through blood vessels (Restucci et al., 2003; Sorenmo 2011). We can say that this phenotype feature is due to lymphangiogenesis which is typical in malignancies, involving formation of new vessels from preexisting lymphatic vessel (Tamela and Alitalo 2010, Fidler 2011). In our study, peritumoral lymphatic vessel density assessment showed that there are numerous lymphatic vessels at the tumor periphery, in the adjacent tumor area, at the tumor-mammary parenchyma connection, compared with low lymphatic vessels density inside of the tumor. All these tumors metastasize through the lymphatic system, the first quantifiable station being the sentinel lymph node. But until the appearance of metastasis in sentinel lymph nodes, the tumor cells must leave the primary tumor and through the lymphatic vessels, via lymph nodes, populate another distance sites (Achen 2006, Ungheforen et al., 2011). In current veterinary practice, if a mammary gland tumor is diagnosed, the surgical treatment eradicates entire mammary chain together with the sentinel lymph nodes, if they are identified. This is not an appropriate attitude for several reasons: lymph nodes excision carries a significant morbidity with complications such as lymphoedema, pain, numbness, and limited member movement. Nevertheless, if the sentinel lymph nodes are positive for tumor cells, there is a 40% risk that higher next lymph nodes may also be involved in metastatic disease (Stan 2009). Fine needle aspiration biopsy of sentinel lymph node is a minim invasive alternative to surgical excision. But in carnivores it is difficult to specify which nodes are really the sentinel ones. Numerous studies have been conducted by Patsikas et al, related to the lymphatic drainage in healthy and neoplastic mammary glands in female dogs. Their results showed that healthy mammary glands are drained by the ipsilateral lymph centers, cranial by axillary lymph center and caudal by inguinal lymph nodes. They revealed no connection between contralateral lymph nodes or mammary glands. On the contrary, Pereira et al., 2003, have shown that in the presence of mammary tumor the lymph drainage is completely changed, both in terms of recruitment of new lymph nodes and establishment of new connections. Similar results were obtained by our team in a study regarding the cranial thoracic mammary gland drainage, in which we identify the cranial sternal lymph node as a sentinel lymph node simultaneously with axillary lymph nodes (Stan 2009). Also, it was demonstrated the presence of lymphatic connections between contralateral inguinal lymph nodes (Stan 2012). In addition our results are consistent with those of other researchers, about the existence of a lymphatic plexus, located at the medial aspect of the thigh, involved in lymphatic drainage of neoplastic inguinal mammary gland. (Pereira et al., 2003; Patsikas et al., 2006). Based on these findings, it can be stated that the lymphatic drainage of mammary glands in female dog, shows a great variability. These findings are among the few, who studied the lymphatic vasculature in carnivores' neoplastic mammary glands. Therefore, there is insufficient anatomic data concerning lymphatic vascularization in neoplastic mammary glands in the bitches and is a lack of comparative studies focusing on lymphatic vessels in mammary neoplasia. To metastasize in various locations, tumor cells have to cross lymphatic system barriers. If we considered that initial lymphatic's are blind ended, without basement membrane, being fenestrated, it can be said this features are real facilities to tumor dissemination, compared to

blood vessels (Olivier, 2004). Furthermore, our results showing the aberrant distribution, high peritumoral density and sinuous route of the lymphatic vessels, these features could be the morphological explanation of easy entrance of the tumoral cells into the peritumoral lymphatic vessels. In our research, within the tumor the lymphatics appear to be dysfunctional with no content. The explanation is logical if we consider that inside of tumor the interstitial pressure is high due to uncontrolled multiplication of tumor cells. Under these conditions, entry of tumor cells could be partially affected. Another aspect which worth taking into account to explain the low density of intratumoral lymphatic vessels is the possibility that intratumoral lymphangiogenesis is inhibited rather than induced. Padera et al., reported the absence of intratumoral lymph vessels in an experimental induced tumor model in rodents. Therefore, metastatic cells can easily invade preexisting lymphatic vessels or the new formed peritumoral vessels due to induction of lymphangiogenesis by tumor itself. There are studies showing that tumor cells can use as transporting agents chemokines or lymphocyte or antigen presenting cells to gain access into lymphatic vessels, thus increasing the dissemination possibility. Many types of tumors express themselves vascular endothelial growth factors VEGF- C and VEGF-D and the presence of these factors induce active lymphangiogenesis, sentinel lymph nodes metastasis and distant metastasis (Saharinen et al., 2010). All these are leading to a poor prognostic. Level of VEGF-C and VEGF-D and their corresponding receptor are increased in determination made in the presence of breast tumor in woman (Kodera et al., 2011). There is not a correlation between tumor angiogenesis and lymphangiogenesis as long as each process is mediated by the specific markers (VEGF-A and VEGF-B for angiogenesis and VEGF-C and VEGF-D for lymphangiogenesis). Studying dogs and cats carcinomas, it was showed that VEGF is strongly expressed in the cytoplasm of tumor cells, occasionally in carcinoma stroma cells and infrequent in endothelial cells of tumor vessels without a correlation between VEGF and lymphatic involvement. These results are not in agreement with those obtained by Restucci et al, 2010, who showed existence of a strong correlation between VEGF expression and increased density of blood tumor vessels. The same question arises in case of lymphatic dissemination. Both, human and animal experimental models on clinicopathological data, indicate that adjacent tumor lymphangiogenesis is associated with sentinel lymph nodes metastasis (Padera et al., 2002, Sleeckx et al., 2014). These findings are similar to our results of the present research in which we found a high density of peritumoral lymphatic vessels on a large area, all these findings being associated with presence of metastatic infiltration in sentinel lymph nodes. Also, morphological changes of newly formed vessels from the tumor vicinity, with sinuous feature and multiple anastomoses, increased the lymphatic endothelial properties in adhesion of tumor cells, facilitating the spread of cancer.

More recently, it was found that VEGFs secreted by primary tumor, induce lymphangiogenesis in sentinel lymph nodes that drained the tumor territory even before the spread of tumor cells (Steven et al., 2014). Based on these findings and considering our results from present research, we hypothesized that the lymphatic network is already established when the tumor becomes invasive.

Many anti-lymphangiogennic therapies have been proposed, especially in women breast cancer. Kodera et al, have realized a study on VEGF receptors blocking activity, clinically proven to be an inhibitor of tumor angiogenesis, concluded that the same therapy may be beneficial in breast cancer, by suppressing lymphangiogenesis and axillary metastasis. The therapy consists of administration of Sunitinib, an VEGF-3 activity inhibitor. Not only VEGF and their ligands VEGF-C and VEGF-D are involved in lymphatic dissemination (Fidler 2011). Based on the findings that dilatation and spreading of tumor cells are inhibited by administration of non steroidal anti-inflamatory drugs (NSAIDs). Karnezi et al., 2012, have shown a direct link between regulation and involvement of prostaglandins in metastatic dissemination. All these studies

lead to the creation of a new therapy, anti-angiogenic therapy, whose direct target are VEGF, especially the VEGF-C and VEGF-D which has been shown to inhibit lymphangiogenesis and lymph nodes metastases. Therefore, it can be said that lymphatic vessels which are actively involved, both morphologically and functionally in metastatic dissemination, may be considered therapeutic targets in inhibition of tumor dissemination.

CONCLUSIONS

Our results demonstrate that increased peritumoral lymphatic density and a large area of peritumoral lymphatic vessels are associated with the presence of metastasis in sentinel lymph nodes. These features could be considered as prognostic factors in development of mammary tumor in female dog. In veterinary medicine, assessing the efficiency of anti-angiogenic and anti-lymphangiogenic therapy, alone or in combination with chemotherapy, as potential inhibitors of tumor growth and metastasis would be of great interest.

REFERENCES

Achen MG., Stacker SA., 2006. Tumor lymphangiogenesis and metastatic spread-new players begin to emerge. Int J Cancer,119(8):1755-60.

Alitalo K., and M. Detmar, 2012. Interaction of tumor cells and lymphatic vessels in cancer progression, Oncogene, 31(42): 4499–4508.

Fidler I. J., 2011.The biology of cancer metastasis. Semin Cancer Biol. ;21(2):71-78

Karnezis T, et al., 2012 VEGF-D promotes tumor metastasis by regulating prostaglandins produced by the collecting lymphatic endothelium. Cancer Cell, 14;21(2):181-95

Kodera Y, Katanasaka Y, Kitamura Y, et al. Sunitinib inhibits lymphatic endothelial cell functions and lymph node metastasis in a breast cancer model through inhibition of vascular endothelial growth factor receptor 3. Breast Cancer Res.2011;13(3):R66

Olivier 2004. Lymphatic vasculature development, Nature Rev, 4:35-45

Padera TP, Kadambi A,, di Tomaso , et al. 2002. Lymphatic metasatasis in the absence of functional intratumor lymphatics. Science. 296:1883-6.

Patsikas, M. N., Karayannopoulou, M., Kaldrymidoy, E., Papazoglou, L. G., Papadopoulou, P. L., Tzegas, S. I., Tziris, N. E., Kaitzis, D. G., Dimitriadis, A. S. and Dessiris, A. K. 2006, The Lymph Drainage of the Neoplastic Mammary Glands in the B itch: A Lymphographic Study.AHE, 35: 228–234.

Pereira, C. T., Rahal, S. C., de Carvalho Balieiro, J. C. and Ribeiro, A. A. C. M. 2003, Lymphatic Drainage on Healthy and Neoplasic Mammary Glands in Female Dogs: Can it Really be Altered? AHE. 32: 282–290.

Restucci B, Borzacchiello G, Maiolino P, Martano M, Paciello O, Papparella S. 2004 Expression of vascular endothelial growth factor receptor Flk-1 in canine mammary tumours. J Comp Pathol. 130:99–104

Saharinen P, et al. 2010 Claudin-like protein 24 interacts with the VEGFR-2 and VEGFR-3 pathways and regulates lymphatic vessel development. Genes Dev.;24:875–880.

Santos, M., Correia-Gomes, C., Santos, A., de Matos, A., Rocha, E., Lopes, C., & Pereira, P. D. 2014. Nuclear pleomorphism: Role in grading and prognosis of canine mammary carcinomas. The Veterinary Journal, 426-433

Sleeckx, N., Van Brantegem, L., Van den Eynden, G., Fransen, E., Casteleyn, C., Van Cruchten, S., ... & Van Ginneken, C. 2014. Lymphangiogenesis in canine mammary tumours: a morphometric and prognostic study. J Comp. Pathology , 150(2), 184-193.

Sorenmo KU, Rasotto R, Zappulli V, Goldschmidt MH. 2011.Development, anatomy, histology, lymphatic drainage, clinical features, and cell differentiation markers of canine mammary gland neoplasms. Vet Pathol.48(1):85-97.

Stan F, 2009**,** Study of the mammary superficial lymphatic system in bitch, 2009, USAMV Cluj-Napoca Romania. The Ph-d thesis.

Stan F., 2009. Study on the Lymphatic Vascularisation of the Cranial Thoracic Mammary Gland (T1) in Bitch Bulletin UASVM, Veterinary Medicine 66(1):107-113.

Stan F., 2012. Corelation Beetwen Subareolar And Peritumoral Blue Dye Injection To Identify Sentinel Lymph Nodes In Canine Mammary Glands Neoplazia, Lucrări Ştiinţifice USAMV,Iasi,55(1-2), 125 – 132

Steven A. Stacker, Steven P. Williams, Tara Karnezis, Ramin Shayan, Stephen B. Fox, Marc G. Achen, 2014. Lymphangiogenesis and lymphatic vessel remodelling in cancer Nature Reviews Cancer 14: 159–172

Tamela T., Alitalo K., 2012. Lymphangiogenesis; Molecular mechanisms and future promise. Cell.2010;140 (4):460–476.

Ungefroren H, Sebens S, Seidl D, Lehnert H, Hass R. 2011 Interaction of tumor cells with the microenvironment. Cell Commun Signal.; 9:18.

pleomorphism: Role in grading and prognosis of canine mammary carcinomas. The Veterinary Journal, 426-433.

Sleeckx, N., Van Brantegem, L., Van den Eynden, G., Fransen, E., Casteleyn, C., Van Cruchten, S., ... & Van Ginneken, C. 2014. Lymphangiogenesis in ca-

nine mammary tumours: a morphometric and prognostic study. J Comp. Pathology, 150(2), 184-193.

Sorenmo KU, Rasotto R, Zappulli V, Goldschmidt MH. 2011. Development, anatomy, histology, lymphatic drainage, clinical features, and cell differentiation markers of canine mammary gland neoplasms. Vet Pathol.48(1):85-97.

Stan F, 2009**,** Study of the mammary superficial lymphatic system in bitch, 2009, USAMV Cluj-Napoca Romania. The Ph-d thesis.

Stan F., 2009. Study on the Lymphatic Vascularisation of the Cranial Thoracic Mammary Gland (T1) in Bitch Bulletin UASVM, Veterinary Medicine 66(1):107-113.

Stan F., 2012. Corelation Beetwen Subareolar And Peritumoral Blue Dye Injection To Identify Sentinel Lymph Nodes In Canine Mammary Glands Neoplazia, Lucrări Ştiinţifice USAMV, Iasi, 55(1-2), 125 – 132

Steven A. Stacker, Steven P. Williams, Tara Karnezis, Ramin Shayan, Stephen B. Fox, Marc G. Achen, 2014. Lymphangiogenesis and lymphatic vessel remodelling in cancer Nature Reviews Cancer 14: 159–172

Tamela T., Alitalo K., 2012. Lymphangiogenesis; Molecular mechanisms and future promise. Cell.2010;140 (4):460–476.

Ungefroren H, Sebens S, Seidl D, Lehnert H, Hass R. 2011 Interaction of tumor cells with the microenvironment. Cell Commun Signal.; 9:18

.

Non-Invasive Assessment of Sentinel Lymph Nodes That Drain the Tumoral Mammary Glands in Female Dog

Florin Gheorghe STAN

Faculty of Veterinary Medicine, University of Agricultural Sciences and Veterinary Medicine, Calea Mănăştur, 3-5, Cluj Napoca, Romania
*corresponding author: florin.stan@usamvcluj.ro

Bulletin UASVM Veterinary Medicine 73(2) / 2016,
Print ISSN 1843-5270; Electronic ISSN 1843-5378
DOI:10.15835/buasvmcn-vm: 12251

Abstract

Mammary gland tumours occupy a significant place in the pathology of this species. Female dogs that are not spayed after their first heat cycle have a higher predisposition of developing mammary tumours. Most tumours metastasize at distance via the lymphatic system. In these conditions, the sentinel lymph nodes of the mammary glands must be assessed prior to surgical treatment.

Considering the insufficient usage of non-invasive investigative methods of the sentinel lymph nodes, the aim of this study is to describe the sonographic anatomy of the lymph nodes that drain the mammary gland tumours in female dog.

Twelve dog females presenting tumours of the cranial and caudal abdominal mammary glands (A1 and A2), inguinal mammary gland (I) and cranial thoracic mammary gland (T1) were examined (group I). In addition, a control group composed of eight dog females was used (group II). The axillary and superficial inguinal lymph nodes were evaluated using an algorithm composed of gray-scale ultrasound, Doppler technique, contrast enhanced ultrasound (CEUS) and real time elastography. Surgical excision of the sentinel lymph nodes was performed and samples for histopathological examination were taken.

The following ultrasonographic findings revealed on gray-scale examination were suspected for the metastatic infiltration: hypoechoic pattern, round shape, hillus absence and heterogenicity. Doppler technique showed an aberrant and mixed vascularisation of the lymph nodes, while the CEUS revealed incomplete enhancement of lymph nodes parenchyma. On real time elastography, the presence of blue areas in more than 50% from the lymph nodes parenchyma led us to conclude that the lymph node stiffness was caused by metastatic infiltration. Histopathological examination confirmed the presence of the metastatic infiltration in 97% of the examined lymph nodes.

The algorithm composed of gray-scale ultrasound, Doppler technique, CEUS and real time elastography proved to be efficient in diagnosing the metastatic infiltration of sentinel lymph nodes of mammary gland. Further studies are needed to validate the proposed algorithm.

Keywords *ultrasonography, lymph nodes, female dog, mammary gland tumour*

INTRODUCTION

Neoplasia is a global reality, which is rapidly growing in many countries, both in human and veterinary medicine. In female dog, there is an increasing incidence of mammary gland tumour, one of four unsprayed female developing malignant disease (Cassali *et al.*,2014; Stan *et al.*, 2010). It is also important to note that a high number of practitioners, have reported in recent years the diagnosis of malignant melanomas and

lymphomas in veterinary medicine (Goldberg *et al.*, 2004, 2011), especially in pets. The status of regional lymph nodes is a well-known prognosis factor in most malignant tumours in both humans and animals, holding a major impact in choosing the therapy (Nyman *et al.*, 2005; Servais *et al.*, 2011).

Pre-therapeutic staging includes assessment of the extent of the neoplasm through the lymphatic system. The most important lymph node in assessing lymphatic dissemination is the so-called "sentinel lymph node" (Sever *et al.*, 2012; Stan *et al.*, 2010; 2012). Regarding the link between mammary tumour and regional lymph nodes, the reaction of potential lymph node, is related to tumour topography and the direction of lymphatic drainage (Stan *et al.*, 2012; 2013; 2014).

In recent years, non-invasiveness has become a major goal in malignant diseases, since the imaging methods are continuously developing (Alam *et al.*, 2008; Liu *et al.*, 2014; Rubaltelli *et al.*, 2014; Stan *et al.*, 2014). However, lymph node biopsy is currently considered the main procedure to investigate the status of lymph nodes (Sever *et al.*, 2012). Considering that the accuracy of biopsy is only 70-85%, depending on the size of the fragments collected, and it is influenced by errors of sampling and sample processing, there is a tendency of finding an alternate, non-invasive investigating technique for staging malignant disease. The most suitable in this way are the imaging techniques.

This study is fully justified, both from theoretical (establishing the criteria for non-invasive investigation of lymph nodes) and practical considerations (compiling an ultrasonographic diagnostic algorithm), due to many similarities (hormonal status, estrogens-dependent breast tumours) between the lymphatic drainage of the mammary gland (Cassali *et al.*, 2014; Stan *et al.*, 2012) and also the variability of this system in both humans and carnivores.

MATERIALS AND METHODS

The draining lymph nodes of mammary glands belonging to the twelve dog females presenting tumours of the cranial and caudal abdominal mammary glands (A1 and A2, n=4), inguinal mammary gland (I, n=6) and cranial thoracic mammary gland (T1, n=2) were examined. The selection criteria are listed below:

Inclusion criteria	Exclusion criteria
• Subjects with mammary gland tumours confirmed by clinical, imaging and histopathological examinations • Stable general conditions at study beginning • Owner consent	• Subjects with surgically treated tumours • Pregnancy • Unstable general condition

In addition, eight healthy subjects were used as control group. All subjects underwent a clinical examination to highlight the potential associated comorbidities. The axillary and superficial inguinal lymph nodes were evaluated using an algorithm composed of gray-scale ultrasound, Doppler ultrasound, contrast-enhanced ultrasound (CEUS) and real-time elastography.

Gray-scale ultrasound of superficial lymph nodes was performed with Logiq 9® (General Electric) using a multifrequency linear probe (8-12 MHz). Doppler, elastographic and contrast enhanced ultrasound examination modes were available, in either real time or post processing. The following characteristics of the lymph nodes have been assessed: shape, size, (transverse and longitudinal axes), capsule delimitation from adjacent tissues, lymph node parenchyma, ecostructure and ecogenicity and hilum ecogenicity.

Doppler ultrasound pursued the following: the presence of vascular signal in lymph nodes, vascular type (normal vs. altered) and vascular pattern (peripheral vs. central).

For CEUS a second-generation contrast agent (SonoVue - Barraco-Italy) was used in two steps:

1. The suspension was prepared in its original packing. A quantity of 0.4ml SonoVue was injected in the peritumoral area in four distinct points, followed by gentle massage of the injected area. The progression of the contrast agent was followed on the device's screen up the first lymph node, noting the anatomic region where it was found. Also, the time of progression was recorded and the parenchyma's aspect has been assessed.

2. After placing a peripheral venous catheter, an average dose of 0.6ml SonoVue/animal (0.6mlSonoVue/10kg BW) from the freshly

prepared suspension was administrated on the main route of the catheter. On the secondary route, 5 ml of physiological serum was injected. When the contrast injection was done, the ultrasound timer started and the pattern of the lymph node parenchyma in the arterial and venous phases was recorded.

Real-time ultrasound elastography evaluated the region of interest (ROI) around the lymph nodes. The colour-coded signals used for the evaluation of the stiffness of tissues (blue-very hard; red-very soft; yellow-soft; green-intermediate) were registered. This data was stored as digital picture files, and subsequently analyzed by using Adobe Photoshop® to estimate the amount of each colour in the ROI numerically.

In all subjects, a sample for histopathological examination was taken. Lymph node ultrasound guided biopsy was performed in healthy subjects. Surgical excision of the sentinel lymph nodes during the mastectomy in subjects presenting mammary tumours was performed and samples for histological examination were taken. Haematoxylin&Eosin staining was used.

RESULTS AND DISCUSSION

Forty-eight lymph nodes were evaluated. There have been recorded thirty- two lymph nodes in the malignant category, sixteen in the benign category.

Gray-scale ultrasound. Lymph node patterns were described according to Table 1, which shows the chosen parameters and corresponding scores for determining the lymph node pattern (malignant or benign). The gray-scale ultrasound characteristics used to differentiate between benign and malignant lymph nodes are illustrated in figure 1.

Doppler ultrasound used the following parameters: the presence of vascular signal in the lymph node, vascular type (normal vs altered), vascular pattern (central vs peripheral).

Tab. 1. Gray-scale ultrasound

Parameter	Characteristic	
	Benign	Malignant
S/L* ratio	< 0.5	>0.5
Echogenicity	Isoechoic/Hyperechoic	Hypoechoic
Echostructure	Homogenous	Inhomogeneous
Capsule features	Well defined with regular margins	Irregular
Hilum	Present, hyperechoic	Absent
Nr. of points	0	1

*S = short axis, L = long axis

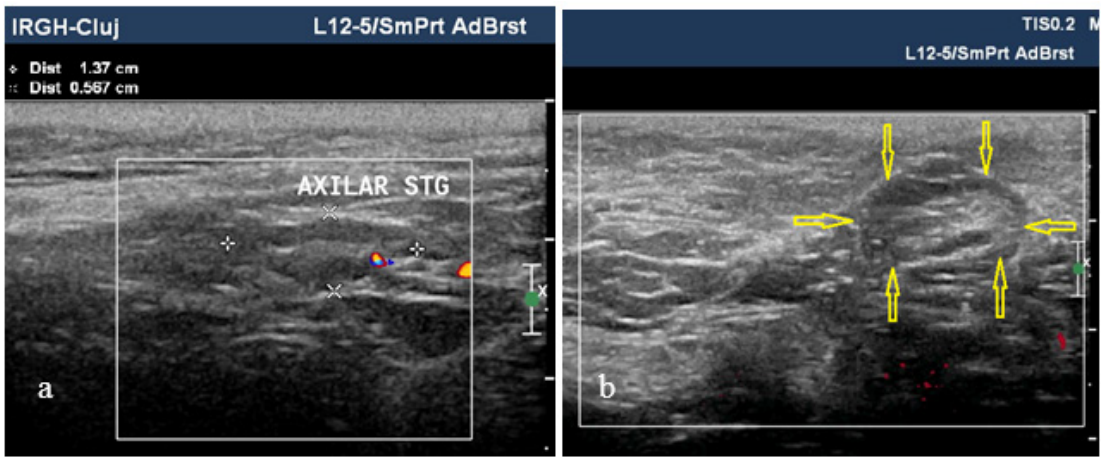

Fig. 1. Grey scale US of normal (a) and pathological (b) lymph node. a) Oval shape, well defined capsule and homogenous echostructure of normal lymph node; b) Rounded shape, irregular appearance of capsule and inhomogeneous echostructure of pathological lymph node - arrows.

Each pattern has a score specified in Table 2 and illustrated in figure 2.

Using **contrast enhanced ultrasound (CEUS)** two patterns of enhancement in sentinel lymph nodes were observed: complete enhancement and partial enhancement with the presence of perfusion defects. Contrast-enhanced ultrasound performed after peritumoral administration of 0.4 ml SonoVue in four points revealed the presence of hypoperfused focal areas of sentinel lymph nodes in eleven subjects from group I. After intravenous administration of contrast agent, the pattern of enhancement was analyzed in both groups. The results and score for each accomplished parameter are detailed in Table 3. The two pattern of enhancement are illustrated in figure 3.

On real time elastography, the colour-coded signals (blue-very hard, red-very soft, yellow-soft

Tab. 2. Color Doppler

Parameter	Characteristic	
	Benign	Malignant
Presence of hilar vascular signal	Present/Absent in lymph node<2mm	Absent
Pattern	Ordered	Chaotic/Unordered
Distribution	Radially from the hilum toward the capsule	Peripheral, subcapsular
Nr. of points	0	1

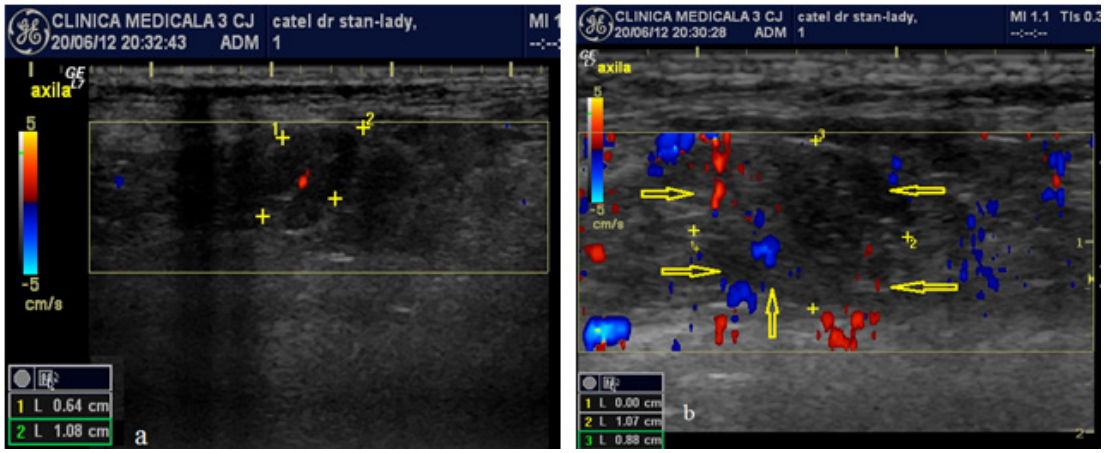

Fig. 2. Doppler US of normal (a) and pathological (b) lymph node. a) The presence of hilar vascular signal in axillary lymph node. b) Chaotic arrangement with peripheral distribution of the vessels in a metastatic lymph node.

Tab. 3. CEUS

Parameter	Characteristic	
	Benign	Malignant
a) peritumoral adm		
Enhancement	Complete, intensive	Incomplete, with areas without contrast agent
Type	Homogenous	Inhomogeneous
Distribution	Centripetal	Aberrant
b) IV adm.		
Enhancement	Complete, intensive	Incomplete with filling defects or absent
Type	Homogenous	Inhomogeneous
Distribution	Centrifugal	Aberrant, distribution delays
Nr. of points	0	1

green-intermediate) were interpretated according to the Table 4.

The result of the gray scale ultrasound and Doppler examination were interpretated as follows:

Number of points less than 4: the nodes were interpretated as benign – (n=16 lymph nodes).

Number of points ranged between 4 and 6 : the nodes were interpreted as uncertain followed by CEUS and real-time elastography (n= 10 lymph nodes).

Number of points more than 6: the nodes were considered malignant (n=32 lymph nodes).

Nowadays the ultrasound exam is the method of first choice in the evaluation of adenopathies by conventional techniques, namely the grey-scale ultrasound and Doppler techniques (Stan 2010; Stan *et al.*, 2012), along with CEUS – Contrast-Enhanced Ultrasound (Stan and Badea 2012). In these conditions, the ultrasound techniques are the diagnostic methods whose values were most often studied. These could indicate a change in the researcher's interest to use the non invasive techniques in lymph node assessment instead of conventional invasive methods. Gray scale ultrasound exam studies the diagnostic value of lymph node parenchyma ecogenicity, ecostructure, short to long axis ratio, hilar pattern and margins in both humans and animals (Dudea *et al.*, 2012; Whitman *et al.*, 2011). According to existing literature the two-dimensional ultrasound exam cannot make a real distinction between tumour-infiltrated lymph nodes (malignant ones) and inflammatory lymph nodes – which can be considered as beningn lymph nodes (Dudea *et al.*, 2012; Nyman *et al.*, 2005; Stan *et al.*, 2010). The performances improved by using Doppler ultrasound in evaluating the lymph vascularisation, but not enough (Furukawa *et al.*, 2007; Stan *et al.*, 2010, 2013).

Contrast-enhanced ultrasound (CEUS), has added a new dimension to diagnostic possibilities,

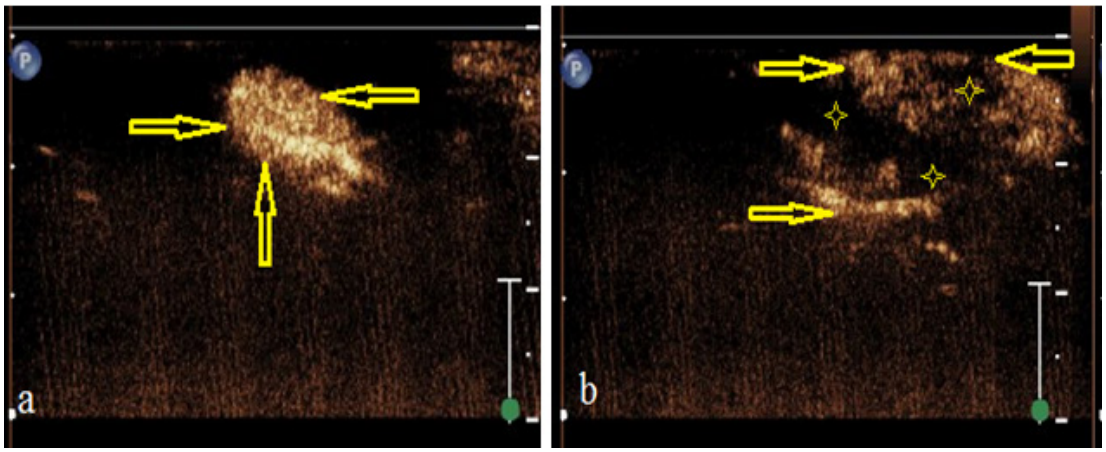

Fig. 3. CEUS of superficial inguinal lymph node. a) Complete, homogenous enhancement in normal lymph node. b) Arterial phase showed several nonenhancing areas within the sentinel lymph nodes of tumoral mammary glands: a hypoperfused mass-asterisks, surrounded by relative normal enhancing of lymph node parenchyma – arrows.

Tab. 4. Real-time elastography

Parameter	Characteristic	
	Benign	Malignant
Stiffness, Quantified by the software in colour nuances	a)The whole lymph node is soft, mostly green, yellow or turquoise b) >50% of lymph node is green, with presence of small yellow or turquoise hyperechogenous nodules c) < 50% of lymph node is blue	>50% of lymph node is blue >50% is blue except for some hyperechogenous nodules All lymph node is blue and/or shares the color with surrounding tissue Hard lymph node colored blue on the edges, with necrotic areas – green/red
Nr of points	0	1

by establishing an accurate diagnosis of focal lesions and trying to find its utility in assessing lymph nodes status (Goldberg *et al.*, 2004, 2005; 2011). By using the peritumoral injection of Sonaziod in 63 Sinclair swine with melanoma, Goldberg and al., (2011) stated the importance of this method in lymphatic mapping and its ability to localize the sentinel lymph nodes in cases of unpredictable drainage pathways. However, their results have shown that the differentiation between the benign and malignant lymph nodes was limited using only lymphosonography. Analysis of characteristic parameters of the method such as washing curves, transit times and quantifying the amount of contrast, improved the method, especially in describing the free lymph nodes (Stan *et al.*, 2014).

Another imaging technique is ultrasound elastography (real-time elastography), which quantifies the degree of tissue stiffness. Diagnostic methods based on this technique seem to be promising (Alam *et al.*, 2008; Das *et al.*, 2011; Lenghel *et al.*, 2012). In real-time ultrasound elastography, visualising the stiffness of the tissue requires transposition in colour mode, each colour signifying a level of stiffness. Thus, very hard tissues are represented by dark blue and intermediate shades of green, soft tissue are yellow and very soft ones are red. Evaluating this colours by using a special software, certain scores of elasticity can be calculated (Dudea *et al.*, 2012; Lenghel *et al.*, 2012). Based on four or five color-coded patterns of lymph nodes, an elasticity score was proposed for the metastatic lymph nodes of the head and neck in squamos carcinoma. Alam *et al.*, (2008) established five elastographic patterns of lymph nodes based on the distribution and percentage of hard areas (or high elasticity) in lymph node parenchyma; pattern 1 being an absent or very small hard area to pattern 5, in which the hard area occupied the entire node. In this study the cut-off line between benign and malignant lymph nodes was set between pattern 2 and 3. Recently, Lenghel *et al.*, (2012) report a very good specificity and sensitivity in the differentiation between malignant and benign lymph nodes using the combined gray-scale appearance and elastographic images. The elastographic score that also includes the structural changes was based on eight patterns (Lenghel *et al* 2012). Our study proposed an elasticity score of four patterns, trying to include the structural changes that indicated tumour infiltration too.

Currently, there is no standard of non-invasive lymph node staging in veterinary medicine. The current surgical approach by total excision of the lymph node without a prior investigation is an invasive procedure with potential risk of complications. It presents a high degree of intraoperative subjectivity and even errors in proper identification of the first lymphatic drainage station may occur. We consider that it is time to change the mainstream approach of tumour staging investigation in veterinary medicine with a non-invasive and less expensive alternative.

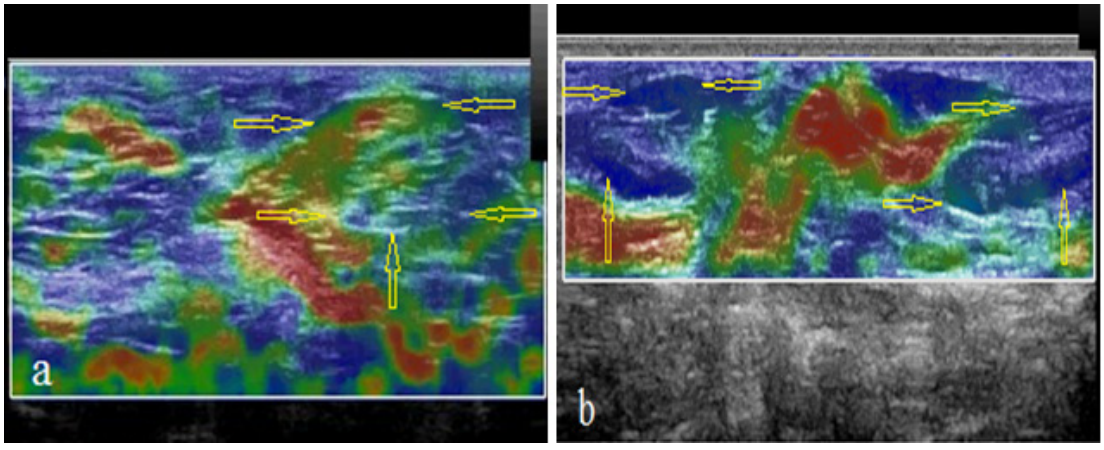

Fig. 4. Real time elastography of sentinel lymph nodes. a) Benign lymph nodes were mostly green; b) Hard lymph nodes revealed by the blue color present in all lymph node (the superficial inguinal lymph nodes) indicate the presence of metastatic infiltration.

CONCLUSIONS

The combination of the four ultrasound techniques used in the current study is a premiere. They were represented by: grey-scale ultrasound, Doppler ultrasound, contrast-enhanced ultrasound and real-time elastography. By using this algorithm, the metastatic infiltration of sentinel lymph nodes of mammary gland was assessed. These preliminary results are the first ones reported in veterinary medicine. Unfortunately, the statistical analysis is not relevant due to the low number of clinical cases, this being one of the major limitations of the proposed algorithm. Further studies are needed to confirm the accuracy of the diagnosis and to compare the results to those obtained by CT or MRI.

REFERENCES

1. Alam F, Naito K, Horiguchi J, Fukuda H, Tachikake T, Ito K. (2008). Accuracy of sonographic elastography in the differential diagnosis of enlarged cervical lymph nodes: comparison with conventional B-mode sonography. AJR Am J Roentgenol. 191:604-610.
2. Cassali *GD,* Lavalle GE, Ferreira E, Lima AE, De Nardi AB, Ghever C, Sobral RA , *et al.*, (2014). Consensus for the Diagnosis, Prognosis and Treatment of Canine Mammary Tumors. Brazilian Journal of Veterinary Pathology 7(2):38 - 69.
3. Das D, Gupta M, Kaur H, Kalucha A (2011). Elastography: the next step. J Oral Sci;53:137-141.
4. Dudea SM, Lenghel M, Botar-Jid C, Vasilescu D, Duma M (2012). Ultrasonography of superficial lymph nodes: benign malignant. Med Ultrason 14: 294-306.
5. Furukawa MK, Kubota A, Hanamura H, Fujita Y, Furukawa M (2007). Diagnosis of cervical lymph node metastasis of head and neck squamous cell carcinoma: usefulness of power Doppler ultrasonography and elastography. MEDIX (Suppl) :20–23.
6. Goldberg BB, Merton DA, Liu JB, (2004).Sentinel lymph nodes in a swine model with melanoma: contrast-enhanced lymphatic US. Radiology 230:727–734.
7. Goldberg BB, Merton DA, Liu JB, Murphy G, Forsberg F. (2005). Contrast-enhanced sonographic imaging of lymphatic channels and sentinel lymph nodes. J Ultrasound Med 24:953–965.
8. Goldberg BB, Merton DA, Liu JB, *et al* (2011). Contrast-enhanced ultrasound imaging of sentinel lymph nodes after peritumoral administration of Sonazoid in a melanoma tumor animal model. J Ultrasound Med 30:441–453.
9. Lenghel LM, Bolboaca SD, Botar-Jid C, Baciut G, Dudea SM. (2012) The value of a new score for sonoelastographic differentiation between benign and malignant cervical lymph nodes. Med Ultrason 14:271–277.
10. Liu JB, Merton DA, Berger AC (2014), Contrast-enhanced sonography for detection of secondary lymph nodes in a melanoma tumor animal model. J Ultrasound Med 33: 939-947.
11. Nyman, H.T., Kristensen, A.T., Skovgaard, I.M (2005) Characterization of normal and abnormal canine superficial lymph nodes using grey-scale B-mode, color flow mapping, power and spectral Doppler ultrasonography a multivariate study**.** Vet Radiol Ultrasound 46: 404–410
12. Rubaltelli L, Beltrame V, Scagliori E. (2014). Potential use of contrast-enhanced ultrasound (CEUS) in the detection of metastatic superficial lymph nodes in melanoma patients. Ultraschall Med 35: 67-71.
13. Servais EL, Colovos C, Bograd AJ, White J, Sadelain M, Adusumilli PS **(**2011**),** Animal models and molecular imaging tools to investigate lymph node metastases. J Mol Med (Berl) 89:753–769.
14. Sever, AR, Mills P, Weeks J, Jones S, Fish D, Jones P A, Mali W (2012). Preoperative needle biopsy of sentinel lymph nodes using intradermal microbubbles and contrast-enhanced ultrasound in patients with breast cancer. American Journal of Roentgenology 199(2):465-470.
15. Stan F, Gudea A, Baba AI, Feier D, Badea R (2012). Correlation between Ultrasonographic Features and Morphological Pattern after Blue Dye Injection of Normal Superficial Lymph Nodes in Carnivores. Bulletin UASMV Cluj Napoca 69 (1-2):211 – 219
16. Sta, F (2010). Power Dopler ultrasonography vs Color Dopler of the Sentinel Lymph Mammary Glands at Female Dog. Bulletin of University of Agricultural Sciences and Veterinary Medicine Cluj-Napoca. Veterinary Medicine 67 (1): 298-304.
17. Stan F, Damian A, Papuc I, Gudea A, Chirilean I, Dezdrobitu C, Bochis I, Crisan M, Abu Rock Ayman, Irimescu I, Tuns F (2010). The Importance of Ultrasonography in the Exploration of the Superficial Lymphatic System of Carnivores, Bulletin of University Agricultural Sciences and Veterinary Medicine Cluj-Napoca, Veterinary Medicine 67(1): 291-297.
18. Stan F, Badea R (2012). Morphological Identification of Lymph Node Vasculature Using Contrast Enhanced Ultrasonogaphy (CEUS). Bulletin of University of Agricultural Sciences and Veterinary Medicine Cluj-Napoca. Veterinary Medicine 69(1-2):197-203.
19. Stan F, Damian A, Gudea A, Dezdrobitu C, Delia Bob, Martonoș C, Lăcătuș R, Purdoiu R, Papuc I, Bochis I (2013). Normal anatomy of popliteal lymph center, anatomical variants and non invasive assesment using ultrasound techniques. Lucrări Științifice, Seria Medicină Veterinară, Iași 55(3-4): 373-380.
20. Stan F, Gudea A, Damian A, Papuc I, Bochis I, Pentea M (2014). Grey Scale Ultrasound, CEUS and Elastography to Asses Sentinel Lymph Nodes in Mammary Gland Neoplasia in Carnivores. Anatomia, Histologia, Embryologia, 43: Issue Supplement S1: 88.
21. Whitman GJ, Lu TJ, Adejolu M, Krishnamurthy S, Sheppard D (2011). Lymph node sonography. Ultrasound Clinics 6(3): 369-380.

The Institutional Bioethics Committee of University of Agricultural Science and Veterinary Medicine in accordance to Directive 2010/63 /EU of the European Parliament and of the Council on the protection of animals used for scientific purposes approved the study.

Bulletin UASMV, Veterinary Medicine, 69(1-2)/2012
Print ISSN 1843-5262; Electronic ISSN 1843-5378

Correlation between Ultrasonographic Features and Morphological Pattern after Blue Dye Injection of Normal Superficial Lymph Nodes in Carnivores

Florin STAN[1)], Alexandru GUDEA[1)], Alecsandru Ioan BABA[2)],Diana FEIER[3)], Radu BADEA[3)]

[1)] Department of Comparative Anatomy,
[2)]Department of Pathology, Faculty of Veterinary Medicine Cluj - Napoca, University of Agricultural Sciences and Veterinary Medicine, Cluj - Napoca, 3-5, Mănăștur Street, 400372, Romania, flodvm@yahoo.com;
[3)]Department of Ultrasonography, Regional Institute for Gastroenterology and Hepatology (IRGH), University of Medicine and Pharmacy "Iuliu Hatieganu", Cluj - Napoca, Croitorilor Str., No. 19-21, 400162, Cluj-Napoca, Romania, rbadea@umfcluj.ro

Abstract. The present study performs a description of ultrasound anatomy of superficial lymph nodes using gray scale ultrasound, Doppler techniques (color Doppler and power Doppler), compared with a morphological identification method - injection of coloring solutions (Blue Dye), with lymphatic tissue tropism. Eleven subjects were examined (nine female and two male). A total of 58 lymph nodes were assessed belonging to the axillary, superficial inguinal, popliteus, superficial cervical and submandibular lymph centers. Ultrasonographic criteria followed were: shape, size, echogenicity, ecotexture, capsule appearance, hiperecoic band of the hillum and angioarhitecture. For comparison, subcutaneous injection of Blue Dye Evans, 0.5% in 4 subjects was performed. Ultrasound examination detected right and left inguinal, and popliteus lymph nodes in all subjects, axillaries lymph nodes in 10 subjects, cervical superficial lymph nodes in 9 subjects and submandibular in 7 subjects. Normal lymph nodes present oval (fusiform) shape, with a corticomedullary homogenous ecotexture, well defined capsule. The ecogenicity was hypoecoic or isoecoic to the surrounding tissues, with a hiperecoic hilar band. The distribution of vascular flow within the lymph node, assessed by color Doppler techniques, was hilar in 78% of subjects. Power Doppler technique detected with high accuracy the presence of vascular signal in small lymph vessels. Subcutaneous injection of Blue Dye, identified in all subjects the axillary, inguinal superficial, popliteus and cervical superficial lymph nodes. Compared with Blue Dye, ultrasound examination revealed with about the same accuracy the lymph nodes, with 96% specificity and 87% sensitivity.

Keywords: lymph nodes, topography, ultrasound, Doppler ultrasound, blue dye Evans, anatomy

INTRODUCTION

Although technological progress takes its toll on methods for noninvasive investigation of human and animal body, in terms of lymphatic system a perceived shortage on its evaluation methods exists (Olivier, 2004). The lymphatic system is involved in many metabolic processes, immune response and tumor metastasis (Baba A. I., 2007). The in vivo evaluation of these components, vessels and lymph nodes is not easy and is not specific enough, in case of disease. Clinical examination and laboratory evaluation are nonspecific in lymphatic illness. Therefore it is necessary to know the normal aspects made by intravital noninvasive methods, to which pathology may be reported (Badea et al., 2006; Stan et al., 2005). Nowadays, in human medicine, ultrasound is the first method of intention, due to its noninvasiveness (Badea et al., 2010).

There are sporadic descriptions in literature of lymph nodes imaging in veterinary medicine. Compared to human, in which ultrasound is a method of first choice in lymphatic evaluation, veterinary medicine lacks this current practice.

In human cancers prognostic significance of lymph nodes metastasis is well known. Introducing the sentinel lymph node concept made a major change regarding both therapeutic and prognostic attitude (Badea et al., 2006). Furthermore, in recent years in woman breast cancers, histopathologic evaluation of presumptive metastatic lymph nodes is made by biopsy under ultrasound guidance (Frati et al., 2011). Thus, it's possible to avoid lymphoscintigraphy based on radiant products. Classical methods for identifying lymphatic system are based on using dye solutions and radiopharmaceuticals (Pereira et al., 2003). Most used dye solution was ink of China, isosulphan blue and blue dye Evans. The possibility of anaphylaxis if ink of China is used is high, therefore most researchers have conducted their studies on cadavers. Intravital evaluation of lymphatic drainage is made by lymphoscintigraphy using usually radiant ^{99}mTc sulphur colloid and a dye solution injected prior of lymphoscintigraphy. Separately, the two techniques do not provide sufficient accuracy in identifying the sentinel lymph nodes, but applied together an increased detection capability of sentinel lymph nodes is achieved.

Another subject of debate is the choice of site of dye or contrast injection (Frati et al., 2011). Patsikas and Dessiris made their own study regarding identification of healthy and neoplastic mammary draining lymph nodes using subareolar and peritumoral injection of ultrafluid lipiodol (Patsikas, M. N. and Dessiris, A., 1996). Perreira et al. have used both ink of China and 10% fluorescein, injected subareolar and in mammary gland parenchyma to identify the sentinel lymph nodes in the same condition (Pereira et al., 2003). All these researchers note that in condition of neoplastic disease of mammary glands, the pattern of lymphatic drainage is completed changed. Present research correlates two methods in describing the anatomy of superficial lymph nodes in carnivores. The morphological method is injection of blue dye Evans and the noninvasive imaging method is ultrasonography. Starting from the premise that both methods are addressed to superficial lymph nodes, and the fact that most researchers report a substantial increase of sentinel lymph nodes identification if two methods are used simultaneously, we hypothesized that ultrasonography and blue dye injection could make a better assessment on superficial normal lymph nodes of carnivores.

MATERIAL AND METHODS

The study was conducted on eleven subjects (nine female and two males) in two steps. The first part consisted in evaluation of superficial lymph nodes by ultrasound. Ultrasound was performed using a General Electric device, Logique 7, equipped with soft parts module.

A linear transducer with 7-12MHz frequency was used. Ultrasound approach was made taking into consideration the anatomical projections of superficial lymph nodes, respectively submandibular region, lateral cervical region in the middle third, axillary region, inguinal region, and popliteal region. The sections obtained were transversal and longitudinal dependent on lymph nodes location. Ultrasound examination was done in stunning, after acepromazine administration (1mg/kg/bw). Subjects were positioned in supine position. In cases where it was possible, ultrasound examination was performed after clinical palpation of lymph nodes. This was easy for popliteus lymph nodes, inguinal lymph nodes in tiny subjects, and if the thoracic limb could be easily pushed forward the palpation was possible for the axillary lymph nodes. Superficial cervical lymph nodes were palpated in three subjects. Both, manual palpation and

transducer palpation, was performed for lymph node identification in the local area to assess the consistency and lymph node relationship with surrounding tissues. To obtain a good visualization, a mechanical toilet was made followed by the application of an appropriate amount of ultrasound gel, for getting a good contact between transducer and skin surface.

Followed ultrasound criteria were: shape, size, by measuring the two axes: transverse and longitudinal, their report, echostructure, parenchymal echogenicity, lymph capsule appearance and hilum appearance. Doppler technique watched vasculature aspects by following criteria: presence of vascular flow, its lymph node distribution.

In the second part of this study, six subjects were injected using 0.5 % blue dye Evans solution. Since the superficial lymph nodes draining the mammary glands, and given their frequent pathology, blue dye injection was made both periareolar and in mammary gland parenchyma in four adjacent points: cranial, caudal, medial and lateral.

A total amount of 0.4ml blue dye Evans was injected, 0.1ml per injection point. Three subjects were injected in cranial thoracic and cranial abdominal mammary glands, and three other subjects were injected in caudal thoracic, caudal abdominal and inguinal mammary glands.

All injections were made under anesthesia. After injection, for easier penetration and diffusion of the dye in the lymphatic vessels, a slight massage of the injected area was made.Twelve hours later, after general anesthesia, the subjects' euthanasia was made and the stratigraphic dissection was performed. The following aspects were observed: lymphatic drainage of the injected mammary glands, their afferent lymph nodes, their size, macroscopic appearance after blue dye impregnation, location and number of lymph nodes that compound every lymph center.Ultrasound assessment results were compared with those obtained after blue dye administration.

RESULTS AND DISCUSSIONS

Ultrasound examination has been made to all the specimens on the superficial inguinal and popliteus lymph center without any difficulties. Superficial inguinal lymph center consisted of two lymph nodes at five subjects, three lymph nodes at four subjects and only one lymph node at two subjects. Popliteus lymph nodes were unique in the majority of the cases (nine subjects of eleven). The axillar lymph center was detected in ten cases of eleven, in six cases in its composition accessory and proper lymph nodes were found, and in four cases, it was composed only of one lymph node. Hence the superficial position and the caudal disposition from the inguinal mammary gland at 2-3 cm in front of the symphysis pubis, which most of the times was a reference of identification due to its hyperecogenous feature. Superficial inguinal lymph nodes needed a shorter detection time in most of the cases, compared with axillary lymph center. For the axillary lymph center, axillary accessory lymph nodes were easily detected when the thoracic limb was pushing forward because they are placed caudally by olecranon, right under the skin muscle of the thoraces. The olecranon was a point of reference.

At one, two or even three cm (in the case of two large sized subjects-one Rottweiler and one Pit-bull), ventrally from the origin of the thoracodorsal artery, with hypoecogenous feature and vascular signal, proper axillary lymph nodes were detected. The popliteus lymph center was detected in all the subjects due to its facile approach in the popliteal space. Transversal and longitudinal sections were achieved. Lymph nodes were detected in the popliteal conjunctive tissues placed on the descendant branch of the caudal femoral artery. At ultrasound examination, this artery had a hypoecogenous feature presenting a vascular signal at Doppler examination. In most of the cases (nine of eleven), the popliteus lymph center had one lymph node and in two

cases it had two lymph nodes. For the cervical superficial lymph nodes, approach was made on the median third of the neck, in the back side. The cervical superficial lymph node is placed in front of the supraspinatus muscle, close to the cervical superficial artery.

These lymph nodes are relatively easy to identify, if the cervical superficial area is appropriately prepared. They were identified at nine subjects, the majority being double (in seven of nine cases). The submandibular lymph center was identified by ultrasound in the submandibular triangle, ventral-caudaly from the angular process of the mandible. It was composed of two lymph nodes in four subjects and three lymph nodes in three subjects, right under the skin. In four cases, the submandibular lymph nodes were not detected. Caudaly by the submandibular lymph node, the parenchymal structure of salivary glands was detected. On ultrasound examination these glands have a homogenous ecostructure, lightly hyperecogenous compared with lymph node ultrasound pattern. Cranialy by these lymph nodes the facial vein was detected, with hyperecogenous pattern.

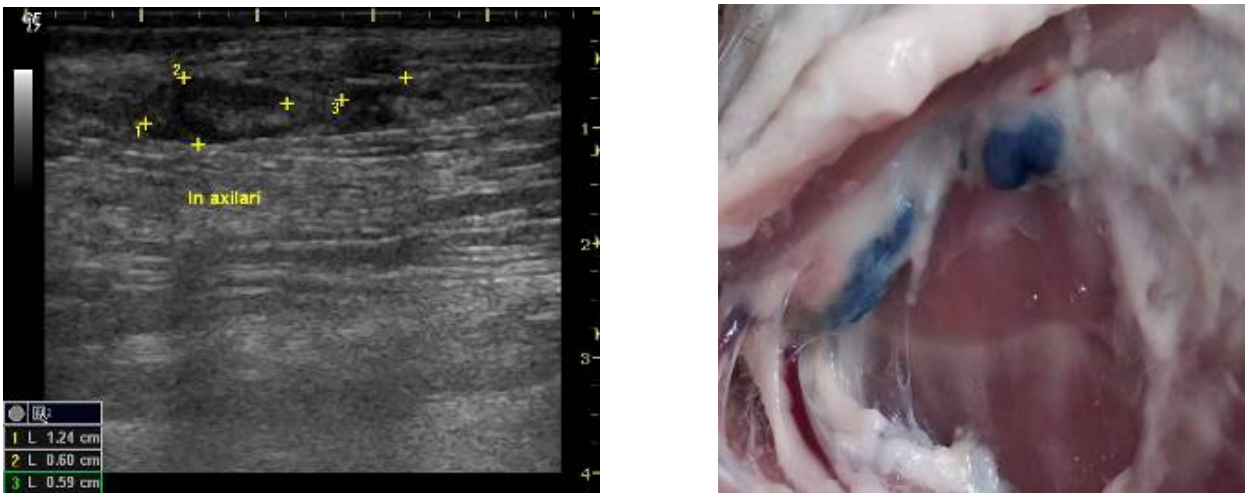

Fig. 1 Axillary lymph center composed by two lymph nodes and the macroscopic view after blue dye injection

The shape of axillary lymph nodes was oval, with a well-defined capsule which clearly delimits the lymph nodes from adjacent tissues. Lymph node parenchyma was homogenous, hypoecogenous or isoecogenous with surrounding tissues. Centrally, lymph node hillus appears linear, hyperecogenous and with a slightly bold aspect, corresponding to blood vessels and supporting fibrous pocket. Axillary lymph node dimensions were variable, determined by measuring the two axes: transversal (short axes) and longitudinal (long axes), ranging between 0.3 / 1.2 and 0.9 cm / 2cm. Ratio between short and long axis was in favor of the longitudinal (less than 0.5, average 0.48.). Same oval shape and composition of lymph center was detected after injection of blue dye solution.

Using ultrasound examination, superficial inguinal lymph nodes appear as a group, composed by two lymph nodes, oval in shape and dimensions ranged by 0,4/1,5 to 1,7/3,5cm, well defined by a smooth capsule and homogenous ecostructure. Size of lymph nodes were determined by measuring the two perpendicular axes, transverse axis (short), and longitudinal axis (long), as in axillary lymph center.

In the popliteal region the structures located posterior to the knee joint were imaged respectively: aponeurotic plane, adipose tissue, vascular-nervous package, popliteal lymph nodes.

Ultrasound image guidance presents some particularities resulting from specific ultrasound approach, in the popliteal space. In cross section, in the top of the screen posterior structures will be located and in the bottom of the screen anterior structures will be located. In longitudinal sections the image remains in the same orientation, but in the left of the screen cranial structures will be located and in right side those located caudal. Compared with axillar and superficial inguinal lymph nodes, popliteal lymph nodes present a less oval shape, axis ratio was between 0.49 and 0.65 (average 0.59), with the same sonographic features as in axillary and superficial inguinal lymph nodes.

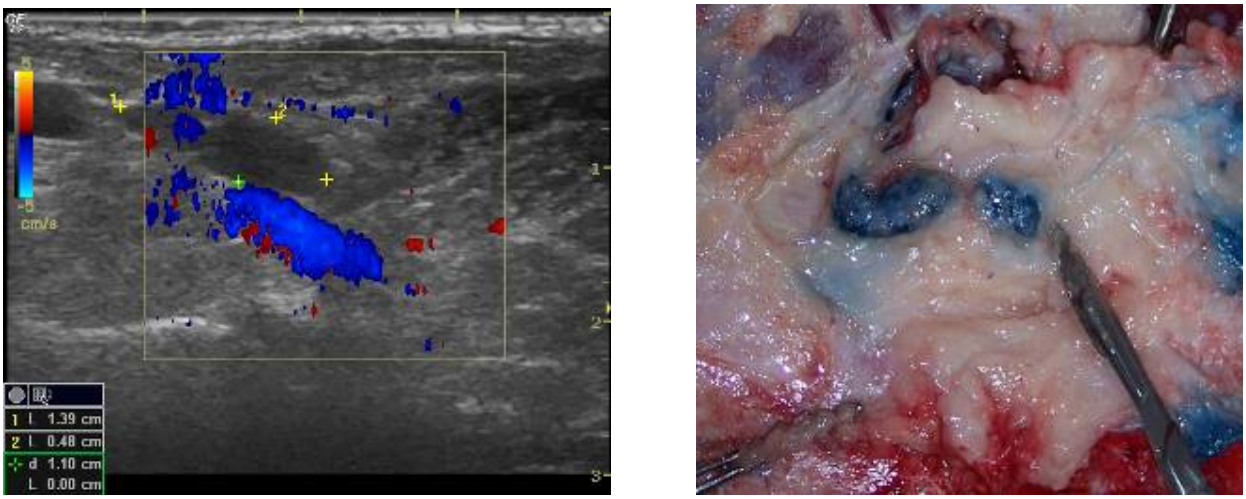

Fig. 2 Grey scale ultrasound of superficial inguinal lymph nodes and appearance after blue dye injection

Submandibular lymph nodes have dimensions between 0,55 / 1,4 cm, with an axis ratio below 0.5. They were found cranially by their enrollment next to the lingual vein, (which have an hypoecogenous feature) and salivary glands. Cervical superficial lymph nodes were rated on the same criteria as above described lymph nodes. Sizes ranged from 0,4 / 1,1 cm and 0,7 / 1,9 cm, with an axis ratio of 0.51. Ecostructure, echogenicity, characteristics of the capsule and hilum were framed in descriptions of other lymph nodes.

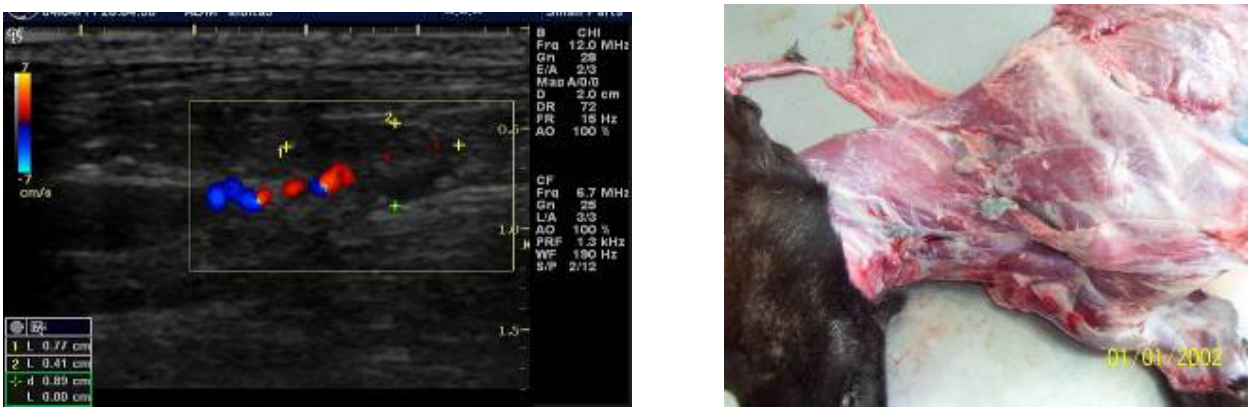

Fig. 3 Color Doppler technique on superficial cervical lymph nodes and their appearance after blue dye injection

Vasculature lymph nodes were assessed by ultrasound Doppler techniques. Information about the presence, direction and mode of vascular distribution into the lymph nodes was obtained. Thus, in lymph nodes bigger than 0.5 cm, vasculature was noted in 84% of lymph nodes, layout of the hilum, ordered toward the lymph nodes periphery.

Small lymph nodes, smaller than 0.5 cm showed no vascular signal (38% of cases). Easiest Doppler techniques were performed on the superficial inguinal lymph center. Power Doppler technique detected more accurately the vascular signals in small vessels of superficial inguinal lymph nodes, popliteus, and submandibular lymph nodes. This technique was applied with difficulty in the axillar lymph center.

Twelve hours later, a regional dissection was performed in order to visualize the lymphatic drainage of blue dye injected in mammary glands. According to it, lymphatic drainage of the mammary glands was performed in two ways: cranial and caudal by the axillary lymph center and superficial inguinal lymph nodes, dependent on the injected mammary gland.

Thus, cranial thoracic and abdominal mammary glands were drained cranial by axillary lymph nodes in five cases and in one case by axillary lymph node and superficial cervical lymph nodes simultaneously. In caudal direction lymph nodes were well impregnated with dye, superficial inguinal lymph nodes in all cases of the drainage of cranial abdominal mammary glands, and the inguinal one. Lymph node shape was oval having a well-defined capsule, crossed in 2-3 spots by afferent lymphatic vessels. In one case we saw a few lymphatic vessels crossing the white line establishing connections between contralateral superficial inguinal lymph nodes. No connections between healthy mammary glands on ipsilateral site were found. Popliteal lymph nodes and the submandibular ones were poorly impregnated with blue dye to a single subject.

In the present study it was demonstrated that the ultrasound can provide valuable information on normal appearance of superficial lymph nodes of carnivores. Lymph nodes are difficult to approach structures. Learning takes time and perseverance and not least experience (Badea et al., 2004, 2010). Description of a lymph node as normal or pathological requires knowledge about the region that it drains, their anatomical topography and normal appearance, and data on variability within the same species (Stan F., 2009). Being located in intermuscular connective spaces or embedded in adipose tissue, the difference in acoustic impedance is low. There are less echogenic interfaces and reflection is weak. Superficial lymph nodes evaluated in the present study belong to the lymphatic drainage of mammary glands in carnivores.

These were located in the subcutaneous tissue, relatively shallow, which facilitated approach on one hand, but on the other hand they were available only after adding the amount of ultrasound gel. Too superficial location presents its disadvantages in the examination process due to small surface that ultrasound must pass through. Aspect is related to the evaluation of submandibular lymph nodes. The most difficult to image were axillary lymph nodes due to their deepest position and embedding in adipose tissue, which echogenicity is similar to the lymph node. For deep located lymph nodes, ultrasound approach is hampered by tissue overlay, transmitted image quality also being affected. Deep located structures require long time for exploration and for each pulse ultrasonic reception.

In present study, lymph nodes shape was oval, elongated, axis ratio was <0.5 which corresponds with data obtained by other researchers (Mayer et al., 2010). In a study in which were compared normal and pathological lymph nodes, it was showed, that the ratio of the two axes is significantly increased in pathological lymph nodes, especially by increasing the value of short axis (DE Swarte et al., 2011). These researchers have found that inflammatory or metastatic

lymph nodes tend to be rounded, without being able to make a distinction between the two categories based solely on this criterion. In human medicine, in skin malignant melanoma and breast cancer, ultrasound is the method of first choice in evaluation and staging. Badea et al. have shown that lymph nodes ultrasound in metastatic disease provides important data for staging.

They showed that the shape, distribution mode of vascularization, echogenicity and ecostructure are profoundly changed (Badea et al., 2010; 2006). In our study only the normal lymph nodes were imaged. Their size was directly related to body weight.

Thus, the large lymph nodes were the superficial inguinal ones, axillary and at least the cervical superficial lymph nodes. Even in the same lymph center, size varies, depending on the number of lymph nodes that compose it (Stan et al., 2010; Stan, 2009), and the presence or absence of components: proper axillary lymph node was larger in the absence of accessory lymph node. Size of lymph nodes evaluated in the present study, was determined by measuring perpendicular axes, in accordance with the requirements of human medicine.

In the absence of diseases, ratio of the transverse and the longitudinal axis must be less than 0.5. In the absence of accessories, axillary lymph nodes have sizes between 0,5 / 1,4 cm up to 1/2, 5 cm, and the accessories when they were present, had dimensions of 0.2 / 0, 7 cm to 0,7 / 1,5 cm. This is due to the lymph nodes' need to drain from a large region. A correlation can be made from these determinations for the purposes of assessing lymph shape: ie. at ratio below 0.5 lymph node is oval shaped, normal, whereas increasing this value, tends to be rounded, which implies the presence of a disease. Lymph nodes visualized by injecting blue dye Evans showed the same size as the ultrasound assessment. Furthermore, as described at ultrasonography, oval shape was recovered at regional stratigraphic dissection (Stan et al., 2007; 2005)

Lymph nodes parenchyma evaluated in the present study was homogeneous, isoecogenous or reduced as compared with hillum or capsule lymph node echogenicity. Higher echogenicity in the hilum is the result of interlocking medullary sinuses at this level, each behaving as an acoustic interface, which partly reflects giving ultrasound hyperecogen appearance. Also, supporting conjunctive sheath has the same acoustic behavior. However, hilum echogenicity was determined in nine of eleven specimens.

In normal lymph nodes, echogenic capsule was delineating well the lymph nodes from the surrounding tissues, fact confirmed by dissection followed by ultrasound examination. Moreover, the fact that at regional dissection, lymph nodes were presented surrounded by adipose tissue, confirms the ultrasounds well visualization of lymph node capsule.

Lymph node vasculature was evaluated by applying Doppler methods. Applying this method in our study, we obtained dynamic images, focused and integrated on functional and anatomical criteria on blood flow characteristics: present of vascular flow and type into the lymph node distribution. The blood flow from the hillum, was noticed in 84% of examined lymph nodes. Hilum is actually normal blood vessel approaches, or in small lymph nodes, hilum is hardly detectable. It can be said in this context that normal lymph nodes vasculature may be more easily detected in larger nodes. In these lymph nodes, blood vessels were visualized at the hilum, with trajectory and direction toward the capsule, being parallel to the longitudinal axis of lymph node, or, parallel to skin surface. We can attribute this observation to the fact that normal superficial lymph nodes were evaluated in this study. Vascular signal was not detected in small superficial cervical lymph nodes and axillar accessories. This corresponds with data from the literature on human lymph nodes, upon which the vasculature of the hilum can be visualized only in node with transverse diameter greater than 5mm (DE Swarte et al., 2011; Mayer et al., 2010).

At power Doppler superficial lymph nodes evaluation, the color appearance of relatively large area image was based on high sensitivity of this technique, which was capable to detected much slower blood flow in small vessels compared with color Doppler technique. This technique has been applied successfully in the superficial inguinal and popliteus lymph node. In axillary, superficial cervical and submandibular lymph nodes, we encountered difficulties in applying this technique because their location near pulsation vessels, proximity of heart, and in case of axillary nodes respiratory movements which led to the unpredictable artifacts.

CONCLUSIONS

In this study we used as golden standard the morphological detection method of superficial lymph nodes by injecting blue dye solution. Basically, combining the two methods, imaging and morphological, we responded to the need for knowledge of normal feature of superficial lymph nodes in carnivores. As in human medicine, it is required to combine several methods to make a lymph node investigation. Ultrasound may be the method of first choice, because its noninvasiveness in lymph nodes evaluation. In veterinary medicine, cytological and histological assessment of presumptive pathological lymph nodes is made by surgical excision. Ultrasound guided biopsy can be easy and minimally invasive alternative in assessment of pathological carnivores lymph nodes.

REFERENCES

1. Baba A. I., 2007**,** Comparative Oncology, Editura Academiei Române, Bucureşti, 2007
2. Badea R, Crişan M, Lupşor M, Fodor L. Diagnosis and characterization of cutaneous tumors using combined ultrasonographic procedures (conventional and high resolution ultrasonography). Med Ultrason. 2010; 12(4): 317-322
3. Badea R, Andrei A, Cosgarea R, Avram B, Lupşor M, Ionescu I, Vasile T, Hica S, Antofie G. Aportul explorării ultrasonografice la diagnosticul şi stadializarea melanomului cutanat malign. Revista Romană de Ultrasonografie 2006; 8 (1-2): 9-20
4. Badea R., DudeaS., Mircea P., Zdrenghea A D., 2006, Tratat de ultrasonografie clinică, vol. 2. –Capul şi gâtul, toracele şi mediastinul, ecocardiografie, vasele membrelor. –Ed. Medicală Bucureşti, 2006.
5. Badea R., Dudea S., Mircea P., Stamatian F., 2004, Tratat de ultrasonografie clinică, vol. 1. -Principii, abdomen, obstetrică şi ginecologie.-Ed. Medicală Bucureşti, 2004.
6. DE Swarte, M., Alexander, K., Rannou, B., D'anjou, M.-A., Blond, L. and Beauchamp, G. (2011), Comparition of Sonographic features of Benign and Neoplastic Deeo Lymph Nodes in Dogs. Veterinary Radiology & Ultrasound, 52: 451–456. doi: 10.1111/j.1740-8261.2011.01808.x
7. Frati, Y. Delpech, A. Bricou, E. Barranger Détection du ganglion sentinelle chez les patientes atteintes d'un cancer du sein à un stade précoce : quel site d'injection en 2011 ?Gynécologie Obstétrique & Fertilité, Volume 39, Issue 11, Pages 620-623
8. Mayer MN, Lawson JA, Silver TI. Sonographic characteristics of presumptively normal canine medial iliac and superficial inguinal lymph nodes. Vet Radiol Ultrasound. 2010 Nov-Dec;51(6):638-4
9. Olivier – Lymphatic vasculature development, Nature Rev 2004, 4:35-45
10. Patsikas, M. N., Karayannopoulou, M., Kaldrymidoy, E., Papazoglou, L. G., Papadopoulou, P. L., Tzegas, S. I., Tziris, N. E., Kaitzis, D. G., Dimitriadis, A. S. and Dessiris, A. K. (2006), The Lymph Drainage of the Neoplastic Mammary Glands in the Bitch: A Lymphographic Study. Anatomia, Histologia, Embryologia, 35: 228–234. doi: 10.1111/j.1439-0264.2005.00664.x

Comparative Study of the Liver Anatomy in the Rat, Rabbit, Guinea Pig and Chinchilla

Florin Gheorghe STAN

Department of Comparative Anatomy, Faculty of Veterinary Medicine, University of Agricultural Sciences and Veterinary Medicine, Calea Mănăștur 3-5, 400372, Cluj Napoca, Romania
** corresponding author: florin.stan@usamvcluj.ro*

Bulletin UASVM Veterinary Medicine 75(1)/2018
Print ISSN 1843-5270; Electronic ISSN 1843-5378
doi:10.15835/buasvmcn-vm:002717

Abstract

In liver surgical and histological research, small rodents are the most used experimental models. Although the small animals liver is typically lobulated and its macroscopic appearance do not resemble that of the compact human liver, a high degree of lobulation equivalence, allow the use of small rodents in biomedical research. The macroscopic anatomy of the liver of the rat, rabbit, guinea pig and chinchilla was studied from a comparative standpoint. The topography, lobulation and the connection elements of the liver were examined by detailed in situ observation and explanted liver of forty specimens.

The rat liver (*Hepar*) consists of four distinct lobes of different size: the left lateral lobe - LLL (*Lobus hepatis sinister lateralis*), the median lobe - ML, the right lobe – RL (*Lobus hepatis dexter*) and the caudate lobe CL (*Lobus caudatus*). The largest lobe was the median lobe. The rabbit liver consists of five lobes: left lateral lobe - LLL, left medial lobe - LML (*Lobus hepatis sinister medialis*), right lobe - RL, quadrate lobe – QL (*Lobus quadratus*) and caudate lobe - CL. The most developed lobe was the left lateral lobe. The caudate lobe had a very narrow attachment on the hilar region. The guinea pig liver show six lobes: left lateral lobe - LLL, left medial lobe - LML, right lateral lobe – RLL (*Lobus hepatis dexter lateralis*), right medial lobe – RML (*Lobus hepatis dexter medialis*), quadrate lobe - QL and caudate lobe - CL. The largest lobe of this specie was the left lateral lobe. In chinchilla liver showed four lobes like in the rat. In the rats the most developed hepatic ligament was the falciform ligament (*Lig. Falciforme hepatis*) which spans from xyphoid process of the sternum and diaphragm to the liver, beginning at the interlobular fissure. The coronary ligament (*Lig. Coronarium hepatis*) was well developed in all rats. Interlobular ligaments connect the left lateral lobe with the upper caudate lobe. In rabbits, guinea pigs and chinchillas the connection elements were represented by the falciform ligament, coronary ligament, right (*Lig.triangulare dextrum*) and left triangular ligaments (*Lig. Triangulare sinistrum*), hepatorenal ligament (*Lig.hepatorenale*) and hepatoduodenal ligament (*Lig. hepatoduodenale*) with varying degrees of development.

Based on detailed study of the macroscopic anatomy of rat, rabbit, guinea pig and chinchilla a proper experimental model in liver research, could be assessed. In this regard, the vascular anatomy of the liver in the mentioned species is of a great importance and it is subject of another report.

Keywords: anatomy, experimental models, hepatic ligaments, liver lobes

Introduction

In recent years, mice and rats are the most used animals both in morphological and functional studies of the liver. Starting from the models used in experimental liver transplantation, anatomical and physiological studies, metabolic and immunological research, the area of interest has expanded in the field of regenerative and pathological studies. In this context, experimental lobar resections of the liver have been practiced on both healthy liver and liver tumors. Particularly of the rodents is that they have the same anatomical organization of the liver, in the sense that each liver lobe has its own pedicle containing a portal triad, namely the corresponding branch of the portal vein, its own biliary pathway and the

arterial branch (Popesco *et al.*, 1997; Stamatova *et al.*, 2012; Quesenberry et Carpenter, 2012). Due to this fact, lobar resections, more or less extensive (Madrahimov *et al.*, 2006) are possible. All these interventions requires a good understanding of the liver's macroscopic anatomy and its vasculature. Due to the facts that rats are the most commonly used in biomedical research because they are easy to maintain and their procurement is cheap, anatomical liver studies have been made most often on this rodent. The rat and chinchillas liver is described as having four main lobes: the right lobe (*Lobus hepatis dexter*), the medial lobe, the left lobe (*Lobus hepatis sinister*) and the caudate lobe (*Lobus caudatus*) (Martins and Neuhaus 2007; Stan 2013; Novak *et al*., 2015), while the guinea pig liver is divided into six lobes, the right and left lobes being subdivided in lateral and medial part (Breazile and Brown, 1976), topography determined by position on the falciform ligament (*Lig. Falciforme hepatis*) and median plane. Thus, the right lateral lobe (*Lobus hepatis dexter lateralis*) - RLL, the right medial lobe (*Lobus hepatis dexter medialis*) – RML, the left medial lobe (*Lobus hepatis sinister medialis*) - LML, the left lateral lobe (*Lobus hepatis sinister lateralis*) – LLL, besides the caudate lobe (*Lobus caudatus*) – CL and the quadrate lobe (*Lobus quadratus)* – QL, are described. An intermediate situation is encountered in the rabbit, in which the liver has five lobes, the right lobe being undivided (Barone, 1997; Stamatova *et al.*, 2012). Another distinguishing characteristic of rats compared to the other three species is the absence of gallbladder (Kongure *etv al.,* 1999; Martins and Neuhaus, 2007). Taking into account the fact that the rodents share the same ancestor with the lagomorphs on the one hand and on the other hand the rabbits are used as much as experimental models as the rodents, this anatomical study performs the comparative description of the lobes of the liver at rat, rabbit, guinea pig and chinchilla.

Materials and methods

Forty animals (ten of each species) were examined. Ten adult male Wistar rats (mean body weight 460±40g) provided from the UMF (University of Medicine and Pharmacy *Cluj*-Napoca) bio base, were used. Also, ten domestic rabbits (mean body weight 980±250g), ten guinea pigs (mean body weight 420±50g), and ten chinchillas (mean body weight 350±60g) were brought from breeding farms in the day of the examination. All animals received care according to the criteria outlined in the "Guide for care and Use of Laboratory Animals". The study was performed with approval of the Bioethics Committee of the University of Agricultural Sciences and Veterinary Medicine, Cluj Napoca. Euthanasia was performed by administration of an overdose of isoflurane (AErrane, Baxter, USA) in all animals. A midline incision of abdominal cavity was performed and the liver, its topography, and connecting elements were recorded. The hepatic ligaments were incised and the liver was extracted from abdominal cavity to be examined separately. Terms were used in accordance with NAV 2012.

Results and discussions

- Topography, borders surfaces and relations with adjacent structures

In the rats, the firm, smooth, dark red liver (*Hepar*) was placed on the cranial abdominal region, half of its volume being situated in the intrathoracic part of abdominal cavity (Figure 1A). It has a compact appearance and a central position, the caudal edges reaching approximately the same level on both sides of the abdominal cavity. On the right side, the caudal edge was made by the right inferior lobe and on the left side by the left lateral lobe. The diaphragmatic or parietal surface (*Facies diaphragmatica*) was smooth and convex, being mostly made by the medial lobes and by the left lateral lobe, and completely covered by the peritoneum. *In situ*, on this surface were visible three lobes: the median lobe, the left lateral lobe (*Lobus hepatis sinister lateralis*), and the right lobe (*Lobus hepatis dexter*). Between the caudate lobe (*Lobus caudatus*), caudal vena cava and the two layers of coronary ligament (*Lig. Coronarium hepatis*), a part of the liver was uncovered by the peritoneum, (*Area nuda*) being in direct contact with the diaphragm. The visceral surface (*Facies visceralis*) was deeply concave being in relation with the stomach, descending duodenum, pancreas, transverse colon and right flexure, spleen, right kidney and right suprarenal gland. With the exeption of the right kidney, that made the renal imprint (*Impressio renalis*), the mentioned structures did not leave visible imprints on the liver lobes. On the visceral surface,

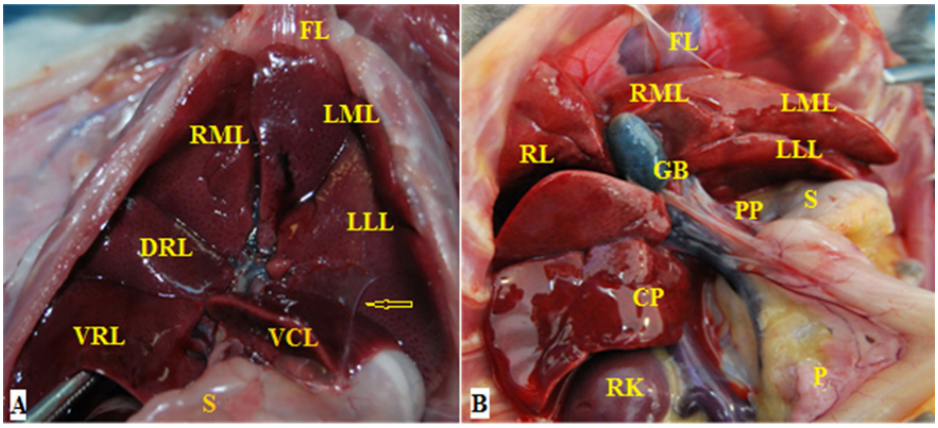

Figure 1. *In situ* visceral surface of the rat-A and chinchilla-B, liver.
LLL-left lateral lobe; LML-left medial lobe; RML-right medial lobe; DRL-dorsal right lobe and VRL-ventral right lobe; FL-falciform ligament; Interlobar ligament-arrow; S-stomach; RK-right kidney; P-pancreas; RL-right lobe; CP- caudate process; PP-papillary process;

covered almost completely by the peritoneum, four lobes were recognized.

In the rabbits, the red-brown liver was positioned almost in intrathoracic part of abdominal cavity. The diaphragmatic surface (*Facies diaphragmatica*) was convex applied on the diaphragm and the visceral surface (*Facies visceralis*) was concave, moulded on the convexity of the stomach (Figure 2C). On the diaphragmatic surface three lobes were visualized, namely two left lobes and one right lobe. Visceral surface show five lobes, separated by deep fissures. The dorsal margin (*Margo dorsalis*) was almost transversally positioned in the manner in which the left lobes of the liver reach the same level as the right lobe. The right margin (*Margo dexter*) is deeply hidden under the hypochondrium and only the caudate process reaches the level of the last rib. The ventral margin (*Margo ventralis*) extends in the epigastric region, stretching between the two costal arcs, up to the level of the seventh rib to the right, and the ninth rib to the left.

In the guinea pigs, two thirds of the red-brown, smooth liver was located in the intrathoracic part of abdominal cavity. It was multilobulated having deep fissures (Figure 2D). Concav diaphragmatic and convex visceral surfaces were noted. On the diaphragmatic surface four lobes were visualized while on the visceral surface six lobes were identified. The visceral surface was in relation with stomach, duodenum, right colic flexure, pancreas and right kidney. The ventral margin of the gallbladder exceeds the ventral border of the liver. On the visceral surface the gallbladder was attached to its fossa (*Fossa vesicae felleae*), between the right medial lobe and quadrate lobe.

In chinchillas, as in guinea pigs, two-thirds of the liver mass was situated in intrathoracic part of abdominal cavity (Figure 1B). Diaphragmatic concave surface showed three lobes, while the convex visceral surface showed four main lobes. The visceral surface was in contact with stomach, duodenum, duodenal lobe of the pancreas, jejunum, and right kidney. It has a light brown colour and a smooth appearance.

- **Liver lobes and hepatic ligaments**

In the rats, the liver presented four lobes: left lateral lobe - LLL, middle or median lobe - ML, right lobe - RL and caudate lobe – CL, of varying sizes. Except for of LLL the rest of the lobes presented subdivisions (Figure 3A).

The left lateral lobe – LLL, occupied the left part of the epigastric region and the left hypochondriac region. It has no subdivisions. The free part of this lobe was placed ventral to the stomach, covering two third of the stomach, cranial to the caudate lobe and slightly dorsal to the middle lobe. Its medial part was covered by the left middle lobe but the dorsal part of the lobe lies in close relation with the diaphragm. It has an oval shape and has no fissures. The left lateral lobe presented a narrow pedicle bound with the intrahepatic cava vein and a small base attached to the left median lobe.

The middle lobe of the rat liver – ML, was the largest lobe of the liver. It was located just under the diaphragm, and makes a large part

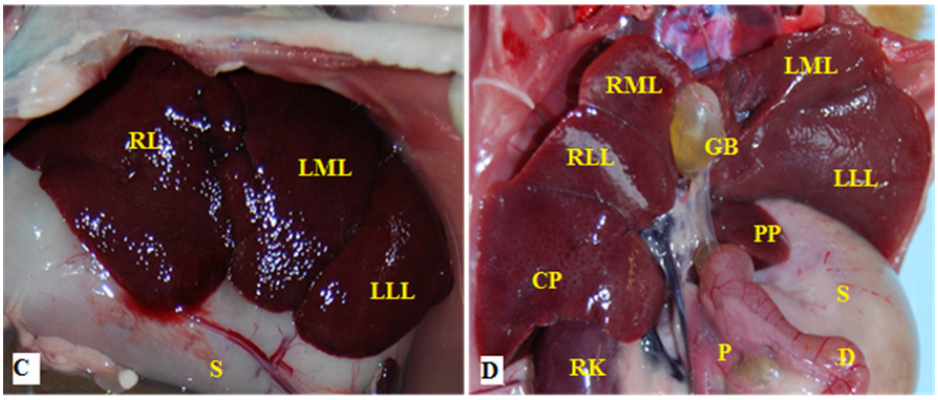

Figure 2. *In situ* liver of the rabbit-C and guinea pig-D.
LLL-left lateral lobe; LML-left medial lobe; RL-right lobe; RML-right medial lobe; RLL-right lateral lobe; CP-caudate process; PP-papillary process; QL-quadrate lobe; GB-gallbladder; RK-right kidney. S-stomach; P-pancreas; D-duodenum;

of the parietal surface. A deep fissure (the main fissure or umbilical fissure, divides the lobe in two portions: a small left middle lobe - LML and a large right middle lobe - RML. The ratio between the two middle lobe divisions was 1:3. The left middle lobe was bound with left lateral lobe. A large base of the middle lobe surrounded almost entire circumference of the cava vein.

The right lobe – RL, was divided by a deep horizontal fissure into two small overlapped portions: the dorsal - DRL, or superior, right lobe and the ventral - VRL, or inferior, right lobe. The two right lobes were located on the right side of the cava vein. On the parietal surface the right lobes were almost completely covered by the right middle lobe. The dorsal right lobe has a large base. The ventral right lobe shows an obvious renal imprint.

The caudate lobe was located ventral to the left lateral lobe, on the left part of the cava vein. A small paracaval portion of the caudate lobe surrounded the cava vein making the connection between the caudate lobe and the ventral right lobe. The proper caudate lobe (or Spiegel lobe) was split into two portions, one as ventral caudate lobe - VCL or anterior, and a dorsal portion as dorsal caudate lobe - DCL or posterior caudate lobe. The VCL has a narrow pedicle, and it lies on the ventral surface of the stomach, being covered by the ventral layer of the lesser omentum. The DCL lies on the dorsal surface of the stomach being in close relation with the gastric lobe of the pancreas and with the spleen. Also, the DCL was covered by the dorsal layer of the lesser omentum.

The falciform ligament was complete in all subjects, making the attachments of the liver with the diaphragm and ventral abdominal wall. In its free margin, the round ligament (*Lig. teres*) was present. The coronary ligament has two layers: the upper layer and the lower layer. The upper layer extended from the upper margin of the bare area to the diaphragm. The coronary ligament was continued on the right side by the small right triangular ligament. This ligament connected the right margin of the DRL to the diaphragm. The left triangular ligament connected the dorsal part of the parietal surface of the left lateral lobe to the diaphragm. Between the LLL and the DCL an obvious interlobular ligament was present.

In all examined rats the caudal cava vein has an extended intrahepatic path.

The gallbladder was absent, usually each lobe being drained by its own bile duct. The common bile duct was formed by the union of the main hepatic ducts.

In the rabbits, the liver presented five lobes: the left lateral lobe - LLL, the left medial lobe - LML, the right lobe - RL, the caudate lobe - CL and the quadrate lobe - QL (Figure 4C). In rabbit the right lobe was single, while the left lobe was subdivided in left lateral and left medial lobes. Almost the half of left lateral lobe was covered by left medial lobe, the first one being entire visualized on the visceral surface. On the lateral edges, the left lateral lobe showed small incisures, less numerous and smaller on the other lobes. The right lobe had an oval shape, twice long as wide and covered the half of the left medial lobe on the diaphragmatic surface. The caudate lobe was well

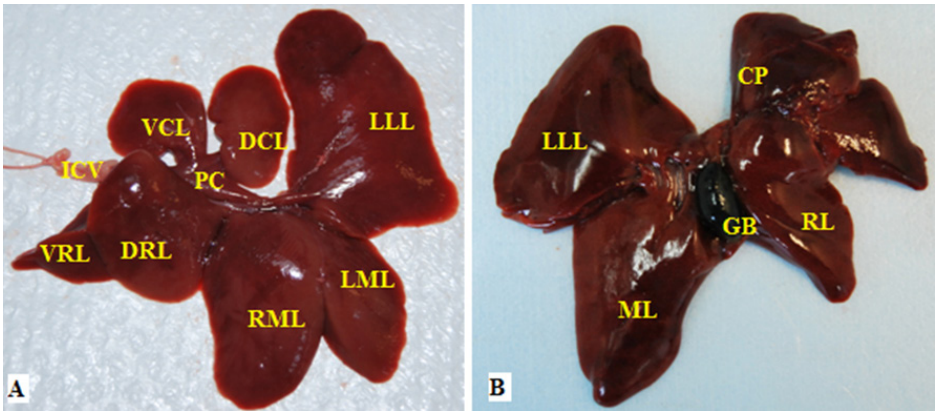

Figure 3. The rat – A and the chinchilla – B liver lobes.
LLL – left lateral lobe; LML – left middle lobe; RML – right middle lobe; DRL- dorsal right lobe; VRL – ventral right lobe; ICV – inferior cava vein ligated; PC – paracaval portion; VCL – ventral caudate lobe; DCL - dorsal caudate lobe. In chinchilla, the notch of the middle lobe - ML and the divisions of the right lobe - RL are not shown in this picture. CP – caudate process;

developed having a narrow attachment on the hilar region. The caudate lobe was divided into two parts: the caudate process (*Processus caudatus*) and the papillary process (*Processus papillaris*). The caudate process exceeds the right liver lobe and shows an obvious renal imprint. The papillary process was rounded in rabbit. The quadrate lobe was small, less visualized, being attached to the gallbladder fossa.

Regarding the hepatic ligaments in rabbit, the absence of the round ligament (*Lig. teres*) was noted. The falciform ligament starting from hillus, was large but very thiny on its insertion on diaphragm and was found in all rabbits. In eight rabbits the right triangular ligament was small, being attached to the right lobe of liver near the caudate process. We noticed the presence of a well developed left triangular ligament extended from the left lateral lobe to the diaphragm in all rabbits. The hepatorenal ligament connected the right lobe of liver to the right abdominal wall having a long parietal insertion.

The gall bladder lies in a deep depression of the caudal surface of right lobe, had cylindrical shape, its ventral border did not exceed the ventral edge of the liver.

***In the guinea pigs*,** the liver showed six lobes: the right lateral lobe - RLL, the right medial, lobe - RML, quadrate lobe - QL, left medial lobe - LML, left lateral lobe - LLL and caudate lobe - CL (Figure 4D). The most developed lobe was the left lateral lobe. This lobe showed no incisures as in rabbits, only a small incision on the lateral edge of the left lateral lobe was noted. The quadrate lobe was well defined in the left side of gall bladder. The rounded shape of gall bladder exceeded the ventral border of the liver. The gall bladder was attached to a fossa on the quadrate lobe and showed an obvious swelling on the beginning of the cystic duct. The caudate process was well demarcated showing the right kidney imprint. The papillary process has triangular shape and was subdivided by a deep cleft in two small segments. Regarding the liver connection elements, in guinea pigs, the presence of a large falciform ligament which connects the diaphragmatic margin of quadrate lobe to xiphoid process of the sternum, extending backward to the ventral abdominal wall, was visualized. The position of this ligament indicates the line division of the liver into right and left territories. The dorsal extremity of falciform ligament was continued by a conspicuous coronary ligament, like a short circular fold, connecting the dorsal border of the liver with the middle aponevrotic region of the diaphragm. Also, a small bare area was present. The left triangular ligament, a lateral continuation of the coronary ligament on the left side, was present in all subjects, connecting the left lateral lobe of the liver with the diaphragm. Regarding the right triangular ligament, this structure was present in seven subjects. The hepatoduodenal ligament was made by the lesser omentum passing from the lesser curvature of the stomach and from the duodenal ampulla to the visceral surface of the liver. In its thickened margin on the right side three important structures were identified, namely the common bile duct, hepatic artery and portal vein. Also, a free edge of this

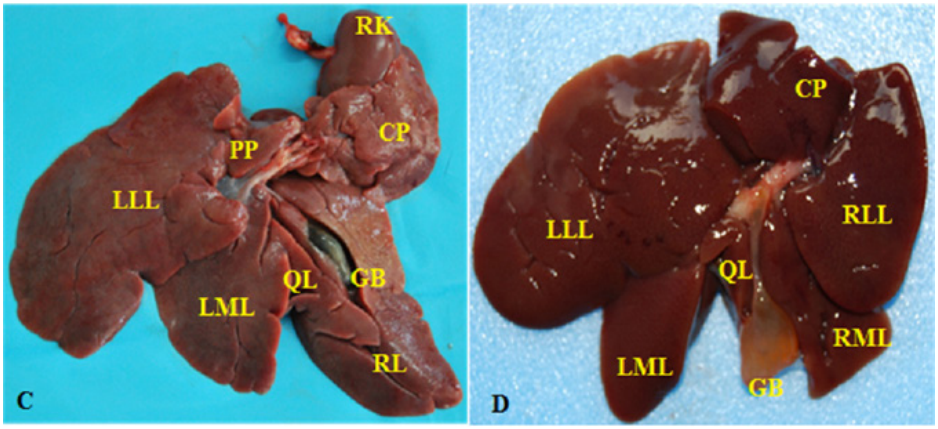

Figure 4. Visceral surface of the rabbit-C and guinea pig-D liver.
LLL-left lateral lobe; LML-left medial lobe; RL-right lobe; RML-right medial lobe; RLL-right lateral lobe; CP-caudate process; PP-papillary process; QL-quadrate lobe; GB-gallbladder; RK-right kidney.

ligament with cranial insertion on the cystic duct, has descended along to the common bile duct to make the caudal insertion on the duodenal lobe of the pancreas. Gastrohepatic ligament was well individualized connecting the lesser curvature near to the right side of the esophagus with the papillary process of caudate lobe. The hepatorenal ligament has a particular insertion. Cranial insertion of hepatorenal ligament was visualized on the ventral border of the caudate process, then glide down medial to the ventral surface of the right kidney and on the ascending duodenum.

In the chinchillas, the liver showed four distinct lobes: the left lateral lobe – LLL, the middle lobe - ML, the right lobe - RL and the caudate lobe - CL. The LLL was unique without divisions (Figure 3B). It has an oval shape, its visceral surface covering the stomach fundus and the ventral surface of this organ. The ML was the largest lobe being subdivided into two portions: a largest left middle lobe (LML) and a smaller right middle lobe (RML). The RL was divided into two pyramidal parts: a lateral part and a medial part. The caudate lobe or Spiegel lobe was well developed. The larger caudate process located at the right side of the cava vein has a wide renal imprint and the small papillary process was located on the small curvature of the stomach. On its base the caudate lobe was attached to the left lobe.

The falciform ligament connected the middle lobes with the diaphragm extending to the level of the umbilicus. The coronary ligament was very small and the left and right triangular ligaments were almost untraceable. The wide hepatoduodenal ligament contained a system of parallel bile ducts which opens at several points in the proximal duodenum.

The oval shape gallbladder has been visualised on the visceral surface, sitting on its fossa on the delineation between the right middle lobe and the right lobe of the liver, its ventral border being covered by the right lobe.

In scientific literature there are numerous descriptions of the gross anatomy of the mammalian liver, but most of them lack of in situ presentation and pictures. This paper performed a thorough description of the macroscopic anatomy of the liver of the most common small animals used in liver research in order to provide comparative macroscopic anatomical details of the liver of the rats, rabbits, guinea pigs and chinchillas. Also with a great importance in liver comparative studies, especially in surgical approach, is the liver vasculature, but this aspect is subject of another ongoing research.

The most studied model in liver research is undoubtedly the rat. Its liver macroscopic anatomy was rated as being closest to the human liver anatomy. Kongure *et al.*, (1999) have compared the rat and humans livers, showing that the divisions of the rat liver correspond to the human liver segmentation made by Couinaud (1994). However, differences exist, and were pointed out by the Martins and Neuhaus (2007). Among them and in concordance with this research are those related to the macroscopic anatomy. The rats liver is multilobulated, divisions of the lobes are distinct, and the left and right territories has approximately the same volume, the gallbladder is absent, while human liver is compact, the lobes

have no clear external divisions, the gallbladder is present and the left territory is smaller than the right territory (Martins and Neuhaus, 2007). Moreover, the fact that each lobe has its own pedicle containing a portal triad, makes the rats the most suitable animal models in liver surgical research.

Between rats, rabbits, guinea pigs and chinchillas there are numerous similarities and differences. The similarities are related to the division in two main territories, the right and the left territory with approximately the same sizes in mentioned species. This aspect is less mentioned in anatomical studies cited (Nowak *et al.*, 2015; Stamatova *et al.*, 2012; Pérez *et al.*, 2005; Pérez and Lima, 2007). Using as delineation landmark the falciform ligament, in this report, the lobes were delimited as right lobes and left lobes.

However, in rat in chinchilla, the middle lobe was shared of both territories, but in rats the right middle lobe was largest compare to the smallest right middle lobe in chinchillas.

The liver surfaces are the same in most of mammals: parietal and visceral surfaces. In rats, the diaphragmatic surface was continued with a surface in direct contact with the diaphragm, aspect mentioned by the Martin and Neuhaus too. The degree of convexity of the diaphragmatic surface was less pronounced in rabbit, due to the presence of a voluminous cecum in this specie.

The rat liver is multilobulated as in other mammals (Barone, 1997) and lobes nomination is made after portal vein ramifications (Couinaud, 1994; Kongure *et al.*, 1999; Martins and Neuhaus, 2007). Our macroscopic assessment is similar with the mentioned authors. However, the rat liver divisions are differently interpreted by various authors due to a great individual variability (Madrahimov *et al.*, 2006; Popesco *et al.*, 1990). In this report, the caudate lobe and the right lobe subdivisions have been named according to the veterinary medicine nomenclature, after their dorsal or ventral position corresponding to the superior or inferior denomination of other authors (Kogure *et al.*, 1999; Madrahimov *et al.*, 2006; Martin and Neuhaus, 2007).

Commonly in rodents there are described four liver lobes: left, right, caudate, and middle lobe (Quesenberry, 2012).). In rabbits subdivision of the left lateral lobe into left lateral and left medial parts and the presence of quadrate lobe pointed out the presence of five lobes (Barone, 1997; Stamatova *et al.*, 2012). In the guinea pigs the presence of deep notches between the lobes lead to the identification of six distinct lobes, which is similar to those reported by Cooper and Schiller (1975), Breazile and Brown (1976). In chinchilla, the presence of four lobes was reported by the Novak *et al.* (2015) too, but they don't mention a clear division of the caudate lobe.

Regarding the hepatic elements, the present report described in all mentioned specie the presence of the five hepatic ligaments, with variable degree of development (Stan, 2013, 2014). The most constant was the falciform ligament, which was complete in rats, guinea pigs and chinchilla, being reduced at hepato-diaphragmatic part in rabbits (Barone, 1997). A noteworthy aspect is the presence of an interlobular ligament in rats, between dorsal caudate lobe and left lateral lobe, pattern which was described by the Madrahimov (2006) too.

Conclusion

The present study shows that an accurate knowledge of the morphology of the liver in experimental models underpins the achievement of safely experimental surgery, organ transplantation and training in liver research.

Acknowledgments. This research did not receive any specific grant from funding agencies in the public, commercial, or not-for-profit sectors.

References

1. Barone R (1997). Anatomie comparée des mammifères domestiques Tome 3. Splanchnologies I. Appareil digestif et respiratoire. Edition Vigot, (pp. 507-559).
2. Breazile JE, Brown EM (1976). Anatomy. In: J. E. Wagner & P. J. Manning (Eds.), The Biology of the Guinea Pig (pp. 53–62). New York: Academic Press.
3. Cooper G, Schiller AL (1975). Anatomy of the Guinea Pig. Cambridge (Mass.): Harvard University Press, (pp. 417).
4. Couinaud C (1994). The paracaval segments of the liver. J Hepatobiliary Bil Pancreat Surg, 2: 145–151.
5. Kongure K, Ishizaki M, Nemoto M, Kuwano H, Makuuchi M (1999). A comparative study of the anatomy of the rat and human livers. J Hepatobiliary Pancreat Surg, 6: 171–5.
6. Madrahimov N, Dirsch O, Broelsch C, Dahmen U (2006). Marginal Hepatectomy in the Rat: From Anatomy to Surgery. Annals of Surgery, 244: 89–98.
7. Martins P N, Neuhaus P (2007). Surgical anatomy of the liver, hepatic vasculature and bile ducts in the rat. Liver Int, 27: 384–392.

8. Nowak E, Kuchinka J, Szczurkowski A, Kuder T (2015). Extrahepatic Biliary Tract in Chinchilla (Chinchilla laniger, Molina). Anat Histol Embryol, 44: 236–240.
9. Pérez W, Lima M (2007). Anatomical Description of the Liver, Hepatic Ligaments and Omenta in the Coypu (Myocastor coypus). International Journal of Morphology, 25: 61-64.
10. Pérez W, Möller R, Martin E (2005). Peritoneal Folds of the Rabbit (Oryctolagus cuniculus). Anatomia, Histologia, Embryologia, 34: 167–170.
11. Popesko P, Rajtova V, Horak J (1990). A Colour Atlas of the Anatomy of Small Laboratory Animals, Volume One: Rabbit and Guinea Pig. London: Wolfe Publishing
12. Quesenberry Katherine Carpenter JW (2012). Ferrets, Rabbits and Rodents: Clinical Medicine and Surgery. (3th ed.). St. Louis, Missouri, USA: Elsevier.
13. Stamatova-Yovcheva K, Dimitrov R, Yonkova P, Russenov A, Yovchev D, Kostov D (2012). Comparative imaging anatomic study of domestic rabbit liver (*Oryctolagus cuniculus*). Trakia Journal of Sciences, 10:57-63.
14. Stan F (2013). Comparative Study of the Stomach Morphology in Rabbit and Chinchilla. Agro Life Scientific Journal, Bucuresti, Romania, 2: 73-78.
15. Stan F (2014). Topographical anatomy of guinea pigs kidneys. Scientific Papers Veterinary Medicine Timisoara, XLV: 114-123.

MORPHOLOGICAL PARTICULARITIES OF THE TEETH CROWN IN GOLDEN JACKAL (Canis aureus moreoticus)

Article · January 2016

CITATIONS
0

READS
323

1 author:

Florin Stan
University of Agricultural Sciences and Veterinary Medicine
32 PUBLICATIONS **57** CITATIONS

SEE PROFILE

Scientific Works. Series C. Veterinary Medicine. Vol. LXII (2)
ISSN 2065-1295; ISSN 2343-9394 (CD-ROM); ISSN 2067-3663 (Online); ISSN-L 2065-1295

MORPHOLOGICAL PARTICULARITIES OF THE TEETH CROWN IN GOLDEN JACKAL (*Canis aureus moreoticus*)

Florin STAN

University of Agricultural Science and Veterinary Medicine Cluj-Napoca, Faculty of Veterinary Medicine, Calea Manastur No. 3-5, 400372, Cluj-Napoca, Romania

Corresponding author email: florin.stan@usamvcluj.ro

Abstract

A thorough understanding of dental and oral anatomy is essential for a proper recognition of all members of the carnivore species and to recognize the various signs of disease. As long as the golden jackal spreading in Eastern Europe is steadily increasing, this study aims to present a detailed description of morphological features of golden jackal dental anatomy in order to be used in clinical practice and research. The anatomical crowns of the teeth from superior and inferior jaws of seven golden jackals were examined. The complete dental formula for the permanent dentition in golden jackal is I 3/3 C1/1 PM4/4 M2/3 x 2=42teeth. The inferior dental arch is anisognathic, narrower and shorter compared to the superior dental arch. The superior incisors are located slightly rostral from the inferior incisors. Their size increases from the central to the lateral incisors, each incisor crown showing a prominent cingulum and three tubercles. The canine teeth were similar in length and width, having a simple crown. The first premolar is the smallest on both dental arches, having one tubercle, while the second and third premolars have in addition a small distal tubercle. The superior forth premolar and the first inferior molar form the carnassials tooth. The superior carnassial has three distinguishing lobes: paracone, metacone and protocone. The upper molars have a short, wide and highly rough anatomical crown. The inferior carnassial is the strongest tooth with a three-lobed pattern. Inferior molars are smaller than those of the superior arch. The morphology of the crown of the golden jackal teeth is similar to that described in dogs.

Key words*: teeth crown, golden jackal, dentition.*

INTRODUCTION

The golden jackal is the most typical member of the genus Canis, having a medium size and no outstanding features. Despite to its phenotypic and genotypic features the golden jackal resembles the grey wolf and coyote rather than the black-backed jackal, side-striped jackal and Ethiopian wolf. Because of this, the most frequent comparisons were made with wolfs. Nevertheless, in scientific literature, there are few anatomical reports of various anatomical systems of the golden jackal, and a detailed morphological description of it has not been made. Compared to wolves, the golden jackals'projections of the skull is less developed. Even though the canine teeth are large and strong, they are thinner than wolfs' and the carnassials are weaker. Its relatively short facial region, weaker teeth row are related to the jackal's diet, composed of small birds, rodents, small vertebrates, insects and carrions. Denied carrion or prey, it feeds on fruits and seeds. This eating behaviour has imposed the occurrence of certain specific characteristics of the dentition. Every tooth, no matter its form and function has the same elements. The structures are crown, enamel, cementum, dentin, pulp, root and periodontal ligament. Anatomical crown is the part of the tooth that is occlusally located to the dentino-enamel junction, or the portion of the dentin of a tooth that is covered by enamel. The clinical crown is the portion of a tooth that is above the gingival margin or the exposed part of a tooth within the mouth. In the present study has been performed a detailed description of the clinical crown of the teeth in golden jackal in comparison with the domestic dog. Domestic dogs possess a heterodont, a diphyodont dentition with anelodont and brachyodont teeth (Evans and De Lahunta 2013). Compared to dogs, horses have hypsodont teeth (Konig et al. 2014). Rabbits have heterodont, diphyodont, with all teeth being elodont (aradicular hypsodont) (Quesenberry and Carpenter 2012, Stan 2014). Those three examples are the most representative among animals. The dental

formula for primitive carnivores consists of 44 teeth (three incisors, one canine, four premolars and three molars in each quadrant) but the evolved carnivore's dentition shows several adaptations to diet (Evans and de Lahunta, 2013). Domestic dog's teeth have short crown, covered only by a thick layer of enamel, obvious neck and long roots covered by cement (Barone 1997).

MATERIALS AND METHODS

Seven adult golden jackals (*Canis aureus moreoticus*) were examined, four male and three female. The subjects were hunting harvest, being part of an ongoing study of the anatomical description on various systems in golden jackal. The oral cavity and teeth were examined before and after exposure of the oral cavity. To expose the oral cavity, an incision was made on each side, starting from lips commissure, in horizontal line and parallel to the mandibular arch, followed by a vertical incision, along the recurved mandibular branch. The entire study was conducted in accordance with the Protocol on Medical Ethics and in compliance with the Directives 63/2010 of the European Parliament and of the Council on the Protection of Animals Used in Scientific Research.

RESULTS AND DISCUSSIONS

The particular anatomical configuration of the viscerocranium in jackal gives the oral cavity a long and narrow appearance (Figure 1). The wide oral slit, starting from the oral angles reaching close to the carnassials.

Figure 1. Viscerocraniumof the golden jackal with elongated appearance of the oral cavity. Wide oral slit exceeds the carnassials plan-arrow

The dental formula contained 42 teeth in all subjects:

$$I:\frac{3}{3};\ C:\frac{1}{1};\ P:\frac{4}{4};\ M:\frac{2}{3}=21\times 2=42.$$

There were no differences in shape, number and disposition between the dentition of males and females. In dogs, Lorber et al. (1979) found differences between male and female canine crown, male having longer and wider canine crowns.

Generally, in mammals the shape, position and even number of teeth can differ according to age, breed and subject (Barone 1997). Thus, canines have 32 decidual and 42 permanent teeth. In diphyodont mammals the variations of number and shape are obvious, especially regarding the decidual and permanent dentition.

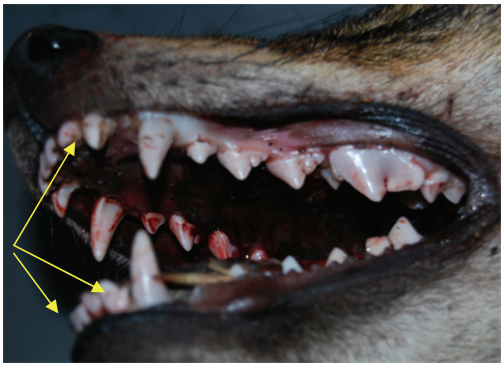

Figure 2. The short incisors crown compared with the large crowns of the majority of the teeth

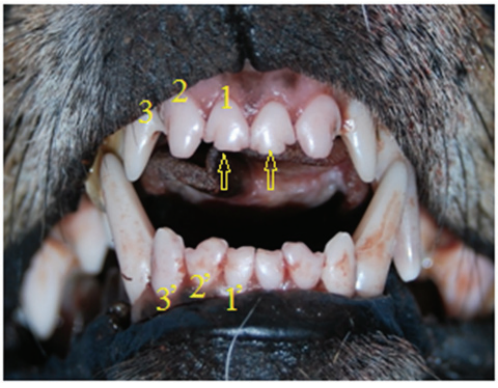

Figure 3. The short incisors crown with central prominent lobe, visible on the central incisors-arrows. Their size increased from central-1 to middle-2 and lateral-3 incisor teeth.

In canines, when the first premolar is considered deciduous, the dental formula is as follows:

$$i:\frac{3}{3};\quad c:\frac{1}{1};\quad \mathrm{m}:\frac{4}{4}=16\times 2=32,$$

In studied subjects, the incisor teeth (*Dentes incisivi*) had a short crown (*Corona dentis*) compared to the large crown of the premolar and molar teeth (Figure 2 and 3). More developed on the superior arch, their size increased from the central to lateral incisor, being rostral slightly arched (Figure 4). Their crowns were flattened and laterally compressed, heavilyfixed. The oclusal border (*Margo occlusalis*) of the crown has shown three salient cusps (lobes), the middle one being more prominent (Figure 4). The smooth vestibular surface (*Facies vestibuaris*), convex in all directions was slightly narrowed towards the neck of the teeth (Figure 4).The lingual surface (*Facies lingualis*), slightly swollen near the neck (*Cervix dentis*) showed a strong girdle (*Cingulum*) in all subjects. Its extremities from the base of the cuting edge were more obvious and formed on each side a small tubercle. The cingulum concavity delimited a small recess which subdivided the large prominent central tubercle. This tubercule was disposed along the cutting edge.The large contact surfaces (*Facies contactus*) from the incisor neck show a sharp reduction before their ending on the cingulum extremities. The oclusal border, like a delicate pointed arch (ogive), was surrounded at its base

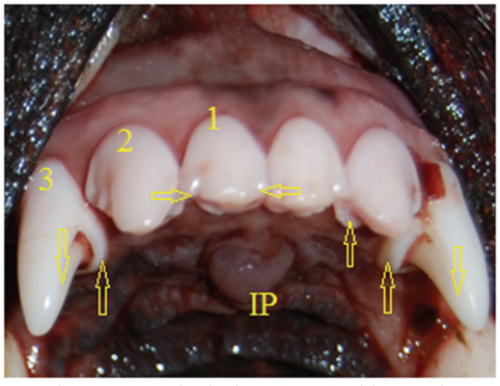

Figure 4. Superior incisors (1,2,3) with smooth, convex appearance of vestibular face. Strong cingulum on the lingual side-up arrows delineated two tubercles on its extremities-horizontal arrows, and a long, narrow central lobe of the lateral incisors-down arrows. IP-incisive papilla

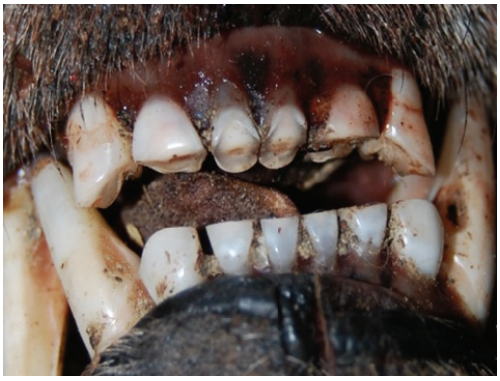

Figure 5. The tooth wear starting from the central lobe of incisors leave the occlusal surface, thick and straight. Note the obvious reduction of the crowns starting from the middle incisors and stump appearance of teeth

by the two tubercles that marked the end of the cingulum (Figure 4). These tubercles were separated from the central cusps by a small notch.Therefore, this three-lobed appearence, with a prominent central lobe like a „clover" shape or like a „lily flower" is similar with the pattern described in canines (Evans and de Lahunta 2013). This disposition announces the three tubercules pattern of the premolars and molars. The incisors neck was well marked in all subjects.

In older subjects (2 subjects) it was noticed a conspicuous wear of the teeth (Figure 5). The wearing was started primarily on the cutting edge of the central lobe (on the ogiva), which was shortened up to the two tubers on the edges (Figure 5). In this way, the occlusal edge

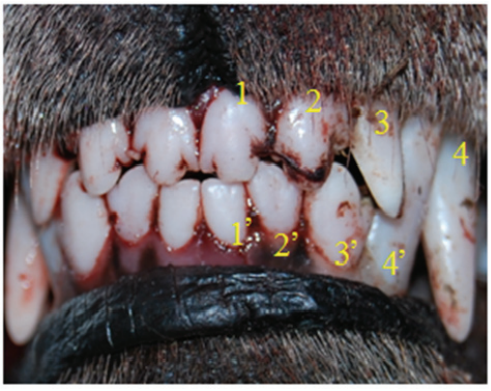

Figure 6. Superior incisors (1,2,3) are located rostral to the inferior incisors (1', 2', 3'). The superior canine tooth (4) is separated by lateral superior incisor by an interdental space, matching the inferior canine tooth (4'), in scissor like appearance

became straight and thick, the “lily flower” disappeared and the levelling appeared. The crown was strongly reduced, taking the form of a stub, the incisors distancing themselves from one another. Gums also suffered a marked process of retraction, emphasizing the appearance of stump incisors. The wear was most evident on the central incisors, progressing towards the middle and the lateral incisors (Figure 5). The wear process described here is similar to that of carnivores (Evans and de Lahunta 2013). There were few differences of size, pattern and disposition between the superior and inferior incisors. Regarding the incisors dimensions, the central were smaller than the middle, which in turn were smaller than the lateral. The obvious difference was shown on the upper jaw. Upper incisors were almost two times stronger than those of the same rank from the lower arch (Figure 4, 5 and 6). Prominent cingulum and stronger central lobe, well separated from the marginal lobes, were well defined characteristics, especially at the central incisors. The lateral incisors showed a long and sharp central lobe in absence of the distal lobe; resembling somewhat and in a small way, the canine pattern. In the occlusion of the arch the lower canine is positioned slightly distal and opposite from the superior lateral incisor.

The upper incisors exceeded rostrally to the lowers, so that, during occlusion, the sharp edges of their lingual surfaces are positioned over the vestibular surface of the lower incisors (Figure 6 and 7). Also, from the superior lateral incisor to the superior last premolar, the upper and lower teeth alternate in their disposition in the dental arch. This type of dentition is called "scissor" dentition and is described especially in dogs (Evans and de Lahunta 2013). Moreover, the central incisors only partially cover their counterparts and the adjacent parts of the inferior middle incisors. In turn, the middle superior incisors cover the occlusal edge of the two inferior lateral incisors. The superior lateral incisors were placed between the inferior lateral incisors and inferior canine teeth, a small diastema separating them from the upper canines. The dolichocephalics canine breeds retain this disposition, while brachiocephalic breeds have a marked inferior prognathism, in which the superior incisors and canines are placed more at varied distances behind their counterparts, reducing their effectiveness of cutting (Barone 1997, Verstraete and Tsugawa 2015). On each jaw, the dental arches (A*rcus dentalis superior et Arcus dentalis inferior*) described an arc, the upper one being wider and stretched compared to the lower jaw arch. The inferior dental arch showed a deeper curvature, was narrower and shorter compared to the superior arch.

Canines (*Dentes canini*), or "fangs" as they are called, were highly developed, conical shaped, having a distal (caudal) and concave tilting. Compared with the incisors, canine’s neck was less marked (Figure 8). The vestibular surface was convex and smooth. The lingual surface was crossed by a lingual groove limited by a

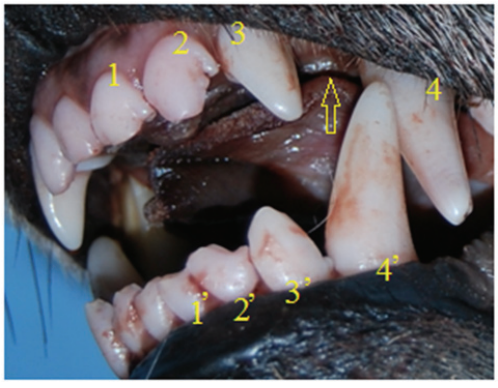

Figure 7. The crown of superior lateral incisors-3, are largest and slightly hooked caudally similar with the next canine tooth. A small *diastema*-arrow, separated the lateral superior incisors from the canine teeth

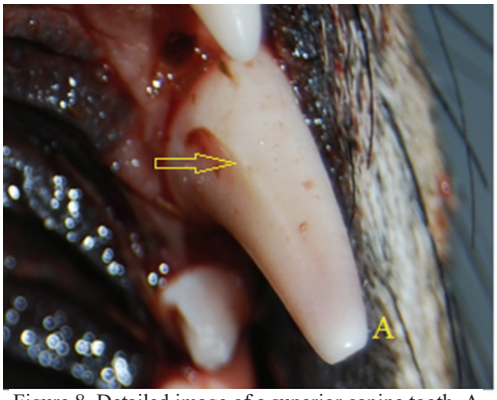

Figure 8. Detailed image of a superior canine tooth. A small ridge on the lingual side-arrow delineates a reduced groove. Note the conned shape, distally oriented and rounded apex-A, of the canine tooth

small ridge at the edge of its mesial surface (Figure 8).The superior canines appeared stronger than the lower ones, their roots being twice as long as the crown. On the distal edge, near the cingulum the canines' circumference was visibly increased. The canines were less titled on the vestibular surface, their crown being less outwards inclined. In occlusion, the lower canine is placed in front of the upper canine, which in turn, sits next to a small diastema. This diastema separates the lower canine from the first premolar (Figure 9).

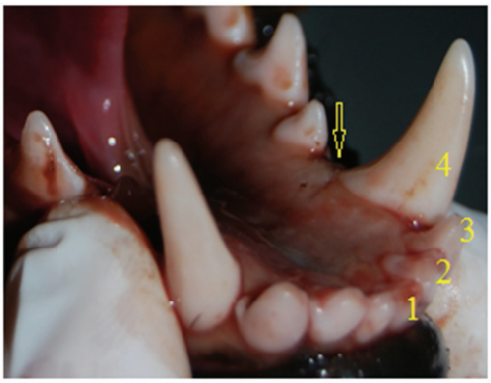

Figure 9. A small *diastema* separate the inferior canine tooth-4, from first premolar tooth-arrow

According to the anatomical rule, on each arch the premolars (*Dentes premolares*) and molars (*Dente smolares*) were classified in mesio-distal direction (rostro-caudal) in: precarnassials, carnassial or sectorius (*dentes sectorius*) and postcarnassial or tuberculosis teeth (Figure 10). Thus, the last upper premolar tooth will be described as upper carnassial and the first lower molar tooth as lower carnassial tooth. These teeth were the largest shearing teeth on both dental arches. These characteristics are similar to those of domestic dogs (Barone 1997, Evans and de Lahunta 2013). Except the last two molars, due to their blade like pattern, slicing and chapping function, on each arc all teeth have achieved a perfect secodont type of dentition. In dogs, deciduous dentition includes on the upper jaw, besides the incisors, two precarnassials, the carnassial and one postcarnassial or tuberculosis tooth. The lower jaw includes three precarnassials and one carnassial tooth (Barone 1997). In the deciduous dentition the first premolar is sometimes described as a precursor, lacking the permanent tooth (Verstraete and Tsugawa 2015), but in accordance with this paper, rather it should be considered a persistent deciduous tooth (milk) continuing in the permanent dentition. The rest of the teeth resemble the shape and disposition as in adults, but are smaller, sharper, having narrower cusps. Their occlusion is as in adults.

The permanent dentition of the golden jackals from the present study included six cheek teeth (premolars and molars) on each superior quadrant and seven cheek teeth on each inferior quadrant (Figure 10). The first three premolar teeth are the precarnassial teeth. The first was smallest with a simple, pointed crown, whose lingual surface shows a small cingulum and a reduced distal lobe (Figure 11). The next two premolar teeth, larger than the first, slightly

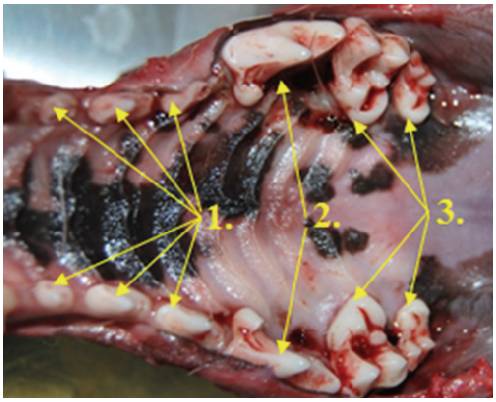

Figure 10. The upper precarnassials-1, carnassials-2 (premolars) and postcarnassials (molars)-3 teeth. Note the strong development of the carnassials and postcarnassials teeth

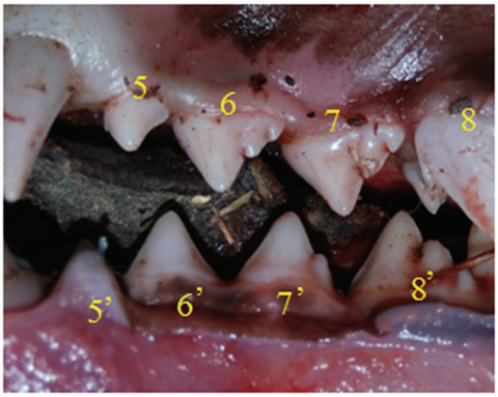

Figure 11. Upper-5,6,7 and lower 5', 6', 7', 8' premolar teeth (precarnassials). The last upper premolar-8 is the carnassial or sectorial tooth

flattened and compressed laterally show three lobes: a prominent intermediate lobe, a short and slightly detached mesial lobe and a long distal lobe (Figure 11). The last precarnassial tooth has a prominent cingulum and a well delineated distal tubercle (Figure 12).

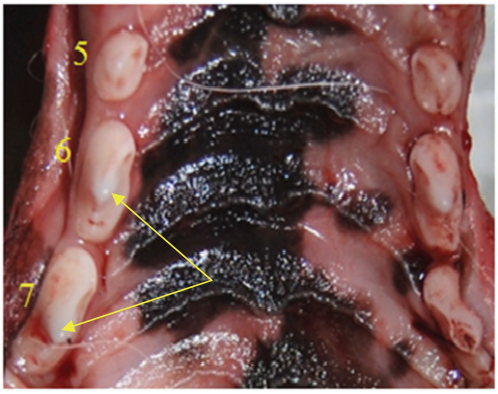

Figure 12. A small, simple crowned of the first upper precarnassial and a well developed intermediate lobe-arrows, of the last precarnassials-6,7

The superior carnassial (or the last premolar tooth) was the stongest tooth on the quadrant. (Figure 13). Three lobes were identifyed: two of them were stronger, being the tooth body, the mesial lobe, named *paracone,* being more prominent than other lobes. The mesial lobe was connected by a sharp ridge to the distal lobe, named *metacone*, which was smaller than the mesial lobe. The third lingual lobe, named *protocone,* was like a reduced, accessory lobe which was connected to the base of the main lobe (paracone) by a girdle or a small crest (Figure 13).

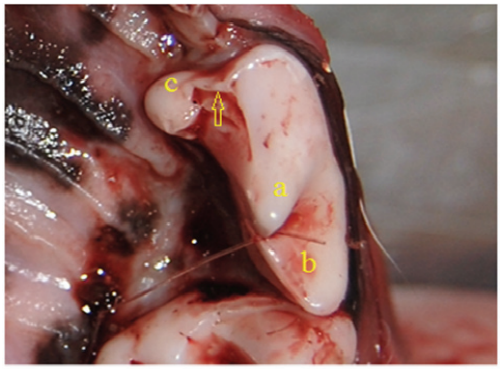

Figure 13. The upper carnassial. a-the mesial lobe (paracone); b-the distal lobe (metacone); c-the lingual lobe (protocone) connected by a small ridge to the base of paracone-arrow

The last two upper molars (or postcarnassial teeth) were well developed (Figure 14). Their crown, short and wide, very rough, was much more developed in the transverse direction than inthe mesio-distal direction. The first postcarnassial tooth (or tuberculosis tooth) was longitudinally shorter than the carnassial, but more developed transversally. Its crown was bordered by a girdle (cingulum), which was extended up to the vestibular surface at the base of two vestibular cusps (Figure 14). Of the two cusps, the mesial one, named *paracone,* was taller. On the lingual surface the cingulum inflated to form a large and short rounded lingual lobe, named *protocone.* Its occlusal surface was subdivided in small tubercles among which the heels of the lower carnassials tooth, affront.

The last postcarnassial tooth (or last molar), was smaller, the two vestibular cusps being reduced and the lingual lobe, *protocone,* being slightly larger, but less mamelonated (Figure 14).

The lower precarnassials were the four lower premolars (Figure 15). The first premolar, like its superior counterpartbut smaller than it, presented a cingulum too and a reduced distal tubercle. The following precarnassials were larger. Their crowns were three-lobed, presenting like the superior premolars, a stronger distal lobe (metaconid) extended in mesio-distal direction. From the second to the fourth premolar, the subdivision of this lobe was clearer.

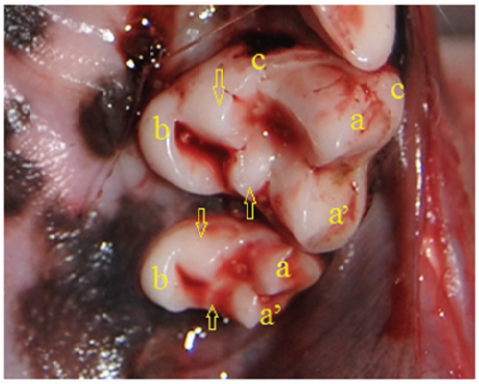

Figure 14. The upper postcarnassials. a (paracone) and a'-the two vestibular cusps; b-lingual rounded lobe (protocone) subdivided in two small tubercles-arrows. c-cingulum

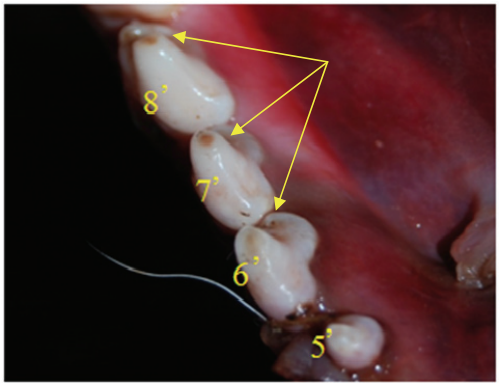

Figure 15. Lower precarnassials 5', 6', 7', 8'. The first premolar-5' is small. The distal lobe (metaconid) is prominent and subdivided, starting from the second premolar-arrows

The lower carnassial appeared stronger than the superior carnassial (Figure 16). The cingulum was relatively small, but the crown was clearly three-lobed. The intermediate lobe, sharp and strong (protoconid) was obviously flanked at its base by a small accessory tubercle distalo-lingual oriented (Figure 16). The mesial lobe (paraconid), shorter, was nevertheless visible, slightly reduced on the lingual part. The short but large caudal lobe has been subdivided into two secondary parts-vestibular (metaconid) and lingual (entoconid).

These parts were separated by a depression, adapted to receive the upper postcarnassial relief, called "heel".

The lower postcarnassials were the last two molars, much smaller than those from the upper arch. The first postcarnassial (or the second molar tooth), held a low crown, slightly wider mesio-distal than in the transverse direction. Its occlusal surface was mamelonated, the distal tubercles being the lowest. The third (or last molar), was very small, having a simple, rounded, less mamelonated crown (Figure 17).

Occlusion of the molar arch was highly efficient on the carnassials tooth due to the maximum development of these teeth. Carnassials teeth were convex on the vestibular side; their aggregate draws a kind of rostral narrow lira, especially on the upper jaw. In the inferior arch the carnassials where less divergent in caudal (aboral) direction. Thus, lower carnassials slid over the lingual surface of the upper counterparts and over the vestibular adjacent lobes of the superior postacarnassials. The sharpest and higher lobe (protoconid) of the lower carnassial, sits in the notch of the first postcarnassial tooth (between metacone and protocone), while the heel facing strong protocone of the upper postcarnassial. Therefore, this complex is permanently sharpened. Because of its positioning in the caudal part of the oral cavity this complex can apply maximum force, easily scissoring the toughest elements, (bones and tendons) without a possible separation. Other teeth have very limited role. Precarnassials are not adjacent; they are arranged alternately, inferiors being placed rostral to the superiors. Due to the reduced volume, the last postcarnassials have only a very superficial action, most often, the inferior postcarnassials are not in contact with their superior counterparts. These features are specie characteristic and are not related with the breed variations of jaws, compared to the incisors disposition, which is strongly related to the breed.

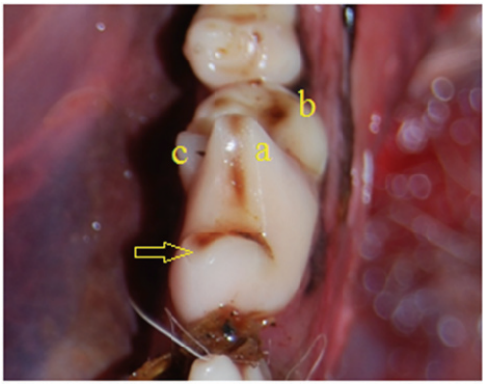

Figure 16. The lower carnassial tooth. The strong intermediate (protoconid) lobe-a. The caudal lobe was subdivided in vestibular (metaconoid)-b and lingual (entoconid)-c lobes. Small accessory tubercle at protoconid base-arrow

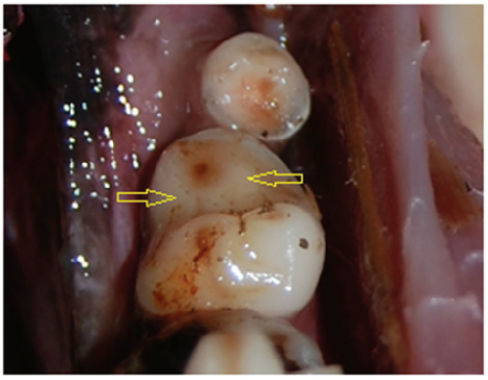

Figure 17. Small distal tubercles-arrows, of the first lower mamelonated postcarnassial tooth, and the smallest last lower precarnassial tooth

In dog the Triadan system is available to identify specific teeth. The number of a tooth is composed of three digit number each of it indicate: the first (in a system of hundreds) indicate the quadrant of the dental arch,1(00) being the upper right; 2(00) being the upper left 3(00) being the lower left and 4(00) being the lower right quadrant. The next two digits indicate the location of the tooth related with the median line, the 01 digit indicate the first central incisor, or the most mesial position of the tooth (Verstraete and Tsugawa 2015). Due to the similarities presented in this paper the Triadan system could be used for reference of the specific tooth in golden jackal.

CONCLUSIONS

The Golden Jackal dentition is similar to that of the dog being: diphyodont, heterodont, brachyodont and secodont type of dentition. In Golden Jackal, the upper dental arch is slightly longer than the lower one, the upper teeth occlusion beind made on the lingual side of the upper teeth, in a "scissor" like action.

Similar to domestic dogs, the Golden Jackal have specialized functional pair of sectorial (carnassials) teeth that consist of the last upper premolar and the first lower molar.

The Triadan system could be used to reference specific teeth in Golden Jackal.

REFERENCES

Barrone, R., 1997. Anatomie comparée des mamiferes domestique, Tome III, Spanchnologie, Appareil digestif, Appareil respiratoire, Ed. Vigot, Paris.

Evans Howard E., de Lahunta Alexander 2013 Miller's Anatomy of the dog, 4th Edition, Saunders, Elsevier Inc.

Lorber M, Alvo G, Zontine WJ., 1979. Sexual dimorphism of canine teeth in dogs, *Arch Oral Biol* 24:585–590,.

Quesenberry, Katherine E. J. W. Carpenter, 2012. Ferrets, Rabbits and Rodents, Clinical Medicine and Surgery, Third Edition, Saunders Elsevier, Missouri

Stan F., 2014, Comparative morphological study of oral cavity in rabbits and guinea pigs. Scientific Works. Series C. Veterinary Medicine, Vol. Lx (1), 27-32.

Verstraete F.,Tsugawa AJ., 2015, Veterinary Dentistry: Self-Assessment Color Review, Second Edition, CRCpresss.

NAV Nomina Anatomica Veterinaria, fifth edition, 2012.

Anatomical Particularities of Male Reproductive System of Guinea Pigs (Cavia porcellus)

Article · November 2015

DOI: 10.15835/buasvmcn-vm:11410

1 author:

Florin Stan
University of Agricultural Sciences and Veterinary Medicine
36 PUBLICATIONS **83** CITATIONS

SEE PROFILE

Anatomical Particularities of Male Reproductive System of Guinea Pigs (C*avia porcellus*)

Florin STAN
Department of Comparative Anatomy, Faculty of Veterinary Medicine, University of Agricultural Sciences and Veterinary Medicine, Cluj-Napoca, Romania
**Corresponding author: flodvm@yahoo.com*

Bulletin UASVM Veterinary Medicine 72(2) / 2015,
Print ISSN 1843-5270; Electronic ISSN 1843-5378
DOI:10.15835/buasvmcn-vm: 11410

Abstract

Currently the pet area shares a great diversity by promoting many exotic species and increasingly expanding existing ones, particularly those of small size. To perpetuate these species a decisive role it has integrity and urogenital health. For this reason and in order to obtain more docile animals, influencing their sexual behavior, veterinarian interventions in order to sterilize, or other curative or preventive maneuvers are required. Knowing in detail the morphology of genitourinary apparatus is crucial for a correct surgical approach. The aim of this study is to achieve a detailed anatomical description of the components of male reproductive system in guinea pigs. Regional stratigraphic dissection was applied on 10 subjects. Macroscopically the components of male genitalia were examined.

Wide opening of inguinal ring was present in all subjects. Ovoid testicle shows a well developed epididymus and a considerable amount of surrounding fat tissue. The glans penis is well represented, being present a small os penis within the dorsal surface of the entire length of glans. The seminal vesicles are the most developed sexual accessory glands, having a coiled pattern, blind ended, and stretching until the abdominal cavity. Prostate and coagulating glands are located at the base of seminal vesicles in close relationship. The prostate is composed of two lobes, dorsal and ventral lobe united by a transversal isthmus. Lobulated coagulating glands show pyramidal pattern being located caudal to the bladder. Bulbouretral glands were small, ovoid and lobulated.

Both gonads and accessory sexual glands were well-developed in guinea pigs.

Keywords: *anatomy, guinea pig, male, reproductive system*

INTRODUCTION

Exotic pets include numerous species belonging to different orders: carnivores, lagomorphs, rodent and many others. Among these, rodenta has a special place due to the high number of species. They represent a significant share of all pets because of their low body weight, gentle character and ease of maintenance, all these based on numerous information available regarding their necessities. All this led to an increasing share of these species as pets, raising the level of addressability with the practitioner in both health problems and counseling owners about reproduction. On the other hand, their usage as experimental model is well known, guinea pigs being chosen as subjects in many studies. However, anatomical data related to the morphology of the reproductive system is scarce in the literature compared to dogs and cats (Barone 2001), which are used as reference in most cases. This justifies the need of knowledge regarding the anatomy of different exotic species to satisfy the need for improvement in nurturing and medical care, especially surgery.

Anatomical particularities of mammalian reproductive system are the result of ontogenetic development, which in males is primarily related to the development and migration of the

testicles into the scrotum. In rabbit and rodent the inguinal ring remains open through the animal's life (McCracken *et al.*, 2008; Quesenberry and Carpenter 2012). In these cases, testicle displacement is physiological compared to most mammals in which after migration to the scrotum, the inguinal ring closes. The morphology of the reproductive system contains accessory sexual glands alongside essential organs that produce spermatozoa – the testicles. In rodents, these contain the following formations: vesicular glands, coagulating glands, prostate and bulbo-uretral glands with small variations between species. Morphological development of accessory genital glands is influenced by multiple factors: hormonal, environmental, seasonal variations related to reproductive activity during mating season (Pelletier, 2002; Nishino *et al.*, 2004).

The aim of the present study is to achieve a detailed morphological description of the male reproductive system in guinea pigs (C*avia porcellus*), the topography of essential reproductive organs and accessory sex glands.

MATERIALS AND METHODS

A group of 6 male guinea pigs were used, with weights between 380 and 650 grams from breeding farms. The subjects were treated according to *Directive 2010/63 /EU of the European Parliament and of the Council on the protection of animals used for scientific purposes* and the Institutional Bioethics Committee of University of Agricultural Science and Veterinary Medicine approved the study. Euthanasia was performed by inhaling an overdose of Isoflurane (Baxter Health Care Corporation, USA). The subjects were positioned in dorsal decubitus performing the extension and fastening of thoracic and pelvine members. The abdominal cavity was opened by performing an incision along the white line until reaching the pubis. The digestive organs which presented topographical relations with components of the reproductive system were identified and then removed to achieve a clearer visualization. After *in situ* photography the genital apparatus has been removed from the pelvic cavity, identifying each component. The terms were in agreement with NAV 2012.

RESULTS AND DISCUSSION

Testicles and sperm ducts (*Testis, ducti genitalis*)

In examined subjects the testicles were located in the perineal region, on both sides of the urethra opening. The slightly flatened aspect of testicular bursa (Bursae testis) was more visible due to brown coloring of the skin in the projection region (Fig. 1). After incision and sectioning of regional skin, the testicles were well visualized because their extraabdominal location, being enclosed in a significant ammount of adipous tissue. In contact with the ventral abdominal wall, between the ventral musculature of the abdominal wall and the skin, the ovoid testicles were dorso-lateral oriented with a slight ventro-medial tilt (Fig. 1). Sectioning of the external layers has highlighted the pink colored testicles, with a dorso-laterally located epididimus (Epididymis). The epididimus components (head, body and tail) were easily identified due to their well development. The head of the epididymus (*Caput epididymis)*, was very coiled and covered with adipous tissue being continued through the epididimus body ventrally positioned by deferent ducts. The tail of

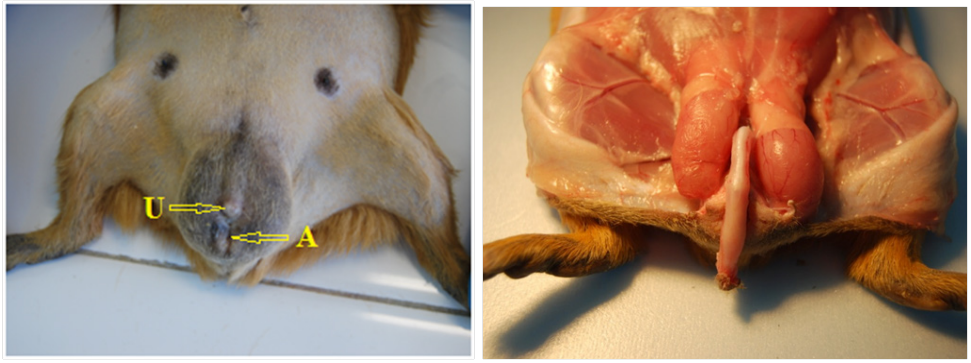

Fig. 1. External appearance of testicular bursa with urethral orifice (U) located cranial to the anus (A)-left and oval shape of testicles-right, in guinea pigs

the epididymus was very obvious due to excesive coiling being continued by the deferent duct (*Ductus deferens)* of 1-2 mm diameter (Fig. 2). The ductus deferens presented a relatively tortuous route in the proximal segment, later to become approximately 1.5-2.5mm in diameter. Whitish, the paired vas deferens were well visualized due to outline clear, smooth and relatively straight path (Fig. 2). Before opening the urethra, the ducts showed a slight enlargement in size and a very short common route. Testes sizes were between 20-30mm long and 12-18mm cross section.

Accessory sex glands

We identified the following accessory sex glands in all subjects: seminal vesicles (*Glandulae veziculares*), coagulating glands, prostate glands (*Glandula prostata*) and bulbourethral glands (*Glandula bulbourethralis*).

The seminal vesicles showed a particular pattern being tubiform, cylindrical and vermiform, blind ended, well developed, having the largest size of the accessory sex glands with a length between 100-120mm and 5-14mm large. Located dorsal to the bladder and ventral to the ureters the vesicular glands presented an upward path surpassing the pelvic cavity directing deep in the abdominal cavity. The distal segments were positioned on both sides of the descending colon (Fig. 3). Each vesicular gland presented a broad and well vascularised ligament. The opening of vesicular glands was made median in uretra into a median cleft (*colliculus seminalis*) together with the ductus deferens opening.

Caudal to the bladder in all subjects we identified the pair coagulating glands, with pyramidal shape, lobulated, being disposed latero dorsal near the seminal vesicles (Fig. 4). Also, these glands were directly related to the prostate gland, being arranged cranio-dorsal to the dorsal lobe of the prostate.

The prostate gland was located immediately caudal to the bladder neck, caudo medial to the coagulating glands and lateral to the seminal

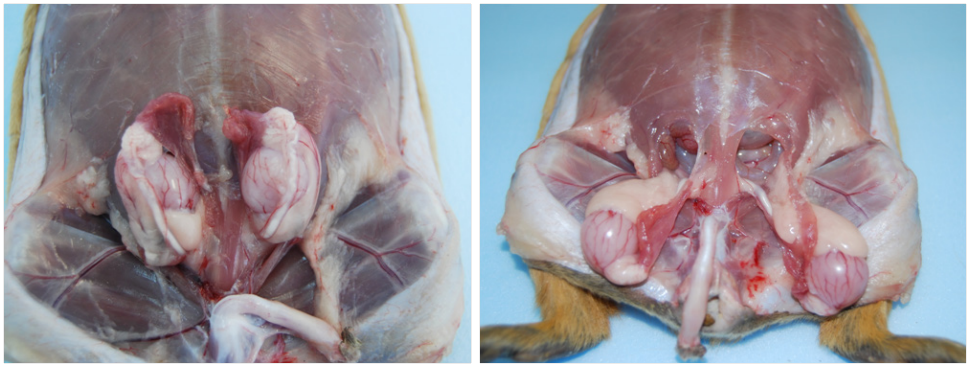

Fig. 2. Oval shape of testicles and clear visualization of deferens ducts and epididymus tail – left and the presence of a large amount of fat on cranial pole of testicles and large inguinal rings – right.

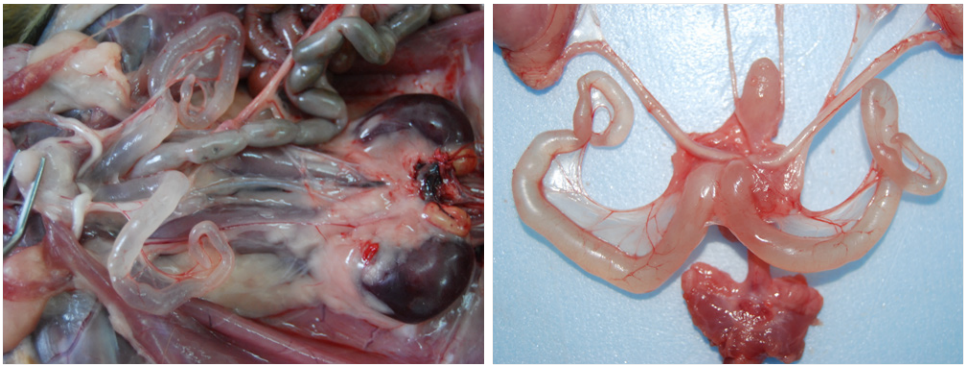

Fig. 3. The tubiform blind ended appearance of vesicular glands located dorsal to the bladder and deferens ducts - left and a well developed ligament of each vesicular gland – right.

vesicles basically being surrounded between the specified components, in its turn surrounding the urethra (Fig. 4). Larger dorsal lobe was joined by a small isthmus to the ventral lobe, smaller in size. Prostate gland with coagulating glands appeared like a common structure without presenting a joint capsule (Fig. 4).

Bulbourethral glands, small, have been identified on both sides of the urethra, on the ischial arch segment of the urethra, ventral to the rectum and dorsal to the pubic symphysis (Fig. 4).

In the initial segment, the penis was attached to the ischiatic arch by the ischio-cavernous muscle while the distal segment was included in the prepuce. Two portions of the penis were recognized: the penian body and glans both of the same calibre with lengths between 45-85mm and 4-7mm circumference. The junction of the two segments was well individualized (Fig 5). The penis was "S"-shaped. We also identified a penian os situated dorsally along the penian glans. In its retracted position the penis was situated ventrally to the pubic symfysis, between the latter and skin. Along all the penis glans until the uretral ostium we identified prominences like small spurs arranged in parallel lines situated dorso-laterally and ventrally, with the ones in the dorsal region having a discontinuous aspect opposed to the ones in the ventral region which were continuous.

In the ventral side of the penis, ventrally from the extrapelvine urethra, in the caudal segment of the penis, we identified the presence of an intormittent sac which open in a transversal slit, caudally from the urethral ostium (meatus). Inside this formation two slightly curved downwards keratinaceous styles were identified. Their insertion was at the cranial segment of the intromittent sac. In living subjects a slight pressure on the penis base lead to its externalization.

DISCUSSION

The variety of information related to the reproductive system of domestic animals is already recognized taking into account the commercial or

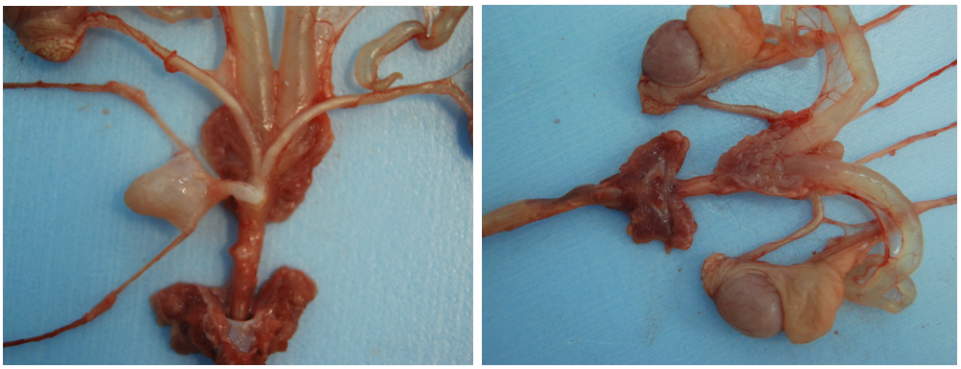

Fig. 4. The prostate gland topography and the coagulating glands – left. The prostate and coagulating glands compose a single structure without a common capsule – right. The topography of bulbourethral glands caudally to the prostate – right.

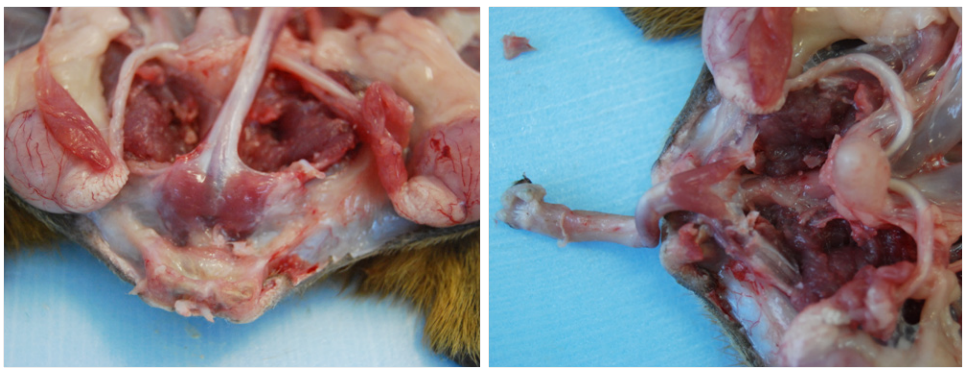

Fig. 5. The guinea pigs penis and its ischio cavernous muscle attachment – left and the S shape of penis – right.

productive aspect. However, the morphological descriptions of the reproductive system of exotic species used as pets or as experimental models are relatively few. From all this, rodents and lagomorphs, especially mice, rats and rabbits receive more attention because they are used in various medical experiments (Vasquez and Del Sol 2002 Suckov *et al.*, 2005; Knoblahgh and True, 2011). Reproductive components are relatively similar in most species and include principal organs - testes, spermatic ducts and accessory sex glands (Barone 2001). Development of these components is influenced by various factors such as hormone composition and androgenic stimulation being of the highest importance (Cepeda *et al.*, 2006). Other factors include the components itself, namely the presence or absence. In the latter scenario, the remaining organs take over the function of the missing one. Environmental factors, time of year and mating season also influence the morphology and function of the reproductive apparatus (Gotteich *et al.*, 1998; Nishino *et al.*, 2004; Breed *et al.*, 2014).

Morphology of main organs of the reproductive system in guinea pigs is common with that of other species like cattle, sheep, swine, lagomorphs and even humans. The caudal-lateral orientation and a slight dorso-ventral tilt is common in most rodents and lagomorphs (Barone 2001, Cooper et Schiller, 1975). Also, the extraabdominal topography with the possibility of intraabdominal migration is present in rabbit as well. During fetal development the testicle descent through the inguinal channel into the scrotal pough takes place in two morphologically distinct phases, each controlled hormonally by secretions from the testicles themselves, with direct implication upon the gubernaculum testis. From the caudadl pole of the kidney, the testicles migrate through the inguinal channel following the lengthening of the gubernaculums and suspensor ligament regression conditioned by testosterone production (Hutson *et al.*, 2009, 2015).Thus, in some animals the descent is complete since the fetal phase(cattle) or only approaching birth(horse)(Barone 2001). The testicles migration through the life make guinea pigs and rabbit to have functional cryptorchidism The extraabdominal loction of the testicles is of great importance for sperm production because of the low temperature necessary for this process. The control for low temperature maintenance is done by contraction of the dartoic layer and testicular cord which bring closer or take further the testicles from the body.

The guinea pigs epididymis have common characteristics with those of most mammals. The pronounced coiling of head and of the tail of the epididymis is usually found in rat, hamster, chinchilla and in rabbit (Barone 2001). The vast amount of fat covering the head of the epididymis found in guinea pigs and and other rodents is not so well represented in rabbits. Due to this pattern the need of surgical closure of the inguinal ring, in orchiectomy might be controversial. Some authors claim that this amount of fat just might have a protective effect. In our opinion, to prevent postoperative herniation suturing is necessary due to considerable width of the inguinal ring and the possibility of migration of fat from inguinal ring. More over this fat is removed during the orchiectomy. Thus, this anatomical peculiarity of testicles in guinea pigs has direct implications in orchiectomy.

Open or closed surgical approach is the most appropriate for the rodents due to the easy anatomical closure by suturing the inguinal rings which are much broader in guinea pigs than in rabbits. Abdominal laparoscopic approach is appropriate to juveniles or in rodents whose testicles migrate extra-abdominally only in reproductive seasons such as sqiurel or prairie dog (Linetz 2000).

Accessory sex glands in guinea pigs were the seminal vesicles, coagulating glands,, prostate glands and bulbourethrale glands. In mammals the presence of accessory sex glands is variable, in terms of topography, number, size and especially shape. The largest diversity is found in rodents, the four components being present in rats (*Rattus rattus*) (Knoblahgh and True, 2011), chinchilla (*Chinchilla lanigera*) (Cepeda *et al.*, 1999; Calamar *et al.*, 2014) and spoted paca (*Agouti paca*) (Borges *et al.*, 2014) while in rabbits are found vesicular glands, well-developed prostate and rudimentary bulbourethrale glands which can be observed only ventrally due to their small size (Barone 2001). In capybara only the prostate and vesicular glands were reported (Ferandez *et al.*, 2010). Regardless of the presence or absence of some or other accessory sex glands their topography is the same in all species – the following are attached to the uretra in caudal direction: vesicular glands,

coagulating glands, prostate and bulbourethral glands.

Our results regarding the tubular, vermiform blind ended and slightly coiled pattern, of vesicular glands are similar to those described in chinchilla (Calamari *et al.*, 2014). The fact that these glands are well represented is due to their function in secretion of seminal fluid as part of the sperm in a range of 50%, both in guinea pigs and chinchilla. Its production is important because in these species after copulation, in the vaginal plug the composition produced by the vesicular glands has a high percentage. Like in rats (Sukov *et al.*, 2005; Knoblahgh and True, 2011), vesicular glands opening in guinea pigs are common with the vas deferens opening compared with the spotet paca which present separate openings of deferents ducts and seminal vesicles (Borges *et al.*, 2014).

The topography of the coagulating gland described in this study, - located latero dorsal to the vesicular glands and craniodorsal to the dorsal lobe of the prostate - is similar to that described in chinchillas (Cepeda *et al.*,2006) and gerbil (Pinheiro *et al*., 2003). In rats the coagulating glands are located on the medial sides of the vesicular glands (Knoblahgh and True, 2011) being referred to as anterior prostatic lobes. In rodents the similarity regarding the coagulating glands is related to their close proximity to the prostate gland, even if their opening are at different levels of the urethra (Pinheiro *et al.*, 2003; Quesenberry and Carpenter 2012). Domestic species like dog, horse, ram, goat and bull lack coagulating glands (Barone 2001)

In animals, prostate gland description shows the presence of several lobes, compared to man in which the prostate gland is a singular organ (Gray 1918). In chinchilla the presence of two lobes was described, the right and left, dorsal located to the junction of the seminal vesicles with urethra, united by an isthmus (Cepeda *et al.*, 2006; Calamari *et al.*, 2014). These descriptions are similar to our results in guinea pigs, in which the prostate gland was composed of two lobes: a well developed dorsal lobe and a small ventral lobe. Neuhaus et al., 2001 made the same description in guinea pigs using a different terminology: cranial and caudal lobe. In rats, according to Knoblahgh and True, 2011, the prostate gland has four lobes: anterior, dorsal, lateral and ventral, sometimes the dorsal and lateral lobes being identified as the dorsolateral lobe. The dorsal lobe surrounds the urethra while the ventral lobe is arranged below the urethra and caudal to the bladder neck. Due to the similar structure of the coagulating glands with the prostate, these glands are sometimes called the anterior lobe of the prostate, being attached to the lesser curvature of the vesicular glands (Knoblahgh and True, 2011).

The ferret (*Mustela putorius*) shared the same characteristic regarding the presence of the prostate gland as single organ, considerably increased in size (1.5/0.6cm), as in humans, surrounding the urethra (Jakobs and Podar, 1986). Moreover, in ferret the prostate is the only accessory sex gland. The most controversial descriptions of the prostate are in rabbits. In this species thr prostate is composed of three parts: proprostata, prostate and paraprostata (Holts and Foote 2005; McCraken *et al.*, 2008). The proprostate is the segment located caudally from the vesicular glands and cranially to the prostate while the prostate and paraprostate are located cranially to the bulbourethral glands. These glandular structures open at the intrapelvine urethra on both sides of the seminal culliculum (Vasquez and Del Sol 2002;).

The bulbourethral glands in guinea pigs are situated caudally to the prostate, dorsally to the urethra and dorsolaterally to the ischiocavernous muscle. The same topography has been described in rats (Knoblahgh and True, 2011), chinchillas (Cepeda 1999) and agouti (Menezes *et al*., 2010). A particular aspect of these glands is that they are located more caudally on the urethra, not being in the close proximity of the prostate, as is in humans (Gray 1918; Barone 2001; Knoblahgh and True, 2011). The lobulated, oval shape is common to rats and guinea pigs while in rabbits these glands only have the latter characteristic.

A particularity of the penis in guinea pigs revealed by our study is the presence of the intromittent sac, situated ventrally to the urethra and the two keratinoceous styles whose insertions are cranially in the mentioned structure. During the erection the two keratinoceous styles are externalized. This aspect has been previously reported in guinea pigs (Weir 1974; Cooper and Sdchiller 1995) and agouti (Molineau *et al*., 2006, 2009). Also the presence of the small spur-shaped formations at the on the penian glans was described in agouti (Molineau *et al.*, 2005) spoted

paca (Borges *et al*., 2014) and even cat (Barone 2001). Even if the role of the proeminences on the intermitent sac is not known (Cooper and Schiller 1997) their presence alongside the spur-shaped formations anchor the penian gland in the female vagina, contributing to the stimulation of spontaneous female ovulation.

The presence of the penian os is common to guinea pigs, chinchillas, (Cepeda *et al*., 2006) and rats (Knoblahgh and True, 2011) but not to rabbits in which, on the other hand has been observed a free extremity of the penis (Queensbery and Carpenter, 2004). Also the topography of rabbit's penis is different from the one we observed in guinea pigs, in which the penis is situated between the two testicles. This aspect can be considered an advantage while castrating rabbits due to the possibility the prescrotal approach compared to guinea pigs for which two incisions are necesary.

A complete description including histological research on the reproductive system in guinea pigs is the subject of another ongoing study which will be published in the future.

CONCLUSION

The morphology of the genital apparatus in guinea pigs shows many similarities with that of rodents.

In guinea pigs the position of the testicles in scrotal pouches without an obvious scrotum, their oval shape and overall conformation and topography is common to that of rats, chinchillas, rabbits, ferrets and other rodets.

The open state of the inguinal canal throughout all their lifespan, allows the intraabdominal migration of the testicles, similar to rabbits.

In guinea pigs the accessory genital glands are: vesicular, coagulanting, prostate and bulbourethral.

The vesicular glands are well represented with a vermiform aspect similar to chinchillas, extending deep into the abdominal cavity.

The prostate has two lobes: a well-developed dorsal one and a smaller ventral one.

Presence of the intromitent sac is unique to histricomorphs.

REFERENCES

1. Barone R (2001). Splanchnologie II. In: Anatomie comparée des mammifères domestiques. Tome quatrième, Triosième edition, Paris, 242.
2. Borges EM, Branco E, Lima AR, Leal LM, Leandro Luiz Martins LL, Reis ACG, Cruz C, Machado MRF, Miglino MA (2014). Morphology of accessory genital glands of spotted paca (Agouti paca Linnaeus, 1766). Animal Reproduction Science 145:75–80.
3. Breed WG, Leigh CM, Aplin KP, Shahin AAB, Avenant NL (2014). Morphological diversity and evolution of the spermatozoon in the mouse-related clade of rodents. J Morphol 275:540–547.
4. Calamar CD, Patruica S, Dumitrescu G, Bura M, Dunea IB, Nicula M (2014). Morpho- histological studies on the male genital apparatus of Chinchilla laniger. Scientific Papers Animal Science and Biotechnologies 47(1):275-280.
5. Cepeda C, Raquel Adaro A, Luis Y Penailillo G Paola (2006). Variaciones Morfométricas de la Próstata de *Chinchilla laniger* (MOLINA, 1982) y de la Concentración de Testosterona Plasmática Durante un Ciclo Reproductivo Anual. Int J Morphol [online] 24(1):89-97.
6. Cepeda R, Adaro L, Penailillo P, Orostegui C (1999). Variaciones morfologicas e stacionales de las glandulas bulbouretrales de la chinchilla (*Chinchilla laniger*), en cautiverio. Rev Chilena Anatom 17 :59–66.
7. Cooper G, Schiller AL (1975). Anatomy of the Guinea Pig. Harvard University Press, Cambridge, Massachusetts, 403.
8. Fernandez DS, Ferraz RHS, Melo APF, Rodrigues RF, Souza WM (2010). Análise histológica das glândulas uretrais da capivara (Hydrochoerus hydrochaeris). Pesq Vet Bras 30(4):373–37.
9. Gotteich A, Hammel I, Yogev L, Terkel J (1996).Quantitative microscopic changes in the mole rat's accessory Sex organs duringan annual cycle. Anat Rec 246(2):231-237.
10. Gray H (2000). Anatomy of the Human Body. Lea&Febiger, Philadelphia,1918; Bartleby.com, 2000. www.bartleby.com/107/.
11. Holtz W, Foote RH (1978). The anatomy of the reproductive system in male Dutch rabbits (Oryctolaguscuniculus) with special emphasis on the accessory sex glands. J Morphol 158:1–20.
12. Hutson JM, Li R, Southwell BR, Newgreen D, Cousinery M (2015). Regulation of testicular descent. PediatrSurg Int 31(4):317-25.
13. Hutson JM, Nation T, Balic A, Southwell BR (2009). The role of the gubernaculum in the descent and undescent of the testis. Therapeutic Advances in Urology 1(2):115-121.
14. Jacob S, Poddar S (1986). Morphology and histochemistry of the ferret prostate. Acta Anat 125:268-273.
15. Knoblahgh S, True L (2011). Comparative Anatomy and Histology: A Mouse and Human Atlas. Elsevier Science, Burlington, 285-309.
16. Linnetz LJ (2000), Abdominal approach to castration in a prairie dog. Exotic DVM 2(5):19–22.
17. McCracken TH, Kainer R, Carlson D (2008). Color Atlas of Small Animal Anatomy: The Essentials. Blackwell Publishing, USA, 72.
18. Mollineau WM, Adogwa AO, Garcia GW (2009). The Gross and Micro Anatomy of the Accessory Sex Glands of the

Male Agouti (*Dasyprocta leporina*). Anatomia, Histologia, Embryologia 38:204-207.

19. Mollineau W, Adogwa A, Jasper N, Young K, Garcia G (2006). The Gross Anatomy of the Male Reproductive System of a Neotropical Rodent: the Agouti (Dasyprota leporina). Anatomia, Histologia, Embryologia: Journal of Veterinary Medicine Series C 35(1):47-52.
20. NAV Nomina Anatomica Veterinaria, fifth edition, 2012.
21. Nishino T, Wedel T, Schmitt O, Biihlmeyer K, Schönfelder M, Hirtreiter C, Schulz T, Kiihnel W, Michna H (2004). Androgen-dependent morphology of prostates and seminal vesicles in the Hershberger Assay Evaluation of immunohistochemical and morphometric parameters. Ann Anat 186: 247–253.
22. Pelletier G (2002). Effects of estradiol on prostate epithelial cells in the castrated rat. J Hist Cytoc 50(11):1517-1523.
23. Pinheiro PF, Almeida CD, Segatelli TM, Martinez M, Padovani CR, Martinez FE (2003). Structure of the pelvic and penile urethra relationship with the ducts of the sex accesory glands of the Mongolian gerbil. J Anat 202(5):431-444.
24. Quesenberry K, Carpenter JW (2012). Ferrets, Rabbits and Rodents: Clinical Medicine and Surgery, 3 ed.
25. Suckow M, Weisbroth S, Franklin C (2005). The Laboratory Rat, Second Edition (American College of Laboratory Animal Medicine), Academic Press, Toronto.
26. Vasquez B, Del Sol M (2002). Complejo prostatico en el conejo (*Oryctolaguscuniculus*). Rev Chil Anat 20:175-180.
27. Weir BJ (1974). Reproductive characteristics of hystricomorfh rodents. Symp Zoology Soc London 34:265-446.

Scientific Works. Series C. Veterinary Medicine. Vol. LXI (1)
ISSN 2065-1295; ISSN 2343-9394 (CD-ROM); ISSN 2067-3663 (Online); ISSN-L 2065-1295

HEART TOPOGRAPHY AND PERICARDIC LIGAMENTS OF GUINEA PIGS

Florin STAN, Melania CRIȘAN, Aurel DAMIAN, Cristian DEZDROBITU, Cristian MARTONOȘ and Alexandru GUDEA

University of Agricultural Sciences and Veterinary Medicine of Cluj-Napoca, Faculty of Veterinary Medicine, Mănăștur Street, No. 3-5, Cluj-Napoca, Romania, Email: flodvm@yahoo.com

Corresponding author email: flodvm@yahoo.com

Abstract:

Small rodents are the most used experimental models in research related to cardiovascular and respiratory system. The guinea pigs occupy a leading position. However, detailed anatomical descriptions of the thoracic cavity of this specie are relatively few in the literature. Compared to mice, rats or hamsters, widely used in research, electrocardiogram waves are similar to humans, making the guinea pigs to be the choice model for studies related to cardiac arrhythmias, and in particular, pharmacological studies. Using gross dissection of the thoracic cavity of ten guinea pigs, this study aims to achieve a detailed description of the heart topography and pericardial ligaments in guinea pigs. Occupying the majority of the narrow thoracic cavity, in the middle mediastinum, in guinea pigs, like all mammals, heart is double layer coated by the pericardium. It lies in the median plane, slightly oriented to the left at the level of 2nd-4th intercostals space and approximately at 1 cm cranial to the xiphoid appendix. External thin walls of the atria are separated from the ventricles by the grooves of coronary arteries and veins, showing multiple branches in all specimens studied. Ventrally and dorsally the ventricles are separated by two shallow interventricular sulci. Pericardial ligaments are well represented and are generated by reflection of the fibrous pericardium on the neighbouring structures, making heart attachment, mechanic protection of the heart and its great vessels.

The following ligaments were visualized in all subjects: sterno-pericardial ligaments (cranial and caudal), in four subjects being joined by a thin blade of adipose tissue; phreno-pericardial ligaments (central-strong, left-shorter, missing in two subjects and right-long); dorsally the verterbro-pericardial ligaments which connect the pericard to the spinal cord, more developed on the left side, forming sheaths for the aorta and for the large vessels. In conclusion, pericardial ligaments achieved a dynamic balance, constantly modified in relation to the phases of the cardiac cycle, their knowledge being necessary both practitioners and researchers which uses guinea pigs as experimental models in cardiovascular studies.

Key words: *heart, pericardic ligaments, guinea pigs*

INTRODUCTION

Although in recent years there is a conservative attitude of anatomists related to the resumption of anatomical studies or acceptance of new explicit theories or morphologically documented studies, the tendency to complete anatomical descriptions, especially of the animals used as experimental model, is unquestionable and must be accepted. In animals,cardiovascular system adaptation, are referred to morphological particularities due to taxonomic affiliation,environment and physical activity (Barone 1997, Cotofan et al., 2007).It is clearly stated that the heart of mammals share many similarities, beginning from embryonic developmental evolution, as long as the heart is the first organ to fully form and function during the vertebrate development (Kent and Carr, 2001; Kirby 2002). Many of the researches findings claim the presence of the same underlying mechanisms in mammal's heart development, which are considered molecularly and developmentally similar (Harvey and Roshental 1998). However, in adult mammals the sizes, shape and positions of heart vary between species. Currently, in medical research, animal use as experimental model is fundamental in developing new therapies of cardiovascular disease, but the extrapolation of animal data requires that the animal model chosen for testing is similar in anatomy and physiology to that in humans (Paul and Paul 2001). Guinea pigs choice for cardiovascular studies must be primarily based on scientific hypothesis, the degree of species similarities to the human anatomy and the appropriate animal housing and care. This

involves a proper selection of the animal model and a detailed knowledge of its anatomy. The present study aims to provide a detailed description of topography, external conformation and pericardic ligaments of the heart in guinea pigs.

MATERIALS AND METHODS

Ten adult guinea pigs from ages between 1 and 3 years old, both sexes (4 male and 6 female) and varying weights (370-610g) were used. The subjects were part of an ongoing study related on digestive system and were provided by the "Iuliu Haţieganu" University of Medicine and Pharmacy, Cluj Napoca, Romania, bio base. Gross dissection was performed after euthanasia which was made by inhalation of an overdose of isoflurane (Baxter Health Care Corporation, USA). Thoracic cavity was opened by a double incision along the right and left side of the sternum to preserve the ligaments insertion. The ribs were carefully removed and the topography of thoracic organs and their ligaments were photographed using a Nikon D60 digital camera. Terms were used in agreement with NAV 2012. The Institutional Bioethics Committee of University of Agricultural Science and Veterinary Medicine approved the study.

RESULTS

Heart topography

In guinea pigs the heart occupies a relatively large space in the thoracic cavity, extending from the sternum to the vertebral column and leaves only a narrow space for the lungs on each side. Its base, dorsocranially oriented, lies in the midline, at the level of 2nd-4th intercostals space, the apex caudoventrally directed was situated at 1cm distance from xiphoid appendix (Fig. 1). The overall orientation was slightly to the left in caudal direction and a more ventrally tilted long axis of the heart (Fig. 2).

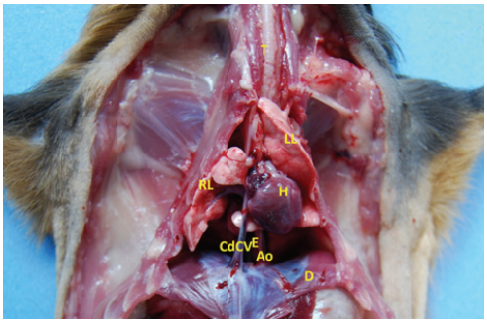

Fig. 1 Heart topography in guinea pigs. H-heart; T-trachea; LL-left lobe of lungs ; RL-righe lobe od lungs;-CdCV-caudal cava vein; E-esophagus; Ao-aorta; D-diaphragm

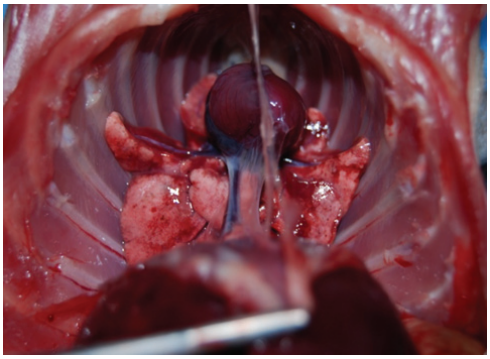

Fig. 2 Note the slightly left orientation in caudal direction and a tilted long axis of the heart

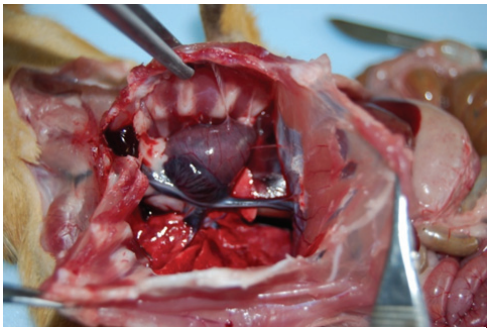

Fig. 3 Right lateral view of the thoracic cavity in guinea pigs. Extended course of the caudal vena cava after passing the diaphragm

The tilted of the heart was limited due to the extensive attachments of the pericardium to the sternum and diaphragm. The auricles were visible on both, right and left sides with the pulmonary trunjk located between them and to the left oriented. The caudal vena cava has an extended course on the right side of median plane (Fig. 3).

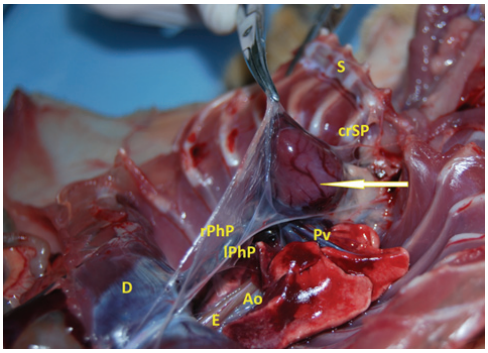

Fig. 4 Well represented arterial vascular supply and venous drainage of the heart-arrow. (S-sternum; crSP-cranial sternal pericardiclig.; rPhP-right phrenico-pericardial lig.; lPhP-left phrenico-pericardial lig.; Ao-aorta; E-esophagus; D-diaphragm; Pv-pulmonary veins)

The aortic arch projects caudally, first on the right then to the left being accompanied by the pulmonary trunk.

In all subjects, the coronary arteries were well observed on the external aspect of the heart running into the shallow coronary groove, with an extensive collateralization of the arteries. Also, an extensive network of intercommunicating veins provides the venous drainage of the heart (Fig 4).

Pericardic ligaments

The heart was enclosed by the fibrous pericardium (*Pericardium fibrosum*), which in cranial direction was fixed at the base of the heart, extends upward on the great arteries and veins, enclosing these vessels; ventrally the fibrous pericardium was attached to the sternum and to the diaphragm by several and obvious ligaments.

Using NAV we systematized the pericardic ligaments in ventral, cranial, dorsal and caudal ligaments.

In all subjects, ventrally, the pericardium was attached to the sternum through the cranial and caudal sterno-pericardic ligaments (*Lig. sternopericardiacum*), which was continuous in seven subjects, showing a small amount of adipose tissue within. The *cranial sterno-pericardic ligament* emerges from the ventral cranial region of heart to be inserted on the dorsal side of the manubrium and on the two small cylindrical vestigial clavicles on the each side. This ligament was a direct continuation of the vertebro-pericardic ligament (right and left), delimiting a space which houses a small amount of adipose tissue, a reminiscent of the thymus in adult animals. The *caudal sterno-pericardic ligament* was detached from the ventral margin of the heart, above the interventricular sulcus to be inserted of the xifoid appendix of the sternum (Fig. 5). This ligament too, was fulfilled with adipose tissue.

Cranially, the parietal pericardium (*Lamina parietalis*) surrounds the aorta and the pulmonary trunk, the inferior and superior vena cava together with the pulmonary veins, being the reflection on visceral layer (*Lamina visceralis-epicardium*) of serous pericardium (*Pericardium serosus*) creating the *pericardial cavity (Cavum pericardii)*. The fusion of the parietal serous pericardium with the fibrous pericardium creates one layer with two surfaces. The fibrous pericardium has little elasticity and by its fusion with the base of the great vessels creates a closed space in which the heart is disposed.

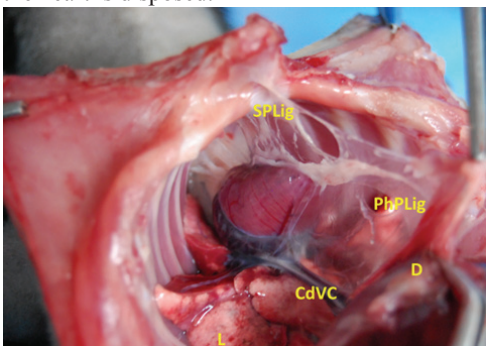

Fig. 5 Overall patern of fibrous pericardium. SPLig-sternal pericardial lig.; PhPLig. Phreno-pericardial lig.; CdVC-caudal cava vein; D-diapragm; L-lungs

In all subjects, dorsal cranial pericardial ligament was short being represented by the *aorto-pericardic ligament* which anchors the pericardium from the aortic arch in cranial direction. This ligament was almost imperceptible due to the relative large place occupied by the heart in thoracic cavity and the close proximity of the heart to the thoracic

inlet. Also, in the middle mediastinum the fibrous pericardium cover the descending aorta making the connection of the pericardium to the vertebral column.

Between the dorsal pericardium and the lungs hilum, covering the vascular and the bronchial elements, the tiny but well visualized *pericardo-pedicular ligaments* were noted. Besides the mentioned ligaments which stabilize relations between the mediastinal organs, in all subjects were identified the connection ligaments between the esophagus and trachea, esophagus and bronchi, and between the esophagus and fibrous pericardium.

The caudal pericardic ligaments were represented by the obvious *phreno-pericardic ligaments, (Lig. phrenicopericardiacum* which connect the caudal margin of the heart with the diaphragm (Fig. 6).

Three ligaments were observed in eight subjects, while in two subjects the left phreno pericardial ligament was missing. The *right phreno-pericardial ligament* was detached from the cranial right ventricle to be inserted on the tendineous center (*centrum tendineum*) of the diaphragm. The *left phreno pericardial ligament* emerges from the apex having an oblique direction for its insertion half divided: one part on the tendinous diaphragm and one part on the costal muscular diaphragm close to the 8th intercostals space. The *central phrenico-*

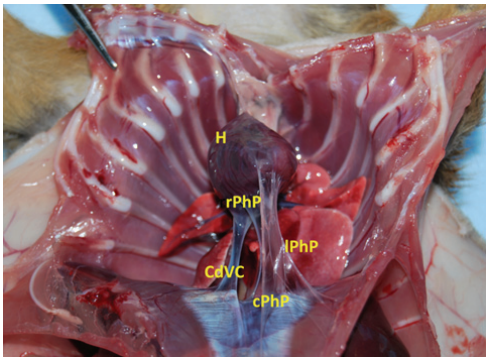

Fig. 6 Phreno-pericardial ligaments and their insertion.rPhp-rightphreno-pericardial lig. ; lPHp-leftphreno-pericardial lig.; CdVC-caudal cava vein; cPhP-centralor ventral phreno-pericardial ligament.

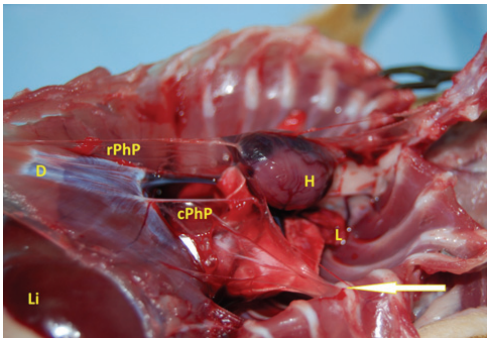

Fig. 7 The left insertion on the 7th rib of pericardium-white arrow

pericardial ligament connected the central part of the tendinous diaphragm with the apex.

This ligament was attached to the right pericardial ligament in five subjects. In two subjects in which the left phrenopericardial ligament was missing,it was well defined a *left lateral pericardial ligament* which emerges from the apex to be inserted on the 7thrib and intercostals space (Fig 7).

Division of the mediastinum A clear division of mediastinum was possible due to the accurate topography of the composing structures in all examined subjects. The cranial mediastinum (*Mediastinum craniale*) was the space between the dorsal side of the sternal manubrium, cranial mediastinal pleura on each side, upper pericardium and the first thoracic vertebrae. It contains several important structures like aortic arch, the final course of superior vena cava, the tracheea, the esophagus, thoracic duct, vagus and phrenic nerves. Also, in the cranial mediastinum a small amount of adipose tissue, a reminiscent of involuted thymus, lying close to the thoracic inlet was found in all subjects. The middle mediastinum

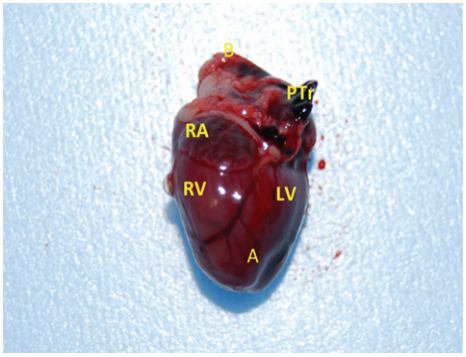

Fig.8 Size, shape and external conformation of guinea pig heart.B-base of the heart; RA-right atrium under the right auricule; RV-right ventricle; A-apex; LV-left ventricle; PTr-pulmonary trunk

(*Mediastinum medium*) was further divided into three spaces: ventral, middle and dorsal. Ventrally, the ventral mediastinum (*Mediastinum ventrale)* was bounded by the sternum and the pericardium dorsally. In this space the sterno-pericardial ligaments, internal thoracic vessels, small lymph nodes were found. The central (middle) space of middle mediastinum was occupied by the great vessels (superior and inferior vena cava, aorta, pulmonary trunk and pulmonary vessels), pericardium and heart. The caudal vena enters into the right atrium after an extended course after passing the diaphragm and caudal mediastinum: the same long trajectory was present of cranial vena cava after the confluence of the right and left brachiocephalic veins. In all subjects the pulmonary veins were well individualized emerging from the well delineated pulmonary lobes. The pulmonary trunk ascends from right ventricle, dorsal and to the left oriented, passing in front of the aorta (Fig. 8). The aorta leaves the left ventricle primary on right oriented, curves dorsally to the left becoming the aortic arch. After the aorta exit the pericardium it arches over the right pulmonary trunk, passing to the left of the trachea and esophagus and entering into the dorsal mediastinum as descending aorta. Dorsal mediastinum (*Mediastinum dorsale)* was the space between the dorsal pericardium and the posterior thoracic walls containing descending

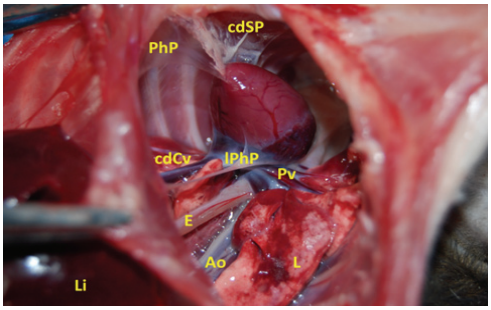

Fig. 9 Caudal view of the thoracic cavity in guinea pigs and its principal structures. cdSP-caudalsterno-pericardiclig.; PhP-phreno-pericardiclig.; cdCv-caudal cava vein,.; Ao-aorta; L-left caudal lung lobe; Pv-pulmonary veins; lPhP-left phreno-pericardiclig.

aorta, thoracic duct, thoracic sympathetic trunk and the thoracic splanchnic nerves. Esophagus passes along the right side of the descending aorta in dorsal mediastinum.

The caudal mediastinum (*Mediastinum caudale*) was a relative large space between the caudal sagital plan which passes under the apex, and diaphragm. It contains the caudal thoracic segments of caudal vena cava, descending aorta, esophagus guarded by the vagus branch (Fig. 9).

DISCUSSION

The heart is located in ventral part of middle mediastinum in large mammals, tend to have a less pronounced left side orientation and a more ventral tilted long axis (Getty 1995; Barone 1997; Crick et al., 2001) if we compare to humans (Goss 1949; Barone 1997). Also, the heart of most animals tends to be elongated having a pointed apex. This feature is absent in dogs which have an ovoid heart with a blunt apex (Evans, 1993), ruminants, which have a pointed apex and a conical shape heart, compare with the blunted apex in sheep (Ghoshal, 1975, Kent 2001) and pigs in which the blunt apex is medially oriented (Cotofan et al., 2007). The conical, elongated heart and pointed apex in rabbit (Schiffmann, 2002) is similar to the guinea pigs heart, but in guinea pigs the hearttend to be more large related on thoracic cavity size, occupying a

disproportionally large part of the thorax and leaves only a narrow space for the lungs on each side.This is in agreement with the report of other studies about the differences that exist in the ratio of heart weight to body weight, which show that adult sheep and adult pigs have a smaller ratio of heart weight to body weight compare to adult dogs, whom ratio was as much as twice the heart weight to body weight than in mentioned animals (Ghoshal et al., 1975; Evans, 1993). The earliest literature data show that the body weight is inversely related to the heart rate and directly related to blood volume and heart weight (Holt 1970; Getty 1975).

In all mammals the apex is formed only by left ventricle, but differences exist in heart orientation. In quadruped standing animals, the heart long axis is oblique, ventro-caudally oriented and slightly to the left. Due to the quadruped posture of animals, the apex of the heart is more ventrally titled toward to the sternum, than in humans, but in guinea pigs this tilting is limited because of extensive attachment of the pericardium both to the sternum and to the diaphragm. Most quadruped mammals tend to have a less pronounced left side orientation and a more tilted long axis of the heart compare to humans, in which the heart is situated with the right atrium on the right, the right ventricle anterior, the left ventricle to the left and posterior, and the left atrium entirely posterior. The apex is projected inferiorly and to the left.

All mammalian hearts lies in the middle mediastinum being enclosed into the pericardium which creates the pericardial cavity around the heart (Barone 1997; Kent and Carr 2001; Cotofan et al., 2007). The mechanical function of the pericardium including the heart fixation in the thorax, prevention of the heart dilatation by maintenance of the heart shape, preventing of excessive movement of the heart with changes in body position and a physical barrier to infection and malignancy are of great importance but not the major one. Also, the pericardium has a secretory function accomplished by visceral layer of serous pericardium, which secrete the pericardium liquid which allows the inner visceral pericardium to glide against the outer parietal pericardium. However, it was proved that the pericardium is not essential for survival, as long as the congenital absence or pericardiectomized human and animals, have no severe adversereaction to removal, or congenital absence (Hammond et al., 1992; Abel et al., 1995). Moreover, in certain condition, the presence of the pericardium, physically constrains the heart function by a depressive hemodynamic influence that limits cardiac output by affecting and reducing diastolic ventricular function (Saunders 2012, Ware 2012; Majoy 2013), feature frequent present in humans too. Equally true is that clinically pericardial disease is one of the most infrequent type of cardiac disease, but morphologically is common, both in humans (Roberts 2005) and animals (Dempsey and Ewing 2011; DeFrancesco 2013). This could be explaining by the differences related to pericardium thickness. Generally, pericardium wall thickness increases with increasing heart and cavities size between the various species. If ovine have 0.32±0.1mm wall pericardial thickness, porcine 0.20±0.1mm, dogs 0.19±0.1mm, humans have between 1-3.5mm wall pericardial thicknesses.Our description of guinea pig pericardium is in concordance with the features found in most of the mammals. Also, in animals the differences of the amount of pericardial fluid are related to the heart dimensions and animal weight. Holt (1970) reported various volume of pericardial liquid in dogs, ranging from 0.5-2.5ml or more in large breed dogs up to 15ml. In small animals, like guinea pigs, chinchilla, rat there are no reports of pericardial liquid volume, further studies are necessary.

In animals, the tiny pericardium is fixed to the great vessels at the base of the heart and is attached to the sternum and diaphragm, although the degree of attachment varies between the species. More specific, the attachment to the tendineus center of the diaphragm is firm and broad in dogs, the phreno-pericardial ligament being the only

constant pericardial ligament reported in dogs. Nevertheless, in dogs, there are reports of the presence of a tiny ligament which detached from the dorsal caudal pericardium to be inserted on the 6th costal cartilage (Kent and Carr 2001). Our results are in agreement with this reports, we describe in two subjects the presence of this pericardo costal ligaments in absence of the left phreno-pericardial ligaments. In ruminants the caudal pericardium is attached to the sternum by a strong sterno-pericardial ligament, only the apex being in contact with the sternum, compare to the extensive attachement to the sternum, in absence of the phreno-pericardial ligaments in horse (Barone 1997; Cotofan et al., 2007).

The presence of a rich coronary collateral circulation in guinea pigs revealed in this study is in accordance with that described in dogs (Ghoshal1975; Koke and Bittar 1978). In the earliest studies related to heart ischemia and in pharmacological therapies for reducing the ischemic size, the dogs were the preferred animal model, but, due to anatomical particularities of coronary irrigation these studies lead to false claim about the efficacy of medication as long as administration in humans did not produce the same results as those observed in dogs. Nowadays, it is well known that the dog have a much more extensive collateral circulation compare to sheep and pigs (Abel et al., 1995). Morphologically, the pig's heart is more similar to the human heart, due to limited collateral coronary circulation, making the swine heart, ideal for acute ischemia studies (Crik et al., 1998). In recent years, small animals are commonly used in cardiovascular disease; the rats have a sparse collateral circulation being a suitable model to heart ischemia (Chorro et al 2009). Due to the extensive collateral circulation in guinea pigs, normal perfusion of heart is maintained after a coronary artery occlusion and infarction does not develop. Another morphological feature of the guinea pigs heart is the smallest diameter of the mentioned vessels which are hard to be verified if the spontaneous or induced reperfusion appears. Nevertheless, the use of guinea pigs as experimental model remains quite important for arrhythmia studies on humans due to the similar electrocardiographic waves (Guo et al., 2009). It was demonstrated that the polarity of T waves is the same of that of QRS complex from human subjects (Watanabe et al., 1985, Roberts et al., 2003, Zaragoza et al., 2011).

Regarding the mediastinum, based on the obvious anatomical components, we realized a detailed division and description of mediastinum spaces. In human the mediastinum is divided by a transversal plane that connects the sternal angle,passes over the pericardium to the intervertebral disc of 4th and 5th thoracic vertebra, into superior and inferior mediastinum, the later being subdivided in anterior, middle and posterior (Goss 1949, Gray's Anatomy, 2008). In animals anatomical descriptions recognizes three spaces: cranial, middle and caudal, with a double division of middle mediastinum in ventral and dorsal (Barone 1997, Cotofan et al., 2007) From a morphologic point of view, and due to extensive feature of pericardic ligaments in guinea pigs, our division of middle mediastinum in ventral, middle (central) and dorsal is justified. The same simple landmarks as in humans could be made: the ventral mediastinum is dorsal to the sternum and ventral to the pericardium, the middle mediastinum contains the pericardium and its components and the dorsal mediastinum is behind the pericardium and ventral to the vertebral column.

All these considerations mentioned above are the base of using both large and small animals as experimental models for the cardiovascular studies. The advantages of large animal models are primarily based to their similarities in heart physiology to humans and ease of instrumentation, but equally true is that maintenance costs are higher which make small animal models more attractive.

CONCLUSIONS

Apart from the differences in size the guinea pig heart is anatomically similar with the most of the mammal's heart.

Guinea pigs have a different type of heart vascularisation meaning the presence of a well developed collateralisation of heart supplying vessels offering a natural degree of protection of ischemic disease.

The tiny but obvious sterno-pericardial and phreno-pericardial ligaments give the guinea pigs heart, a strong insertion and protection into thoracic cavity.

The middle mediastinum in guinea pigs can be divided in three obvious spaces: ventral, middle (or central) and dorsal, each of them containing important and obvious anatomical structures.

REFERENCES

Abel, F.L., Mihailescu, L.S., Lader, A.S., and Starr, R.G. (1995) Effects of pericardial pressure on systemic and coronary hemodynamics in dogs.Am J Physiol. 268, H1593–H1605.

Breazile JE and Brown EM. 1976. Anatomy. In: Wagner JE, Manning PJ, eds. The biology of the guinea pig. New York: Academic Press;:53-62.

Chorro FJ, Such-Belenguer L, López-Merino V. 2009. Animal models of cardiovascular disease. Rev EspCardiol 62:69–84 (English Edition)

Cotofan, V,. Hritcu, V., Palicica, R., Damian, A., Ganta, C., Predoi, G., Spataru, C., Enciu, V., Anatomia animalelor domestice : vol. II : Organologie Timisoara, 2007 Orizonturi Universitare.

Crick, S.J., Sheppard, M.N., Ho, S.Y., Gebstein, L., and Anderson, R.H. 1998 Anatomy of the pig heart: comparisons with normal human cardiac structure. J Anat. 193, 105–119.

DeFrancesco, T. C. 2013. Management of cardiac emergencies in small animals. Veterinary Clinics of North America: Small Animal Practice, 43(4), 817-842.

Dempsey, S. M. and Ewing P. J. 2011.A Review of the Pathophysiology, Classification, and Analysis of Canine and Feline Cavitary Effusions. Journal of the American Animal Hospital Association: 47 (1):1-11.

Evans, H.E. 1993 The heart and arteries, in Miller's Anatomy of the Dog, 3rd Ed. (Miller, M.E. and Evans, H.E., eds.), Saunders, Philadelphia,PA, pp. 586–602.

Getty, R. 1975 General heart and blood vessels, in Sisson and Grossman's The Anatomy of the Domestic Animals, 5th Ed. Getty,R., ed, Saunders, Philadelphia, pp. 164–175.

Ghoshal, N.G. 1975 Ruminant, porcine, carnivore: heart and arteries, in Sisson and Grossman's The Anatomy of the Domestic Animals, 5th Ed. (Getty, R., ed.), Saunders, Philadelphia, PA, pp. 960–1023, 1306–1342, 1594–1651.

Goss, C.M. (ed.) 1949 Anatomy of the Human Body: Gray's Anatomy. Lea and Febiger, Philadelphia, PA.

Gray's Anatomy: The Anatomical Basis of Clinical Practice (40th ed.), Churchill-Livingstone, Elsevier, 2008

Guo, L. Dong, Z. Guthrie, H. 2009. Validation of a guinea pig Langendorff heart model for assessing potential cardiovascular liability of drug candidates. Journal of pharmacological and toxicological methods, 60(2): 130-151.

Hammond, H.K., White, F.C., Bhargava, V., and Shabetai, R. 1992 Heart size and maximal cardiac output are limited by the pericardium. Am J Physiol. 263, H1675–H1681.

Harvey, R.P. and Rosenthal, N. 1998.Heart Development.Academic Press, New York, NY.

Holt, J.P. 1970.The normal pericardium.Am J Cardiol. 26, 455–465.

Kent, G.C. and Carr, R.K. 2001.Comparative Anatomy of theVertebrates, 9th Ed. McGraw Hill, Boston, MA.

Kirby, M.L. (2002) Molecular embryogenesis of the heart.Pediatr Dev Pathol. 5, 516–543

Koke, J.R. and Bittar, N. 1978.Functional role of collateral flow in the ischaemic dog heart.Cardiovasc Res. 12, 309–315.

Majoy, S. B., Sharp, C. R., Dickinson, A. E., & Cunningham, S. M. 2013.Septic pericarditis in a cat with pyometra. Journal of Veterinary Emergency and Critical Care, 23(1), 68-76.

Paul, E.F. and Paul, J. (eds.) 2001Why Animal Experimentation Matters: The Use of Animals in Medical Research. Social Philosophyand Policy Foundation: Transaction, New Brunswick, NJ.

Roberts SJ, Guan D, Malkin R. 2003. The defibrillation efficacy of high frequency alternating current sinusoidal waveforms in guinea pig. Pacing Clin Electrophysiol.;26:599–604

Roberts, W. C. 2005. Pericardial heart disease: its morphologic features and its causes. Proceedings (Baylor University. Medical Center), 18(1), 38–55.

Saunders, A. B. 2012. The diagnosis and management of age-related veterinary cardiovascular disease. Veterinary Clinics of North America: Small Animal Practice, 42(4), 655-668.

Schiffmann, H., Flesch, M., Hauseler, C., Pfahlberg, A., Bohm, M., and Hellige, G. 2002 Effects of different inotropic interventions on myocardial function in the developing rabbit heart. Basic Res Cardiol. 97, 76–87.

Ware, W. 2012. Small Animal Cardiopulmonary Medicine: Self-Assessment Color Review. CRC Press.

Watanabe T, Rautaharju PM, McDonald TF. 1985. Ventricular action potentials, ventricular extracellular potentials, and the ECG of guinea pig. Circ Res. 57:362–373

Zaragoza, C., Carmen Gomez-Guerrero, Jose Luis Martin-Ventura, et al., 2011. Animal Mo dels of Cardiovascular Diseases, J. Biomed Biotec.vol. 497841.

NAV Nomina AnatomicaVeterinaria, fifth edition, 2012.

Scientific Works. Series C. Veterinary Medicine. Vol. LXIV (1), 2018
ISSN 2065-1295; ISSN 2343-9394 (CD-ROM); ISSN 2067-3663 (Online); ISSN-L 2065-1295

MACROSCOPIC ANATOMY OF PANCREAS IN RATS, GUINEA PIGS, CHINCHILLAS AND RABBITS

Florin Gheorghe STAN

University of Agricultural Sciences and Veterinary Medicine, Cluj-Napoca,
3-5 Mănăştur Str. Romania

Corresponding author email: florin.stan@usamvcluj.ro

Abstract

The aim of this paper is to provide a detailed and comparative presentation of macroscopic anatomy of the pancreas, its topography and connection elements among the experimental animal species including rats, guinea pigs, chinchillas and rabbits. Using gross dissection, the pancreas and its connection elements were studied on 10 specimens of each species presented. The triangular form of the pancreas is a common anatomical pattern in rats, guinea pigs and chinchilla with different degrees of development of the three portions. Located reroperitoneally and in relation to the duodenum, spleen and stomach, the three portions are referred as the duodenal, splenic and gastric portion or lobes with the same names. In rabbits, however, the right lobe of the pancreas has a diffuse appearance, being located largely in the mesoduoden compared to the left lobe which has a better defined shape being located in the deep wall of the greater omentum. The pancreas relations in the experimental models studied are with the right lobe of the liver, the portal vein, the right kidney, the caudal cava vein, the aorta and the emergence of the celiac and mesenteric arteries, the profound wall of the large omentum, the stomach and the transverse colon.

Key words*: pancreas, anatomy, experimental models.*

INTRODUCTION

Over the decades, the pancreas in experimental animals was intensively studied related to its physiological component. Since the insulin discovery in 1921 and its direct relationship with the glucose metabolism followed by the research involving the inflammatory, ischemic and neoplastic morbidities, it was clearly stated the need of experimental models in order to achieve a better understanding of local and systemic organic implications (Aghdassi et al., 2011; Cattley et al., 2013; Stan 2014; 2015; 2017). Moreover, pancreatic transplantation required a proper knowledge of pancreas anatomy in experimental animals in order to improve surgical techniques. With the exception of domestic animals, in which the pancreas has been extensively studied, both macroscopically and microscopically, detailed anatomical studies were performed in mouse, rats, monkeys, dogs and minipigs (Suckow et al., 2012; Pandiri, 2014; Tsuchitani et al., 2016). In this study, it was intended to present detailed description about the macroscopic anatomy of the pancreas and especially to emphasize the difference and similarities of pancreatic macroscopic anatomy in the rats, chinchillas, guinea pigs and rabbits, which may guide researchers in experimental studies.

MATERIALS AND METHODS

Ten healthy adult rats, guinea pigs, chinchillas and rabbits were used. The Institutional Bioethics Committee of University of Agricultural Science and Veterinary Medicine in accordance to Directive 2010/63 /EU of the European Parliament and of the Council on the protection of animals used for scientific purposes approved the study. Euthanasia was performed by administration of an overdose of isoflurane. The abdominal cavity was opened and the wall of it were carefully removed in order to visualize and to photograph the pancreas, its relations with the adjacent organs and its connection elements. The pancreas was divided in the following portions: duodenal segment, gastric segment and splenic segment. The duodenal segment was visualized ventrally with a minor procedure as pulling the duodenum caudally and additionally the entire pancreas were reached dorsally since the stomach and spleen were turned cranially.

Terms were used in agreement with the NAV (Nomina Anatomica Veterinaria) 2012.

RESULTS AND DISCUSSIONS

Rat

The pancreas has a lobulated pattern. On the right side it was located in the mesentery of the duodenal loop and transverse colon extending to the dorsal part of greater omentum adjacent to the stomach and spleen (Figure 1).

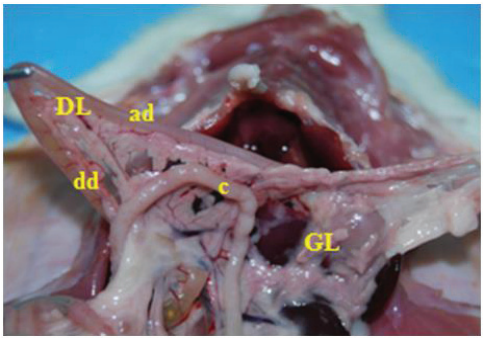

Figure 1. The duodenal lobe – DL of pancreas in rats located in the mesoduodenum. The gastric lobe – GL extends into the dorsal sheet of the greater omentum. dd – descending duodenum; ad – ascending duodenum; c – colon.

On the right side, the right lobe of pancreas (*Lobus pancreatis dexter*) or duodenal lobe was invested in the mesentery between the descending and ascending ansa of the duodenum (*Mesoduodenum*). The splenic lobe, (Figure 2) extends from the duodenal lobe toward to the spleen on the left side of the median plane, being the left lobe correspondent (*Lobus pancreatis sinister*).

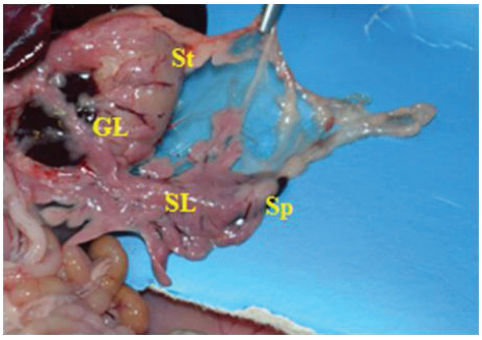

Figure 2. The splenic lobe – SL of pancreas in rats is the most developed and compact lobe. It extends between the duodenal lobe and spleen - Sp. GL – gastric lobe; St – stomach.

It was the most developed and compact lobe of the pancreas in rats. The terminal part of the splenic lobe extends into the gastrosplenic ligament (*Lig. gastrolienale*) (Figure 3).

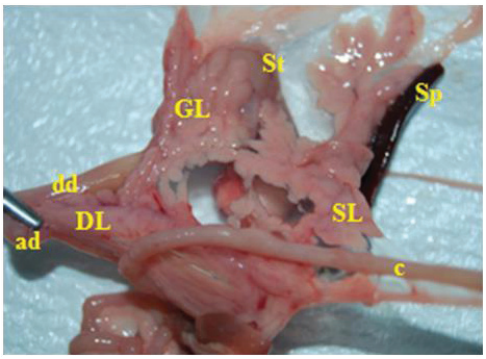

Figure 3. The three lobes compound pancreas in rat: The duodenal lobe – DL; the gastric lobe – GL; the splenic lobe – SL. The caudal part of the duodenal lobe and the dorsal part of the splenic lobe are joined together near to the colon – c.

The gastric lobe was the smallest lobe of the pancreas in rats, extending from the left portion of the duodenal lobe into the dorsal sheet of the greater omentum adjacent to the stomach.

Guinea pig

The pancreas in guinea pig consists of three lobes, each lobe being separated into a number of small lobules. The duodenal lobe lies in close contact with the descending duodenum into the mesentery between the ascending and descending duodenum (Figure 4).

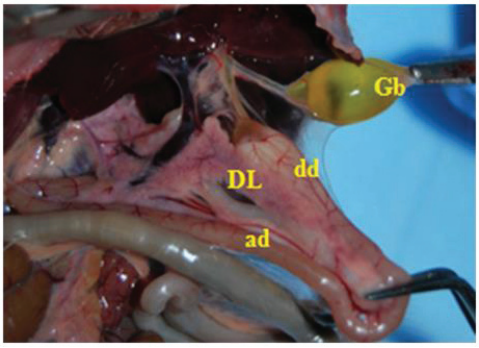

Figure 4. In guinea pig, the duodenal lobe – DL lies in close contact with descending duodenum – dd, into the mesentery between the descendant and ascendant – ad ansa of the duodenum. Gb – gallbladder.

From the proximal portion of the duodenal lobe, the splenic lobe extends to the left, in a caudal direction, near to the dorsal part of the spleen. The compact splenic lobe was the largest lobe of pancreas in guinea pig being fully attached to the gastrosplenic ligament (Figure 5).

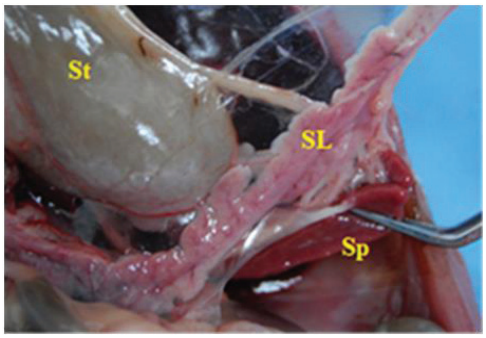

Figure 5. The splenic lobe - SL of pancreas in guinea pig extends caudally to the stomach – St, to the left on the dorsal aspect of the spleen – Sp.

Several islets of pancreatic tissue arranged in a dendritic manner caudally to the fundus of the stomach, and detached from the splenic lobe, formed the gastric lobe of pancreas in guinea pigs (Figure 6).

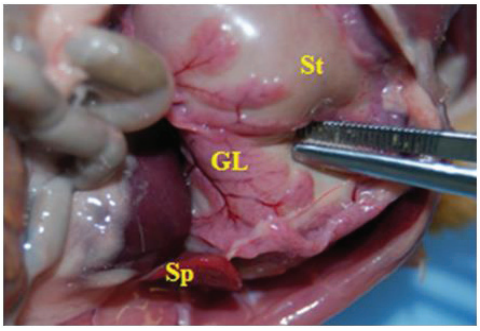

Figure 6. The gastric lobe – GL of pancreas in guinea pig arranged in a dendritic manner caudally to the stomach - St. Sp – spleen.

Chinchilla

In situ the pancreas showed the same three divisions: the duodenal lobe, the splenic lobe and the gastric lobe. The duodenal lobe, corresponding to the right lobe of pancreas (*Lobus pancreatis dexter*) was located adjacent to the duodenum, being attached to the descending loop of duodenum (Figure 7).

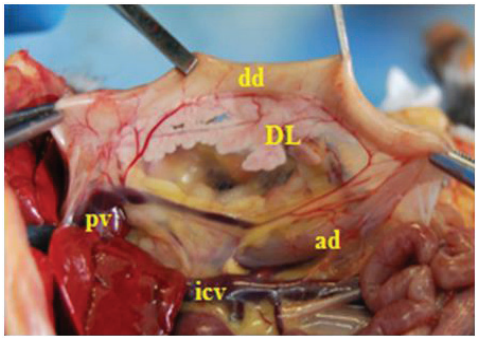

Figure 7. The well defined duodenal lobe – DL of pancreas in chinchilla lies in contact with descending duodenum – dd. The portal vein – pv, passes in close proximity of the caudal portion of the duodenal lobe. icv – inferior cava vein.

Its length does not reach the transverse portion of the duodenum and is not in contact with the ascending loop.

The portal vein was in close proximity to the caudal portion of the duodenal lobe. The left lobe (*Lobus pancreatis sinister*) or splenic lobe has a compact appearance exceeding the caudal edge of the spleen (Figure 8).

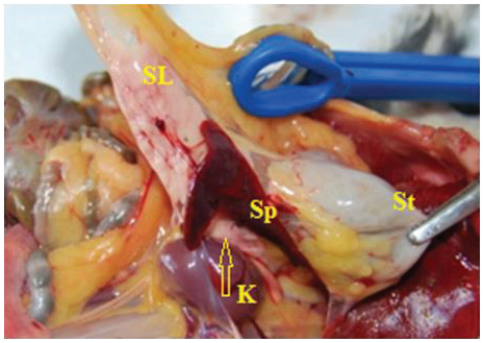

Figure 8. The left lobe of pancreas – SL in chinchilla has a compact appearance exceeding the caudal edge of the spleen - arrow. K –left kidney; St – stomach.

The gastric lobe was dispersed in multiple nodules protruding toward to the stomach (Figure 9). In chinchilla, the pancreas has a triangular shape with irregular margins after removal from the abdominal cavity (Figure 9).

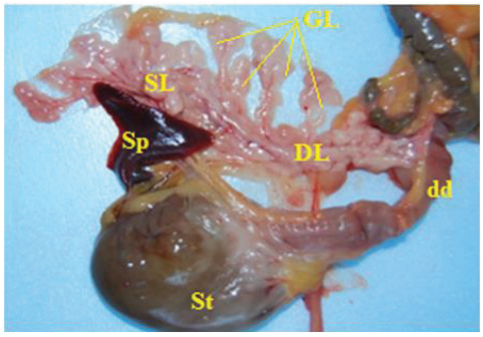

Figure 9. The triangular shape of the chinchillas pancreas. The splenic lobe – SL, was the most developed and compact lobe. The gastric lobe – GL, was dispersed in small portions protruding to the stomach – St. Sp – spleen; dd – descending duodenum.

Rabbit

The major part of the rabbit pancreas is contained into the mesoduodenum, this part being correspondent of the right lobe of pancreas or duodenal lobe (Figure 10).

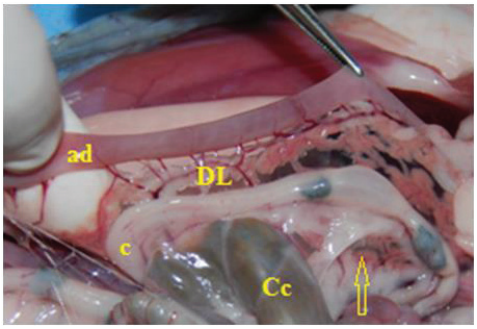

Figure 10. In rabbits, the diseminated glandular tissue of pancreas into the mesoduodenum – DL and arrow, is correspondent of the duodenal lobe. ad – ascending duodenum; c- colon; Cc – cecum.

It appears as a diffused irregular mass of glandular tissue distributed around the pancreaticoduodenal blood vessels and in more close relationship to the ascending ansa of the duodenum (Figure 10). On the lesser curvature of the stomach, and cranial part of the duodenum the gastric lobe was identified. This portion has a slightly condensed appearance (Figure 11).

The left lobe (*Lobus pancreatis sinister*) of the pancreas in rabbits located caudally from the stomach fundus into the wall of greater omentum and in close contact with spleen was assessed as the splenic lobe (Figure 12). This lobe reaches up to the ventral aspect of the left kidney.

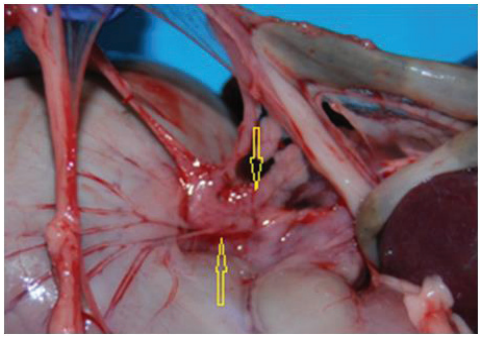

Figure 11. Slightly condensed appearance of pancreatic tissue – arrows, bounded by the lesser curvature of the stomach and cranial part of the duodenum, corresponding of the gastric lobe of pancreas in rabbit.

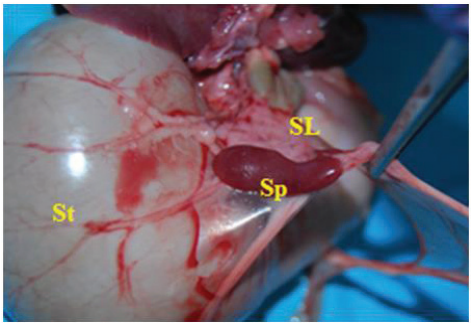

Figure 12. The condensed portion of the left pancreas in rabbits was the splenic lobe –SL. It was extended between the two extremities of the spleen – Sp and the stomach – St.

Due to the fact that pancreas is a target of a numerous diseases, from which the pancreatic cancer and diabetes mellitus are of major importance, this organ is of a great importance both of morphological and clinical interest. Several laboratory animals have been used in a numerous toxicological, pharmacological (Pandiri 2014; Stan 2015) and surgical researches in order to increase the knowledge which can be applied in humans and domestic animals. In this regard, rodents and rabbits are considered good models in clinical and anatomical studies of diverse morphological abnormalities and pancreatic disease (Aghdassi et al., 2011; Stan 2015; 2017; Tsuchitani et al., 2016).

Compared to the human pancreas, which is a compact organ, in experimental animals, the pancreas has a different appearance. Generally, two types of macroscopic anatomy is recognized: a diffuse pattern in which islets of glandular pancreatic tissue are diffusely distributed into the mesentery between the duodenal loop, found in rabbits (Barone 1997; Brewer 2006) and a more compact appearance found in domestic animals, monkeys, minipig and humans (Swindler et al,. 1973; Barone 1997; Evans and de Lahunta, 2013; Tsuchitani et al., 2016). In experimental animals there is an intermediate pattern in which the diffused distribution of the duodenal lobe alternate with a more compact pattern of the left portion (Barone 1997; Katherine Quesenberry and Carpenter 2012; Stan 2017). This is in agreement with our results which showed a compact appearance of the left portion of the pancreas in rats, guinea pigs, chinchillas and in the rabbits. Regarding the right portion assessed as right lobe or duodenal lobe, the diffused pattern of this lobe was the most pronounced in rabbits, while in guinea pigs, rats and chinchillas, the glandular tissue was compact and organized. A possible explanation of this feature is due to the large mobility of the duodenum found in rabbits.

In veterinary medicine and in accordance with the anatomical denomination (NAV) the pancreas is composed by the right and left lobe united through the body. More recent description in experimental animals uses different terms for lobe denomination like duodenal, gastric and splenic lobes (Stan 2017) or gastric lobe, duodenal head and tail (Cattley et al., 2013). In this study for a better comprehension of the macroscopic anatomy the same terms were used. Moreover, these terms have been used because the pancreas portions to which they refer are named after the organs they are in relation with. Therefore, the duodenal lobe was the correspondent of the right lobe of the pancreas or head of the pancreas. In rats, some authors have described the head of the pancreas being composed by the duodenal and parabilliary portion (Tsuchitani et al., 2016). We did not use the parabilliary terms because our results showed that the right lobe was invested into the mesentery between the ascending and descending loop of duodenum at equal distance from the two loops. The gastric lobe described in this study as in the cited literature, has no counterpart in the domestic larger species. In the human, the terms head, neck, body and tail are used to name the different regions of the pancreas. Taking into consideration the anatomical description of pancreas in humans (composed by the head, body and tail), in species presented here, the body of the pancreas extends from the head to the stomach and spleen. In this regard the gastric and proximal part of the splenic lobe is correspondent of the body of the pancreas in the mentioned species. Even in rabbit we showed the presence of a well defined gastric lobe disposed between the lesser curvature of the stomach and spleen, feature founded in other description too (Al-Saffar and Al-Hasnawy, 2014). The compact splenic lobe was found in all species of this study, being the largest lobe in rats, guinea pigs and chinchilla, as it was mentioned in other descriptions (Suckow et al., 2012; Wagner, 2014;). In rabbit this lobe was compact but regarding its length it was shorter than the duodenal lobe. In chinchilla, due to the particular triangular shape of the spleen, the splenic lobe of pancreas, especially the caudal part accounting to the tail of the pancreas, exceed the caudal part of the spleen. This pattern was mentioned by other authors too (Campbell-Ward, 2012; Ozdemir et al., 2013).

Similar with other description of pancreas in Rodents and rabbits (Katherine E. Quesenberry, and Carpenter, 2012; Al-Saffar and Al-Hasnawy, 2014; Wagner 2014), our study highlighted the pancreas partial location into the peritoneum folds between the duodenum, stomach and transverse colon, and partly location between the stomach, spleen, pancreatico-duodenal and splenic vessels. The close relation with the major vessels is of major importance in surgical experiments (Stan 2015). In this regard is worth to be mentioned the ring shape of the body of the pancreas found in a common experimental animal – the minipig. The body of the pancreas in this specie is composed of two separate portions that encompass the portal vein and make the pancreas appear to be „ring-shaped" (Ferrer et al., 2008). This patern is present in horse, pig and sometimes in cattle (Barone 1997). In the

species that were the subject of this study, we have not met this feature.

The macroscopic description of pancreas anatomy is important from the point of view of physiological, pathological and surgical studies. Experimental induction of diabetes, pancreatitis, or transplantation of pancreatic islets should take into account the segmental division of the pancreas in rodents and rabbits as it was shown in this study, the three lobe compound pancreas; the close relationship with the major vessels and the care not to injure the anatomical structure as pancreatic ducts and biliary ducts.

Due to the fact that the present study it was performed on four species, the vascular anatomy of the pancreas and the pancreatic ducts description are subjects of future reports.

CONCLUSIONS

In rats, guinea pigs, chinchillas and rabbit the pancreas presented three well-differentiated portions or lobes. These lobes have been named in relation to adjacent organs: duodenal, gastric and splenic lobe. Related to the human denomination the duodenal lobe is the head of pancreas correspondent; the gastric and the proximal part of the splenic lobe is the correspondent of the body of the pancreas and the caudal portion of the splenic lobe is the tail of pancreas correspondent.

REFERENCES

Aghdassi AA, Mayerle J, Christochowitz S, Weiss Sendler M, and Lerch MM. 2011. Animal models for investigating chronic pancreatitis. Fibrogenesis Tissue Repair. 4: 26.

Al-Saffar F.J. and A.H.A. Al-Hasnawy, 2014. Histomorphological Developmental Study of Advanced Postnatal of the Pancreas of Local Rabbit. Journal of Biological Sciences, 14: 387-402.

Barrone, R.. 1997. Anatomie comparée des mamiferes domestique, Tome III, Spanchnologie, Appareil digestif, Appareil respiratoire, Ed.Vigot, Paris.

Brewer N. 2006. Biology of the rabbit. J Am Assoc Lab Anim Sci 45:8–24

Swindler DR, and Wood CD. Abdomen. Pancreas, Duodenum,and Superior Mesenteric Artery. In: An Atlas of Primate Gross Anatomy: Baboon, Chimpanzee, and Man. DR Swindler and CD Wood (eds). University of Washington Press, Seattle. 214–215. 1973.

Campbell-Ward M. L. 2012. Gastrointestinal physiology and nutrition. pp. 183–192. *In*: Ferrets, Rabbits, and Rodents: Clinical Medicine and Surgery, 3rd ed. (Quesenberry, K. E. and Carpenter, J. W. eds.), Elsevier, St. Louis.

Cattley RC, Popp JA, and Vonderfecht SL. 2013. Liver, Gallbladder, and Exocrine Pancreas. Exocrine Pancreas. In: Toxicologic Pathology: Nonclinical Safety Assessment. PS Sahota, JA Popp, JF Hardisty, and C Gopinath (eds). CRC Press, Boca Raton. 345–356..

Evans Howard E. and de Lahunta Alexander, 2013. Miller's Anatomy of the Dog, 4th Edition, Saunders, Elsevier Inc.

Ferrer J, Scott WE 3rd, Weegman BP, Suszynski TM, Sutherland DER, Hering BJ, and Papas KK. 2008. Pig pancreas anatomy: implications for pancreas procurement, preservation, and islet isolation. Transplantation. 86: 1503–1510..

Katherine E. Quesenberry, J. W. Carpenter, 2012. Ferrets, Rabbits and Rodents, Clinical Medicine and Surgery, Third Edition,Saunders Elsevier, Missouri.

NAV fifth edition 2012.

Özdemir V., Çevik Demirkan A., Akosman M. S. 2013. Subgross and macroscopic investigation of the coeliac artery in the chinchilla *(Chinchilla lanigera)*. Folia Morphol. (Warsz) *7*2: 258–262.

Pandiri, A. R. 2014. Overview of Exocrine Pancreatic Pathobiology. Toxicologic Pathology, 42(1), 207–216

Stan, F. 2014. Anatomical Particularities of the Cecum in Rabbits and Chinchillas. Bulletin of University of Agricultural Sciences and Veterinary Medicine Cluj-Napoca. Veterinary Medicine, 71*(2),* 406-412.

Stan, F. 2015. Rabbits and chinchillas as experimental models. Lucrări Ştiinţifice. Seria Medicină Veterinară. Iaşi, Partea I, , vol 58, p 90-98.

Stan, F. 2014. Topographical anatomy of guinea pigs kidneys. Lucrări Ştiinţifice Medicină Veterinară Timişoara, Vol. XlVII(1), 114-123.

Stan, F., 2017. Anatomical differences and similarities of the pancreas in Guinea Pig (*Cavia porcellus*) and Domestic Rabbit (*Oryctolagus cuniculus*) Lucrări Ştiinţifice Medicina Veterinară Vol. L (2), 355-363 Timişoara

Suckow, M.A., Karla A. Stevens, R. P. Wilson, , 2012. The Laboratory Rabbit, Guinea Pig, Hamster, and Other Rodents, First edition, Saunders Elsevier.

Tsuchitani, M., Sato, J., & Kokoshima, H. 2016. A comparison of the anatomical structure of the pancreas in experimental animals. Journal of Toxicologic Pathology, , 29(3), 147–154.

Wagner Joseph E. 2014. The Biology of the Guinea Pig American College of Laboratory Animal Medicine Academic Press, 317 pag.

CLINICAL SCIENCES

Scientific Works. Series C. Veterinary Medicine. Vol. LXIII (2)
ISSN 2065-1295; ISSN 2343-9394 (CD-ROM); ISSN 2067-3663 (Online); ISSN-L 2065-1295

MACROSCOPIC ANATOMY OF THE GALLBLADDER AND EXTRAHEPATIC BILIARY TRACT IN THE GUINEA PIG (*CAVIA PORCELLUS*)

Florin Gheorghe STAN

University of Agricultural Sciences and Veterinary Medicine,
Cluj Napoca, 3-5 Mănăștur Str. Romania

Corresponding author email: florin.stan@usamvcluj.ro

Abstract

In mammals the variations of the anatomy of the extrahepatic biliary tree have long been recognized. The aim of this study was the macromorphological description of the gallbladder and extrahepatic biliary tract in guinea pigs (Cavia porcellus).Using dissection techniques the gallbladder topography, anatomic particularities regarding the shape and the connecting elements were assessed. Also, the macroscopic appearance of extrahepatic biliary tract and its path was described. The round and well developed gallbladder, exceeds the ventral border of the liver being visible on both, the visceral and the diaphragmatic surfaces of the liver. The gallbladder was connected with the right medial lobe and with the quadrate lobe of the liver by two tiny ligaments. Proximal, the unique cystic duct shows an obvious constriction and a conspicuous swelling. On its path on the hepatoduodenal ligament, the cystic duct joined the left hepatic duct to form the common bile duct. The right hepatic duct drained the right territory of the liver and joined the common bile duct itself. The left territory of the liver and in some cases the quadrate lobe was drained by the left hepatic duct. Distally, the common bile duct shows a unique ampullary dilatation from which a small duct drains into the first segment of duodenum. The major duodenal papilla was located at 1.5 cm distal to the pylorus.

Key words*: gallbladder, extrahepatic biliary tract, macroscopic anatomy, guinea pigs*

INTRODUCTION

The anatomy of the biliary tree involves complex relationship between the liver, intrahepatic biliary canaliculi, bile ductules, gallbladder and extrahepatic biliary tract (Barone 2009; Ellis, 2011). In animals, the obstruction of the extrahepatic tract is frequently present more than it is reported (Bacon et al., 2003; Amsellem et al., 2006; Miwa and Sladky 2016). Considering the many anatomical variations of biliary tract in mammals (Oldham-Ott and Gilloteaux 1997) a proper knowledge of the normal anatomy of the extrahepatic biliary tract is essential in order to prevent its injury during the surgery. Most liver anatomical descriptions contain descriptions of biliary tract too. Due to the extensive use of rats as experimental model in liver transplantation, the most studied is the rat liver (Higgins 1931; Madrahimov et al., 2006). With the exception regarding the absence of the gallbladder in rats, the macroscopic anatomy and connecting elements of the liver resemble the human anatomy of the liver. From the caviomorphs order, the chinchilla's liver was described having four lobes and a well developed gallbladder (Spotorno et al., 2004). The gallbladder is located between the right and medial lobes, having more than one cystic duct and a complex hepatic ducts system (Nowak et al., 2014). In guinea pigs the liver was described having six lobes (Cooper and Schiller, 1975; Breazile and Brown 1976; Stan 2014) and a well developed gallbladder attached to a fossa which delineates the quadrate lobe, drained by a cystic duct which receives several hepatic ducts to form the common bile duct (Higgins 1927; Quesenberry et al., 2004). In guinea pigs, the angioarhitecture, the inervation and the musculature of gallbladder and and bile ducts was assessed by scanning electron microscopy of vascular corrosion casts, histochemical methods and light electron microscopy (Aharinejad and Lametschwandtner 1992; Cai and Gabela 1983). In rabbit, the absence of the common hepatic duct was reported (Brewer

2006). Also, in humans, the biliary tract and its vascular anatomy show numerous anatomical variations (Lamah et al., 2001; Horiguchi and Kamisawa 2010). The aim of this study is to perform a detailed morphological description of gallbladder and extrahepatic biliary tract in guinea pigs.

MATERIALS AND METHODS

Ten adult guinea pigs, four male and six female (mean body weight 420±50g) were used. The Institutional Bioethics Committee of University of Agricultural Science and Veterinary Medicine in accordance to Directive 2010/63 /EU of the European Parliament and of the Council on the protection of animals used for scientific purposes approved the study. Euthanasia was performed by administration of an overdose of isoflurane. The abdominal cavity was opened and the wall of it was carefully removed. The gallbladder topography, its connecting elements and the extrahepatic biliary tract was recorded after the displacement on right and left side of the liver lobes, without altering hilum topography and its components.

RESULTS AND DISCUSSIONS

Gallbladder topography

The rounded shape of gall bladder (*Vesica fellea*) exceeded the ventral border of the liver, being visible both on diaphragmatic and visceral surface of the liver, in all examined specimens (Figure 1).

Its diameter was 9 mm ± 0.3 mm and the total length was 11 mm ± 0.1mm. The gall bladder was attached to a fossa (*Fossa vesicae felleae*) situated at the delineation of the right medial lobe and the quadrate lobe (Figure 1), showing an obvious transition zone at the neck and a small swelling on the beginning of the cystic duct (Figure 2).

Ventral edge of right medial lobe embraces the gallbladder fundus (*Fundus vesicae felleae*) being attached to the later by a small but conspicuous ligament. Also, on the left side, the gallbladder fundus was attached to the quadrate lobe by a second small ligament (Figure 3).

Figure 1 The rounded shape of the gallbladder in guinea pigs. The gallbladder exceeds the ventral border of the liver being visible on both visceral and diaphragmatic surfaces of the liver.

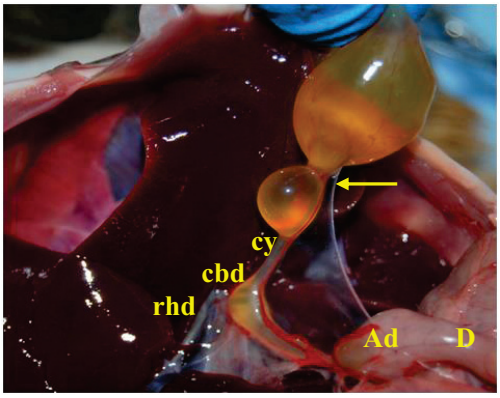

Figure 2 An obvious constriction and a small swelling found at the beginning of the cystic duct - arrow. Rhd –right hepatic duct join the common bile duct –cbd. Ad – ampularry dilatation.

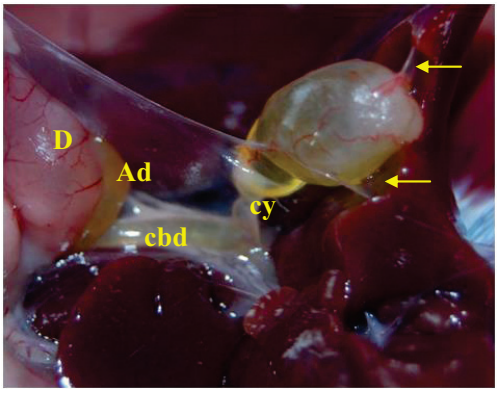

Figure 3 The gallbladder ligaments – arrows. The cystic duct – cy, join the common bile duct – cbd. Ampullary dilatation – Ad, of distal segment of common bile duct. D - duodenum

The extrahepatic biliary tract

The cystic duct (*Ductus cysticus*) diameter was 2 mm ± 0.2 mm making an acute angle with the common bile duct. (Figure 4).

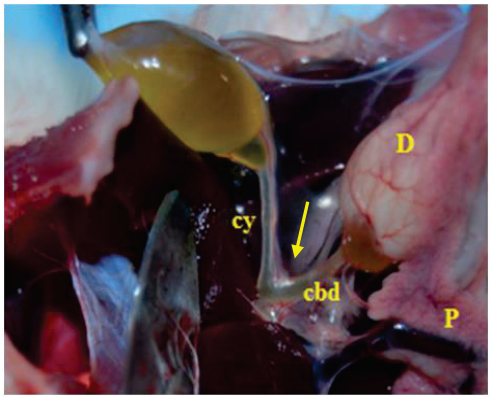

Figure 4 The cystic duct made an acute angle with the common bile duct - arrow

First, the cystic duct joins the left hepatic duct to form the common bile duct, the right hepatic duct draining at short distance after the mentioned union, on the right side of the common bile duct (Figure 5).

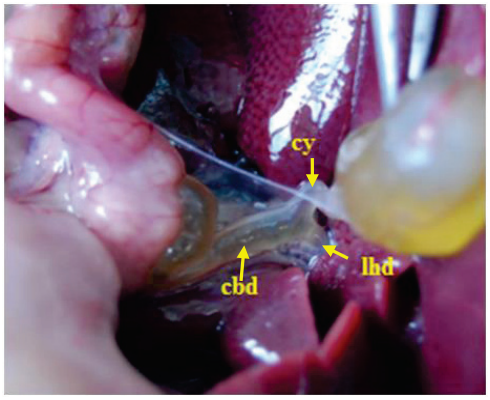

Figure 5 The union of cystic duct – cy, with the left hepatic duct – lhd, to form the common bile duct – cbd.

The right hepatic duct was formed by the union of the hepatic duct that drains the caudate process of the caudate lobe with the channel that drains the right lateral and right medial lobes. The left medial and lateral lobes and the quadrate lobe were drained by the biliary channels which merged to form the left hepatic duct. In three cases the quadrate lobe was drained by a separate channel that joined the cystic duct itself. Distally, above and attached of duodenal wall, the common bile duct shows a unique ampullary dilatation from which a small duct drains into the first segment of duodenum. Proximal of this dilatation the common bile duct showed a small contraction. The opening of the common bile duct observed through the duodenal lumen appeared like a slight elevation of the duodenal mucosa. The major duodenal papilla was located about 1.5 cm distal to the pylorus inside of the first segment of the duodenum (Figure 6).

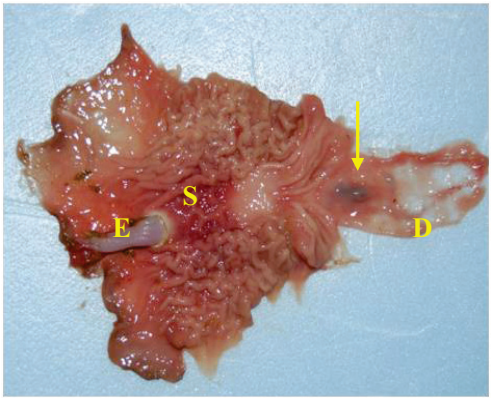

Figure 6 The major duodenal papilla (arrow) located about 1.5cm distal to the pylorus inside of the first segment of the duodenum – D. E – esophagus; S – stomach.

Like most of the mammals, excepting horse, deer, rat, European hamster which have no gall bladder, (Higgins 1931; Shiojiri 1997; Martin and Neuhaus 2007; Barone 2009; Hunyh and Pignon 2013) the guinea pigs show a well developed gall bladder. Different from humans, rabbit, chinchilla and hamster, the guinea pig gall bladder have a rounded shape. However, in contrast with many other species in which the gall bladder is firmly attached and covered by the liver lobes, the guinea pigs gall bladder, exceed the ventral edge of the liver. It was stated that the guinea pigs gall bladder is suspended by a single membrane from the liver with the reminder of the gall bladder hanging freely. Our result pointed out the presence of two small ligaments which connect the medial margin of the right middle lobe on the right

side of the gall bladder and a second one between the gallbladder and the ventral edge of the quadrate lobe. Also, the obvious neck zone constriction is typical for the guinea pigs. This feature and the acute angle formed by the cystic duct with the gall bladder is the morphological explanation of bile stasis. Based on this feature and on the fact that guinea pigs form cholesterol gallstone when given 1% cholestyramine and a weight loosing pellet diet, using guinea pigs as experimental models in gallstone disease in human, is common. The bile stasis, abnormal bile composition, or infections are involved in gallstone formation both in human and guinea pigs (Wagner and Manning 1976). Both in normal or pathological conditions in humans has been found the presence, just below the gall bladder neck, of a dilated pouch at the cystic beginning, named Hartmans pouch (van Eijck et al. 2007; Ellis 2011). In six cases we found an equivalent dilatation, issue that has not been mentioned so far in guinea pigs. As in humans, this is a morphological aspect rather than an anatomic and constant feature.

The gallbladder and the extrahepatic ducts are subject to numerous variations, both in humans and animals, which are best understood by considering their embryological development (Shiojiri, 1997; Uemura et al., 2015). In some animals, including the rat, the deer, the horse and the pigeon, the gallbladder do not develop in embryonic state (Shiojiri 1997; Hisami, 2010; Uemura et al., 2015; Hill, 2017). On the other hand, it was stated that the variability of gallbladder anatomy in mammals is mainly dependent upon diet. Frequent eating of pigeons, rat and deer, which eat almost continuously, imply a continuous secretion and a constant flow of bile from the liver to the intestine, the presence of a gallbladder is not required. In other mammals, like human, cattle, dog or hamster which eats at times the bile is storage and concentrated in the gallbladder, being concentrated one to two times in cattle, four to ten times in dogs and eight to ten times in human and hamster . The anatomical variants of extrahepatic biliary tract include differences in terms of number of ducts, their length, and the manner of union and how the drainage in duodenum is made (Mahandevan 2014). In humans it is clearly stated formation of the common bile duct by joining the common hepatic duct (resulting from the union of the right and left hepatic ducts corresponding to the left and right territories of the liver) with cystic duct (Ellis 2011; Mahadevan, 2014). In rabbit Barone (2009) describe the presence of two hepatic ducts, the left one which drain the left lobes and the quadrate lobe too, joins the cystic duct to form the common bile duct, which receive the right hepatic duct, made by the union of the ducts which drain the right lobe and the caudate lobes. This description is in compliance with the description of Aharinejad and Lametschwandtner (1992) and Jackowiak and Lametschwandtner, (2005), regarding the absence of a common hepatic duct, but the latter authors, studying the angioarchitecture of the rabbit extrahepatic bile ducts and gallbladder, by scanning electron microscopy of vascular corrosion casts, have shown that, there is four or five hepatic ducts which individual join the cystic duct to form the common hepatic ducts. Also, in chinchillas, Novak et al, 2014 state the presence of a complex system of extrabiliary tract by description of multiple cystic ducts which drain the gallbladder together with a multiple anastomosing hepatic ducts running in the hepatoduodenal ligament.

The same pattern was found by Martin and Neuhaus,(2007) who noted that the extrahepatic biliary ducts of the rats are more superficial and also has intercommunicating branches, which implies the existence of a biliary network. Due to the absence of the gallbladder in rats, the common bile duct is made by the junction of the main hepatic ducts. Compare to all mentioned, in guinea pigs the extrahepatic biliary tract is simpler, the absence of a common hepatic duct is obvious and the variability consist of the presence of a different pattern of union of hepatic ducts with the cystic ducts to form the common bile duct, which make the guinea pigs a suitable model to gall stones pathogenesis.

Our results concerning the presence of the distal ampullary dilatation of common bile duct in guinea pigs, are in accordance with those of Higgins (1927) and Cai and Gabela (1983), who also described the common bile duct ampulla and its attachment to the duodenal wall. This is a unique feature of guinea pigs

common bile duct and has not been described in other species.

CONCLUSIONS

The rounded gallbladder of guinea pigs exceeds the ventral margin of the liver. It presents a small constriction and an obvious swelling at the beginning of the cystic duct. The common bile duct is formed by the union of the cystic duct with the left hepatic duct. The common hepatic duct is missing in guinea pig. Distally and attached of duodenal wall, the common bile duct shows a unique ampullary dilatation from which a small duct drains into the first segment of duodenum. The major duodenal papilla opens at 1.5 cm distal to the pylorus.

REFERENCES

Aharinejad S, Lametschwandtner A. 1992. Microangioarchitecture of the guinea pig gallbladder and bile duct as studied by scanning electron microscopy of vascular corrosion casts. Journal of Anatomy. 181:89-100.

Aharinejad SH., Lametschwandtner A. 1992: Microvascular Corrosion Casting in Scanning Electron Microscopy Vienna: Spinger Verlag.

Amsellem, P. M., Seim, H. B., MacPphail, C. M.,Bbright, R. M., Twedt, D. C., Wrigley, R. H. & Mmonnet, e. (2006) Long-term survival and risk factors associated with biliary surgery in dogs: 34 cases (1994-2004). Journal of the American Veterinary Medical Association 229, 1451-1457.

Bacon, N. J. & White, R. A. S. (2003) Extrahepatic biliary tract surgery in the cat: a case series and review. Journal of Small Animal Practice 44, 31-35.

Barone, Robert. 2009. Anatomie comparée des mammifères domestiques. Tome 3. Splanchnologies I. Appareil digestif et respiratoire. Edition Vigot, pp 507-559.

Breazile, J.E., Brown, E.M., 1976. Anatomy. In: Wagner, J.E., Manning, P.J. (Eds.), The Biology of the Guinea Pig. Academic Press, New York, p53–62.

Cai WQ, Gabella G. 1983. The musculature of the gall bladder and biliary pathways in the guinea-pig. Journal of Anatomy; 136(Pt 2):237-250.

Cai WQ, Gabella G. 1983. Innervation of the gall bladder and biliary pathways in the guinea-pig. Journal of Anatomy; 136(Pt 1):97-109.

Cooper G. and A. L. Schiller. 1975. Anatomy of the Guinea Pig Cambridge, Mass.: Harvard University Press. 417 pp.

Ellis, H., 2011: Anatomy of the gallbladder and bile ducts. Surgery 29 (12), 593-596.

Higgins GM, Anderson RM. 1931 Experimental pathology of the liver – Restoration of the liver of the white rat following partial surgical removal. Arch Pathol.; 12:186-202.

Higgins, G.M., 1927. The extrahepatic biliary tract in the guinea-pig. Anat. Rec. 36, 129-147.

Hill, M.A. 2017 Embryology Gastrointestinal Tract - Gall Bladder Development.

Hisami Ando. 2010. Embryology of the biliary tract. Dig Surg:, 27(2);87-9.

Horiguchi S, Kamisawa T. 2010. Major duodenal papilla and its normal anatomy. Dig Surg.; 27:90–93

Huynh Minh, Charly Pignon, Gastrointestinal Disease in Exotic Small Mammals, Journal of Exotic Pet Medicine, Volume 22, Issue 2, April 2013, Pages 118-131.

Jackowiak, H. and Lametschwandtner, A. 2005. Angioarchitecture of the rabbit extrahepatic bile ducts and gallbladder. Anat. Rec., 286A: 974–981.

Lamah M, Karanjia ND, Dickson GH. 2001. Anatomical variations of the extrahepatic biliary tree: review of the world literature. Clin. Anat.; 14: 167–72.

Madrahimov, N., Dirsch, O., Broelsch, C., Dahmen, U. 2006. Marginal Hepatectomy in the Rat: From Anatomy to Surgery. Annals of Surgery, 244:89–98.

Mahadevan Vishy. 2014. Anatomy of the gallbladder and bile ducts Review Article Surgery (Oxford), Available online 8 November

Martins, P. N., and P. Neuhaus, 2007: Surgical anatomy of the liver, hepatic vasculature and bile ducts in the rat. Liver Int. 27, 384–392.

Miwa, Y., Sladky, K. K. 2016. Small Mammals: Common Surgical Procedures of Rodents, Ferrets, Hedgehogs, and Sugar Gliders. Veterinary Clinics of North America: Exotic Animal Practice, 19:205-244.

Oldham-Ott, C. K. and Gilloteaux, J. 1997, Comparative morphology of the gallbladder and biliary tract in vertebrates: Variation in structure, homology in function and gallstones. Microsc. Res. Tech., 38: 571–597.

Quesenberry, K.E., Donnelly, T.M., Hillyer, E.V. 2004. Biology, husbandry, and clinical techniques of guinea pigs and chinchillas. in: Quesenberry, K.E., Carpenter, J.W. (Eds.), Ferrets, Rabbits and Rodents Clinical Medicine and Surgery second ed. Elsevier, New York, pp. 232–244.

Shiojiri N. 1997. Development and differentiation of bile ducts in the mammalian liver. Microsc Res Tech. ;39:328–335.

Stan, F. (2014). Anatomical Differences and similarities of liver and hepatic ligaments in rabbits and guinea pigs. *Anatomia, Histologia, Embryologia*, 43*: Issue Supplement s1* (p.89).

Uemura, M.; Igarashi, H.; Ozawa, A.; Tsunekawa, N.; Kurohmaru, M. et al. 2015. Fate mapping of gallbladder progenitors in posteroventral foregut endoderm of mouse early somite-stage embryos. J. Vet. Med. Sci. 77(5): 587- 91.

van Eijck, F.C., van Veen, R.N. Kleinrensink, G.J. Lange, J.F., 2007. Hartmann's gallbladder pouch revisited 60 years later. Surg Endosc. 21,1122–25.

Wagner J. E and P. J. Manning, 1976. The Biology of the Guinea Pig, New York: Academic Press. 317 pp.

Nomina Anatomica Veterinaria, 5th Edition- Revised 2012.

CLINICAL SCIENCES